**CAPITAL UNIVERSITY OF SCIENCE AND
TECHNOLOGY, ISLAMABAD**

Modeling and Characterization of Ground-to-Air Communication Channel

by

Mirza Muhammad Yasir Masood

A thesis submitted in partial fulfillment for the
degree of Doctor of Philosophy

in the

Faculty of Engineering
Department of Electrical Engineering

2020

Modeling and Characterization of Ground-to-Air Communication Channel

By

Mirza Muhammad Yasir Masood

(PE123007)

Dr. Mohamed Abdel-Maguid, Professor

University of Suffolk, UK

(Foreign Evaluator 1)

Dr. Muhammad Imran, Professor

University of Glasgow, UK

(Foreign Evaluator 2)

Dr. Noor Muhammad Khan

(Thesis Supervisor)

Dr. Noor Muhammad Khan

(Head, Department of Electrical Engineering)

Dr. Imtiaz Ahmad Taj

(Dean, Faculty of Engineering)

DEPARTMENT OF ELECTRICAL ENGINEERING

CAPITAL UNIVERSITY OF SCIENCE AND TECHNOLOGY

ISLAMABAD

2020

I dedicate this thesis to my family for their affectionate love and support.

CAPITAL UNIVERSITY OF SCIENCE & TECHNOLOGY ISLAMABAD

Expressway, Kahuta Road, Zone-V, Islamabad
Phone:+92-51-111-555-666 Fax: +92-51-4486705
Email: info@cust.edu.pk Website: https://www.cust.edu.pk

CERTIFICATE OF APPROVAL

This is to certify that the research work presented in the thesis, entitled **"Modeling and Characterization of Ground-to-Air Communication Channel"** was conducted under the supervision of **Dr. Noor Muhammad Khan**. No part of this thesis has been submitted anywhere else for any other degree. This thesis is submitted to the **Department of Electrical Engineering, Capital University of Science and Technology** in partial fulfillment of the requirements for the degree of Doctor in Philosophy in the field of **Electrical Engineering.** The open defence of the thesis was conducted on **09 July, 2020.**

Student Name :   Mr. Mirza Muhammad Yasir Masood   (PE123007)

The Examination Committee unanimously agrees to award PhD degree in the mentioned field.

Examination Committee :

(a)   External Examiner 1:   Dr. Shahid Khattak,
Professor
UET, Mardan

(b)   External Examiner 2:   Dr. Junaid Mughal,
Professor
COMSATS University, Islamabad

(c)   Internal Examiner :   Dr. Imtiaz Ahmed Taj
Professor
CUST, Islamabad

Supervisor Name :   Dr. Noor Muhammad Khan
Professor
CUST, Islamabad

Name of HoD :   Dr. Noor Muhammad Khan
Professor
CUST, Islamabad

Name of Dean :   Dr. Imtiaz Ahmed Taj
Professor
CUST, Islamabad

AUTHOR'S DECLARATION

I, **Mr. Mirza Muhammad Yasir Masood (Registration No. PE123007)**, hereby state that my PhD thesis titled, '**Modeling and Characterization of Ground-to-Air Communication Channel**' is my own work and has not been submitted previously by me for taking any degree from Capital University of Science and Technology, Islamabad or anywhere else in the country/ world.

At any time, if my statement is found to be incorrect even after my graduation, the University has the right to withdraw my PhD Degree.

(Mr. Mirza Muhammad Yasir Masood)

Dated: 09   July, 2020

Registration No : PE123007

PLAGIARISM UNDERTAKING

I solemnly declare that research work presented in the thesis titled "**Modeling and Characterization of Ground-to-Air Communication Channel**" is solely my research work with no significant contribution from any other person. Small contribution/ help wherever taken has been duly acknowledged and that complete thesis has been written by me.

I understand the zero tolerance policy of the HEC and Capital University of Science and Technology towards plagiarism. Therefore, I as an author of the above titled thesis declare that no portion of my thesis has been plagiarized and any material used as reference is properly referred/ cited.

I undertake that if I am found guilty of any formal plagiarism in the above titled thesis even after award of PhD Degree, the University reserves the right to withdraw/ revoke my PhD degree and that HEC and the University have the right to publish my name on the HEC/ University Website on which names of students are placed who submitted plagiarized thesis.

(**Mr. Mirza Muhammad Yasir Masood**)

Dated: 09 July, 2020

Registration No : PE123007

List of Publications

It is certified that following publication(s) have been made out of the research work that has been carried out for this thesis:-

1. **M.-Y. M. Mirza**, N. M. Khan, A.Jamal and R. Ramer,"Characterization of Spatial Reflection Co-efficient for Ground-to-Aircraft and Satellite-to-Aircraft Communication" *Applied Computational Electromagnetics Society Journal*, vol. 33, no. 1, pp. 56-68, 2018.

2. **M.-Y. M. Mirza** and N. M. Khan,"G2A Communication Channel Modeling and Characterization Using Confocal Prolates." *Wireless Personal Communication*, Springer, 2020, DOI:10.1007/s11277-020-07597-4.

(Mirza Muhammad Yasir Masood)

Registration No: PE123007

Acknowledgements

First and foremost, I would like to thank Allah Almighty for providing me this great opportunity to pursue and complete my doctoral studies. I would like to express my sincere gratitude to my supervisor **Prof. Dr. Noor Muhammad Khan** for his vision, guidance, support and encouragement towards the completion of this studies. His exceptional theoretical concepts, research experience and innovative thinking ability made this work valuable in research community. Working with him has been a great previlage for me and will remain a memorable experience of my life. His critical observation towards every aspect of life is exceptional which groomed me to think and observe more critically. He is a man of rules and ethics. I wish to become a person like him by following his teachings. I pray for his good health and future, and will always remember him in my prays.

I would like to thank all my teachers of the Electrical Engineering Department of the Capital University of Science and Technology (CUST), Islamabad, Pakistan, who build my theoretical and conceptual knowledge. I would also like to thank my ARWiC research group colleagues for providing a pleasant working and research environment.

Finally, I would like to thank my parents, brothers, sisters for their effort, encouragement, motivation, prays and continuous support throughout my Ph.D. studies. I am forever debted to my parents for their support which is the key to complete this degree. I would love to express my sincere love to my nephews and nieces, **Shawaiz**, **Almir**, **Haiqa** and **Alina**, for their sweet lovely prays for my studies. I would also thank my wife and kids, **Rehan Mirza** and **Salaar Mirza**, for dedicating their precious time for my work. At this stage, I cannot forget my paternal and maternal grandparents who always prayed for my good future and wanted to see me at this stage. May Allah bless them a higher place in Jannat-ul-Firdous. Aameen.

(Mirza Muhammad Yasir Masood)

Registration No: PE123007

Abstract

Radio channel characterization is an important field of research which explores the limiting features of the propagation environment and helps designing efficient communication systems. This dissertation presents an in-depth analysis of the A2G/G2A channel models and formulates the problem of G2A channel characterization in the presence of multipaths in a multiple aircraft environment. It is observed that most of the research literature supposedly model G2A channels interchangeably in the same manner as that of land mobile communication links. G2A communications systems are generally equipped with directional antennas for dedicated coverage to flying aircrafts that benefit in increasing range and radio signal strength while restraining interfering signals coming through scattering objects around ground station (GS). This research analyzes G2A multipath channel and thus proposes a geometrically-based physical G2A multipath channel model. The proposed channel model clearly justifies the existence of multipath environment in G2A communication due to the existence of aircrafts in the vicinity of the intended aircraft. This model is based on a three-dimensional confocal prolate spheroids and uses the principle of single-bounce multipath geometry. In order to observe the reflection properties of aircraft, a new term named as Spatial Reflection Coefficient (SRC) is defined and then a novel relationship of the interdependence between RADAR Cross-Section (RCS) and SRC is established. This relationship relates two different terms which are being used differently in two different fields of research. Both terms are inter-dependent and utilize the same input parameters like incident angle, material properties, signaling frequency, polarization and observation angle. The proposed relationship interrelates RCS and SRC which interchangeably help to extract the reflectivity information of a target's surface on the basis of observed RCS. Moreover, this interchangeability between the RCS and SRC will help the researchers of different fields to utilize simulation tools and algorithms of both domains interchangeably. The scattering properties of the body of an Aircraft are analyzed by designing geometrical models of two scenarios, satellite-to-aircraft and ground-to-aircraft. The proposed geometrical models help to estimate the correct incident angles of incoming electromagnetic

(EM) waves impinging on aircraft's surface. Utilizing information of the reflected signal from aircraft's body and the proposed multipath geometry, an expression for the total received power at the intended aircraft is developed. For numerical computations, a quasi-realistic G2A propagation environment is constructed in Matlab®. Simulations for bistatic radar cross section (BRCS) are performed by taking A380® facet-based model on physical optics based simulation software platform POFACET® and power delay profiles (PDPs) are developed. Statistics of the PDPs are then evaluated and the expected data rates of the designed scenario are envisioned. This study highlights the time-dispersive nature of the G2A propagation environment and may become a foundation to observe the communication link performance of G2A applications in recent future. Furthermore, a visualization of the interference caused in wide-beam and narrow-beam G2A communication link scenarios is presented. The proposed model is equally applicable to the networks of passenger aircrafts, flocks of jet fighters and mesh of Unmanned Aerial Vehicle (UAV) drones. This model can also be used to analyze the performance of high data-rate communication links with high mobile speeds over sparsely distributed multipath channels.

Contents

List of Figures

xiv

List of Tables

Abbreviations

A2G	Air-to-Ground
AS	Air Station
BER	Bit-Error Rate
BRCS	Bistatic RADAR Cross Section
CDMA	Code Division Multiple Access
DA2GC	Direct Air-to-Ground Communication
dBsm	Decibels per Square Meter
EAN	European Aviation Network
EM	Electromagnetic
Ev-Do	Evolution-Data Optimized
FDTD	Finite Difference Time-Domain
FMM	Fast Multipole Mthod
G2A	Ground-to-Air
GLSR	Geographic Load Sharing Routing
GO	Geometric Optics
GS	Ground Station
GTD	Geometric Theory of Diffraction
HAP	High-Altitude Platform
HFA	High-Frequency Asymptotic
IFIC	Inflight Internet Connectivity
ILS	Instrument Landing System
LoS	Line-of-Sight
LTE	Long-Term Evolution
MAI	Multiple Access Interference

MIMO	Multiple-Input and Multiple-Output
MoM	Method of Moments
MUD	Multi-user Detection
NEC	Numeric Electromagnetic Code
NLoS	Non-Line-of-Sight
OFDM	Orthogonal Frequency Division Multiplexing
PDP	Power Delay Profile
PL	Path Loss
PN	Pseudo Noise
PO	Physical Optics
PTD	Physical Theory of Diffraction
RCS	RADAR Cross Section
RMS	Root Mean Square
SC	Satellite-based Communication
SDMA	Spatial Division Multiple Access
SNOI	Source not of Interest
SRC	Spatial Reflection Coefficient
TLM	Transmission-Line Matrix
UAS	Unmanned Aircraft System
UAV	Unmanned Aerial Vehicle
UHF	Ultra Hight Frequency
VHF	Very High Frequency

Symbols

P_{D_i} Incident power density

P_{ref} Reflected power

σ Target cross section

P_{D_r} Received power density

Γ Reflection coefficient

E_i Incident electric field intensity

E_r Reflected electric field intensity

σ_{B} Bistatic RADAR cross section

ρ_0 Magnitude of spatial reflection coefficient

P_t Peak transmit power

P_d Received power density

d_1 Distance between aircraft (A_1) and transmitter

G_t Transmit antenna gain

A_e Effective aperture of antenna

h_s Satellite altitude

γ_{A} Angle between the equator (O) and aircraft (A)

γ_{B} Angle between the equator (O) and aircraft (B)

r_E Radius of the Earth

d_{SA} Propagation distance from satellite (S) to aircraft (A)

d_{SB} Propagation distance from satellite (S) to aircraft (B)

β_{A} Angle between satellite (S) and axis of aircraft (A)

β_{B} Angle between satellite (S) and axis of aircraft (B)

β_{C} Angle between satellite (S) and axis of aircraft (C)

η_{A} Angle between satellite (S) and aircraft (A)

η_{B} Angle between satellite (S) and aircraft (B)

h_{A} Aircraft altitude

$r_{\mathrm{C,,max}}$ Maximum radius

Ψ_{B} Angular spread of the beamwidth

α_{A} Angle between ground transmitter and axis of aircraft (A)

α_{B} Angle between ground transmitter and axis of aircraft (B)

α_{C} Angle between ground transmitter and axis of aircraft (C)

A_k k^{th} proximate aircarft

d_k Length of kth propagation path via aircraft A_k

τ_k Propagation delay associated with k^{th} propagation path via aircraft A_k

α_k Attenuation factor associated with k^{th} propagation path via aircraft A_k

h_a Altitude of the intended aircaft

A_0 Intended aircraft

τ_0 Line-of-Sight propagation delay

$\tau_{\max}$ Maximum propagation delay

a_p Minor axis of prolate spheroid

b_p Minor axis of prolate spheroid

c_p Major axis of prolate spheroid

e_p Eccentricity of prolate spheroid

a_{cs} Length of semi-major axes of plane cross-sectioned ellipse

b_{cs} Length of semi-minor axes of plane cross-sectioned ellipse

r_p Radius of pth circle of separation distance

a_{eq} Length of major axis of qth plane cross-sectioned ellipse

b_{eq} Length of major axis of qth plane cross-sectioned ellipse

θ_{Beam} Elevation angle of transmitter beam with aircraft A_0

D_0 Horizontal distance between A_0 and ground station

S_a Scattering aircraft

$d_{\mathrm{GS_q}}$ Distance between ground station and scattering aircraft located at q^{th} prolate spheroid

$d_{\mathrm{S_q A_0}}$ Distance between scattering aircraft (S_q) located at q^{th} prolate spheroid

to aircraft A_0

$d_{\mathrm{GS_q A_0}}$ Distance between ground station to aircraft A_0 via scattering aircraft S_q

c Speed of light

a_{pq} Length of semi-minor axis of qth prolate spheroid

c_{pq} Length of semi-major axis of qth prolate spheroid

Chapter 1

Introduction

1.1   Overview

The advancements in wireless mobile technology have significantly influenced the daily life of every human being through innovative ways of communication, despite one's physical location around the globe. The availability of data services on mobile devices has further enhanced the communication activity in a more suitable and inexpensive way by their integration with real-time applications. These applications facilitated people to stay connected to the world every where and at any time. Due to the growing potential of data-hungry real-time applications, the demand of high data-rate internet access is expected to grow more dynamically in coming decades. This increase in demand is basically for the availability of uninterrupted wireless connectivity with high mobility and guaranteed performance. Rise in demand in recent years was not only seen from the mobile users on the ground but was also observed in the case of the passengers traveling in aircrafts around the globe. To address the demand of in-flight internet, satellite communication system is still one of the major global solutions for the provision of data services to flying aircrafts; however, it is not the best solution for real-time communication services due to its longer end-to-end delays. Therefore, in recent years, the exploration of

new ways to provide high-speed seamless internet connectivity to aircraft passengers has gained the attention of the researchers and development organizations. Air-to-Ground (A2G) and Ground-to-Air (G2A) communication systems are the alternate feasible ways other than the satellite communication systems that can provide high-speed data services with less route delays for data-hungry real-time applications [1]. These links are also a prime requirement of Unmanned Aerial Vehicles (UAVs) to control their operations through ground terminals. The demand of UAV is anticipated to grow exponentially in future due to its immense use in various applications like internet provision, military operations, cargo delivery, weather monitoring, precision farming, firefighting, law enforcement, customs and border patrolling [1–3].

1.2   G2A/A2G Communication

In the last decade, wireless communication has experienced tremendous growth in terms of wireless technology and smart mobile devices efficiency. As a result, an advanced era of airborne internet started that gained the attention of researchers and development organizations who established state-of-the-art methods of providing communication facility to onboard passengers. The earliest communication with airborne vehicles was solemnly for the sake of aeronautical communication between the pilot and the ground crew. The advent of efficient smart mobile devices removed the communication barriers among the people living much far away from each other on the earth. The high usage of internet and global social connectivity of the people demanded the provision of seamless internet connectivity during the flights. To achieve this purpose, satellite-to-aircraft was the first solution of providing internet; however, the longer end-to-end delay, cost inefficiency and high-data rate requirements for data-hungry applications made this option expensive and infeasible. Therefore, the researchers and organizations provided ground-to-air (G2A) and air-to-ground (A2G) solutions that can provide cost-effective coverage with less end-to-end delay and high-data rate as compared to the satellite-based communication systems.

A2G/G2A communication systems has gained attention due to potential of assisting in various field applications that specifically require two-way telecommunications i.e. emergency response, remote sensing, pollution monitoring, earth observation, military applications, meteorological measurements, navigation applications, land and agriculture management. A2G/G2A based communication systems are the possible alternatives of satellite-based communication systems due to their rapid deployment and cost effectiveness. These systems may serve as airborne base stations to provide internet and terrestrial services to land mobile users when the existing terrestrial networks are overloaded due to a large concentration of users in a specific area. These systems may also serve as an efficient and cost-effective relays between satellites and the ground stations. These can cover a large area of earth and are immune to the natural disasters like floods and earthquakes when the infrastructure of terrestrial network get damaged. A2G based communication system consists of high-altitude platform (HAP) flying at an altitude ranging between 17 to 30 km in the stratosphere and can stay in the sky for a long period. Whereas, G2A based communication system radiates upward directed radio beam to provide communication services to flying aircrafts. In literature, various projects address the use of manned and unmanned aerial vehicles. An appropriate design of A2A/G2A communication system necessitates a detailed understanding of multipath propagation geometry between the ground segments and HAPs.

1.3 G2A Communication Scenarios

The Radio spectrum for communication is a scarce resource that requires optimal utilization through efficient spread spectrum techniques. Multiuser spread spectrum systems usually employ a predefined protocol to accommodate multiple users while sharing the same single-access medium. This single-access medium is broken into various channels to provide the same access opportunities for all users in the system. The primary success of a multiuser communication system is that the multiple signals share the same communication resource while maintaining a

manageable interference to other users. Code Division Multiple Access (CDMA) and Space Division Multiple Access (SDMA) are the two well established multiple access schemes to efficiently utilize the communication medium.

G2A Communication Link
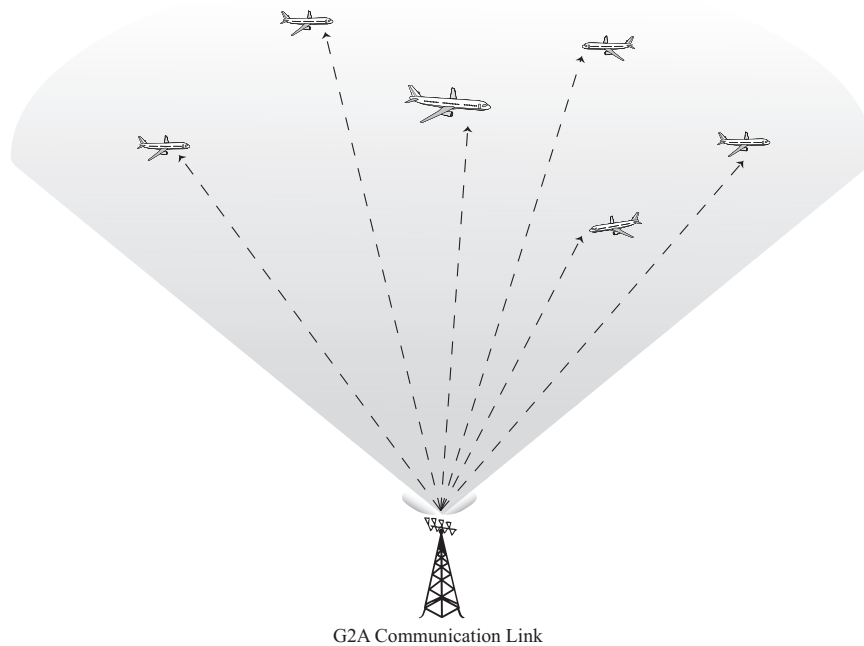
FIGURE 1.1: Illustration of CDMA-based wide-beam communication link scenario.

1.3.1 CDMA

CDMA spread spectrum communication technique was initially developed for military services; however, since 1990, it has been intensively utilized for commercial systems. In CDMA, various users can send information simultaneously over a single communication channel by using their unique orthogonal signature waveforms separately assigned to each active user of the system. This system allocates all resources to every active user instead of allocating different frequencies or time resources to each active user. In this system, a user transmit its narrow band message after multiplying to the spreading sequence having considerable large bandwidth. To detect the message signal addressed to the user, the receiver correlates the received message with the assigned unique orthogonal sequence of the user. Each

active user of the CDMA system independently operates with no knowledge of other users and the signals from other users appears as noise after decorrelation. In CDMA-based G2A communication system, a wide-beam is pointed towards the sky to provide communication services to flying aircrafts. The same methodology of CDMA-based land mobile communication system is used to accommodate multiple aircrafts in the system. The aircrafts can simultaneously transmit/receiver their information symbols by using their unique spreading signatures. An illustrative view of CDMA-based wide-beam communication link scenario is presented in Fig. 1.1.
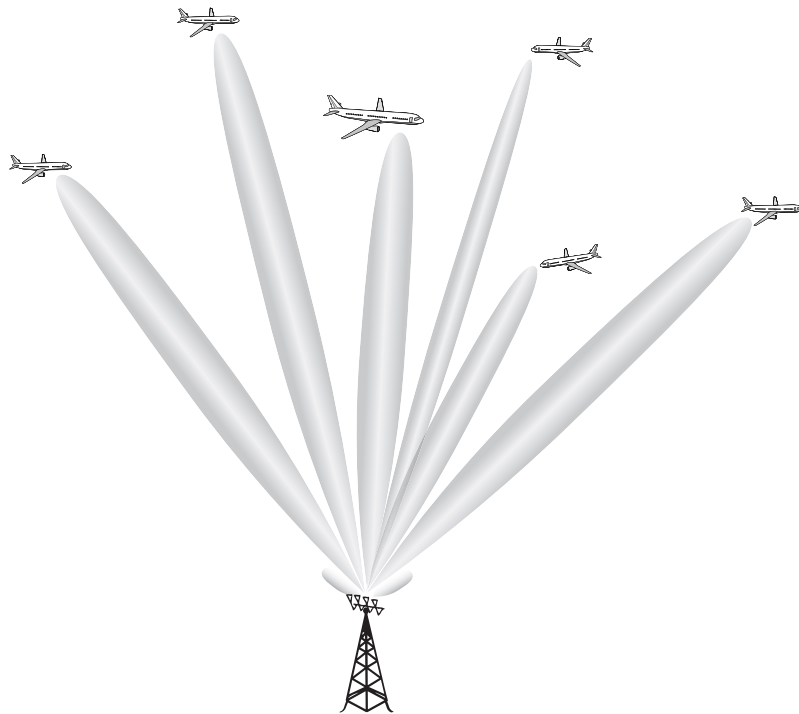
FIGURE 1.2: Illustration of SDMA-based narrow-beam G2A communication link scenario.

1.3.2 SDMA

Spatial Division Multiple Access (SDMA) is the one widely adopted technique in wireless technology that spatially separates airspace for each active user and provides communication services over the same set of frequencies. Its advanced signal processing capability locates each active user in space and radiates separate

directed radio beams towards them instead of transmitting a signal to an entire coverage area. This is the most sophisticated utilization of geographical region that increases capacity, efficiency and coverage range of the communication system with less radiated energy compared to wide-beam/single-beam communication services. This can be integrated with any conventional multiple access technique such as TDMA (Time Division Multiple Access), CDMA (Code Division Multiple Access) and FDMA (Frequency Division Multiple Access). The same working methodology can be employed in SDMA-based G2A communication systems that may accommodate various aircrafts by assigning separate spatial signatures on the basis of their physical locations in geographical airspace in view of the ground station. This permits frequency reuse within the same ground station, provides a high signal-to-interference ratio and utilizes low power levels. The smart antenna capabilities generate nulls to the interfering signals coming from proximate scattering objects that may cause interference to the user of interest. The scenario of SDMA-basad narrow-beams communication links is explained in Fig. 1.2.

1.4 RADAR and Radar Cross Section

RADAR (Radio Detection and Ranging) system is an electromagnetic (EM) system to detect the presence of reflecting objects/target such as air-vehicles, ground-vehicles, people and natural environment. This operates by emitting EM radio waves into airspace and receiving the reflected echo signals from an object/target. The received echo signals not only explore the existence of an object/target but also determine target's location by comparing the received and the transmitted radio signals. The radar system has ability to perform its function over short and long ranges and can operate in snow, rain, fog, haze and darkness. The ability of estimating distances of objects/targets in all weather is the one important aspect of RADARs. The principle of radar is explained in Fig. 1.3 with its basic components. A radar transmitting antenna illuminates a target/object by radiating EM signal energy into airspace and receives a portion of reflected EM signal, as a result of reflection from the object/target, at its highly sensitive receiver.
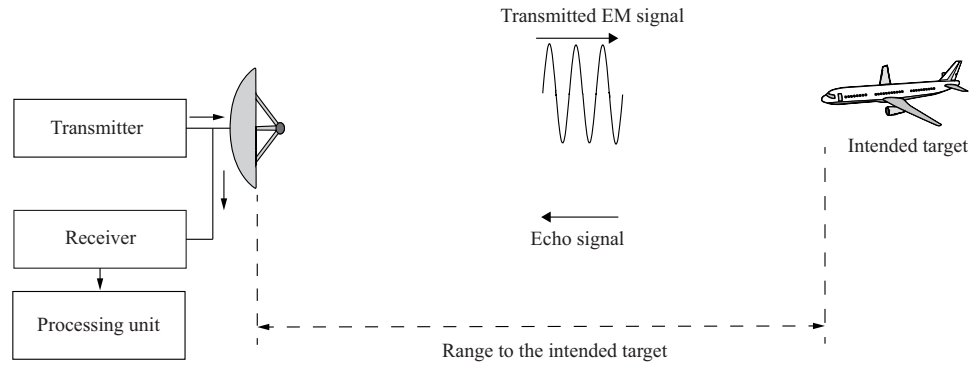
FIGURE 1.3: Basic components of RADAR and its working principle.

The received energy is then delivered to the processing unit of radar system that reveals the presence of the target and determine its geographical location. The range of an object is determined by the measuring the time taken by the transmitted radio wave traveling from RADAR to the targeted object and then back to the RADAR receiver antenna. These can be used detect aircraft, spacecraft, missiles, ships, vehicles, weather formation and terrain. Moreover, the modern use of RADAR covers highly diverse areas, like terrestrial traffic control, flight control systems, antimissile systems, aircraft anti-collision system, space surveillance, ground penetrating radars, geological observations and meteorological precipitation monitoring. Electromagnetic waves when incident on a target, are normally diffract or scatter in all directions. The scattered waves can be separated into two polarization levels; horizontal polarization and vertical polarization. The intensity of scattered or reflected EM waves received at the RADAR receiver antenna that have the same polarization defines the target RADAR Cross Section (RCS). It is a measure that describes the visibility of a target to the RADAR. The RCS is termed as monostatic RCS if the transmitter and receiver are identical; however, it is interpreted as Bistatic RCS when their locations are non-identical. The geometry of both the scenarios is shown in the Fig. 1.4. In terms of scattering methodology, both the terms are identical except the inclusion of bistatic angle in BRCS that makes it different and complex than monostatic RCS.

Assume the power density of an EM wave incident on a targeting object located at range R away from the radar is P_{Di}. The amount of reflected power from the

(a) Monostatic Radar
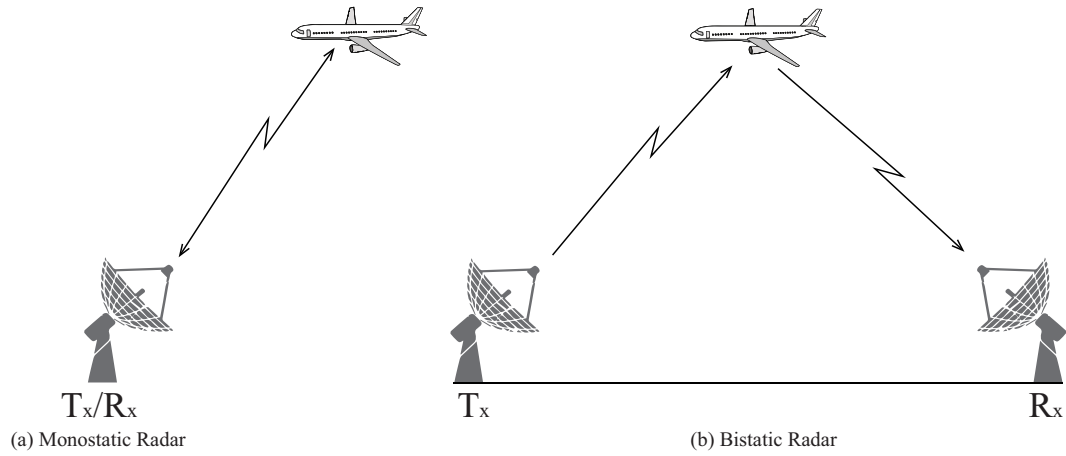
(b) Bistatic Radar

FIGURE 1.4: Geometric comparison between monostatic and bistatic radar.

target can be defined as [4]

$$P_{\text{ref}} = \sigma P_{Di} \tag{1.1}$$

where, σ denotes the target cross section. Whereas, the power density P_{Dr} can be defined as

$$P_{Dr} = \frac{P_{\text{ref}}}{4\pi \text{R}^2} \tag{1.2}$$

solving the above two equations yields

$$\sigma = 4\pi R^2 \frac{P_{Dr}}{P_{Di}} \tag{1.3}$$

1.5 Reflection Coefficient

Reflection is the one important phenomenon of electromagnetic wave theory that occurs when a wave impinges on a reflective surface having a large dimension compared to its wavelength. In practical situations, radio waves are generally reflected by the scattering surfaces such as ground and buildings or any other object between the transmitter and the receiver. A radio wave when reflected from the reflective surface, the intensity of the reflected wave becomes less in comparison to the incident wave. The ratio of the reflected and the incident wave intensity is known as the reflection coefficient of the surface. Fresnel equations are generally used to describe this relation, that depends upon polarization, frequency,

permittivity and conductivity of the reflective surface, and the incident angle of the wave. Moreover, the reflection coefficient of a surface can also be viewed as the transfer function of the reflection process. Since, both amplitude and phase changes are possible at the point of reflection, the coefficient is in general complex. Considering, complex reflection coefficient Γ, the relation among reflected electric field E_r and incident electric field E_i intensities can be described as follows [5–7].

$$E_r = \Gamma E_i \tag{1.4}$$

1.6 G2A Communication Channel

Like traditional land mobile radio channels, propagation of signals in A2G or G2A communication channels is also governed by the same four propagation mechanisms, i.e., reflection, diffraction, scattering, and free-space propagation. The A2G communication channel is generally presumed identical to G2A communication channel; however, radio signal propagation characteristics in these channels make them different from each other. Such differences are essential in modeling large-scale and small-scale fading of A2G or G2A channel environments. In A2G communication, high-altitude platforms (HAPs) are aloft in the air to provide downward communication or internet coverage to ground users. In this scenario, both the transmitter and the receiver are in motion. Whereas, in G2A communication systems, a ground station (GS) fixed at a specific position radiates radio signals to communicate with air vehicles in the sky. Since the primary purpose of a G2A communication system is to provide communication or internet facility to flying aircraft/air-vehicle; therefore, upward directed directional antennas are generally used to serve this purpose. Directional antennas increase coverage and signal strength, while limits the expected interfering signals coming from scattering objects around the GS.
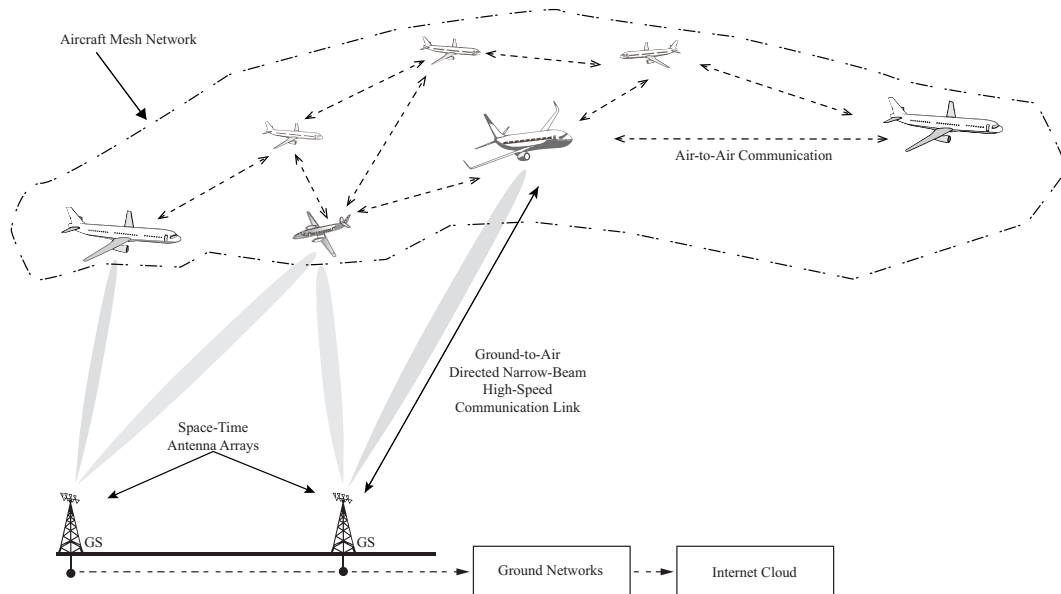
FIGURE 1.5: Provision of internet through ground station.

1.7 Research Objectives

The paramount objective of this work is to analyze G2A propagation environment, to highlight its limiting features that undermine the performance of the communication link and to present its appropriate model. G2A communication environment is generally presumed to be a line-of-sight (LoS) communication environment; however, in reality, the intended aircraft may receive reflected/scattered interfering signals coming from proximate scattering aircraft. Those proximate aircraft may act as scatterers in G2A communication link and may result in degrading communication performance of the link. This dissertation therefore aims at modeling the existence of multipath environment due to the presence of scattering aircraft around the intended aircraft.

1.8 Applications of the Proposed Research

The proposed work may benefit in various modern applications that can be grouped into two main categories, i.e. Airborne internet access and Unmanned aerial vehicles.

1.8.1 Airborne Internet Access

Provision of communication and internet services to onboard passengers for real-time voice or data services through ground stations is the one significant application of the modern-day. Present applications usually require high-speed internet access with a less end-to-end delay to efficiently perform their operations. Therefore, internet provision with slow data-rate cannot fulfill modern-day requirements of onboard passengers. G2A communication links are the one prominent option of providing high-speed internet with less end-to-end route delay. For global coverage, G2A ground station can be installed on various busy air routes on the ground and remote oceanic regions. This work may help to analyze G2A channel properties and to perceive effective data-rates of the communication links.Airborne-Internet

1.8.2 Unmanned Aerial Vehicles (UAVs)

In recent years, Unmanned Aerial Vehicles (UAVs) has gained much importance due to their extensive use in various commercial and defense-related applications. These vehicles are being used in multiple fields, among them, some are border surveillance, rescue missions, medical assistance, delivery of goods, cinematography, scientific researches, surveying, pollution monitoring, disaster monitoring and
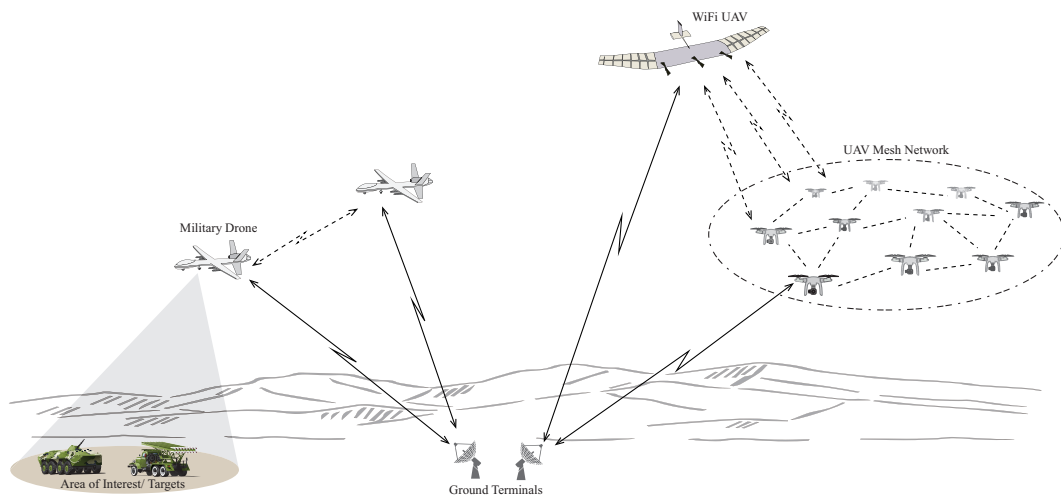
FIGURE 1.6: UAVs application scenarios.

to combat criminal or terrorist activities. The operability and high performance of UAVs highly depend on seamless wireless connectivity through air-to-ground, ground-to-air or air-to-air links. Aerial networks significantly differ from traditional wireless networks because these networks are not just communication networks but also control networks to operate functionality of UAVs from ground stations. Thus, application specific requirements pose challenges over communication range, delay, control, data services, and energy limitations. For instance, aerial filming of a particular event may require high data-rate downlink transferring to the client on the ground, whereas, in applications where UAVs act as data mules, it possibly requires high-data rate at the uplink [8]. In situations when UAVs are equipped to combats with terrorists/criminals, video surveillance and control traffic with high data-rate are needed to mark and hit before losing the target. Hence, it is notable that the performance and operations of UAVs are highly dependent on high-speed data services. Furthermore, UAVs may act as a flying wireless network in which each UAV relays information meant for others and transmit/receive information intended for it. In this situation, at least one UAV needs to be directly connected with the ground station with a high-speed data link. SDMA-based narrow-beam communication links may serve these applications quite efficiently by providing a high-speed communication link with increased range and less end-to-end delay.

1.9 Thesis Organization

Rest of the work presented in this dissertation is organized as follows.
In **Chapter** 2, a detailed review of the existing literature is presented with a critical analysis and discussion to create a gap of this study for problem formulation. The main contributions of this research study is also provided in this chapter. In **Chapter** 3, reflection phenomenon of a transmitted signal in G2A communication link is profoundly analyzed. This chapter explains methodology to develop a relationship between RADAR Cross Section (RCS) and Spatial Reflection Coefficient (SRC). For correct evaluation of incident angles of impinging

Electromagnetic (EM) waves on aircraft's body, a geometric model is proposed and discussed in this chapter for two scenarios, satellite-to-aircraft and ground-to-aircraft. Moreover, details of simulation tool POFACET and the description of aircraft's facet-based model is also provided in this chapter. In **Chapter** 4, existence of multipath environment in G2A communication system due to the presence of proximate scattering aircraft around the intended aircraft is explored and geometrically-based physical G2A channel model is proposed for two propagation scenarios: wide-beam communication link and narrow-beam communication link. In **Chapter** 5, characterization of G2A channel and multi-aircraft interference modeling in presence of scattering aircrafts in the vicinity of intended aircraft is performed. Moreover, this chapter provides expression for total signal power received at the intended aircraft coming from the ground station. Visual interpretation of interference caused in wide-beam and narrow-beam G2A communication link scenarios is also discussed in this chapter. Finally, **Chapter** 6 concludes the thesis with future directives.

Chapter 2

Literature Survey and Problem Formulation

This chapter provides a detailed literature survey to create a gap of this research work. Section 2.1, gives intensive review of the published articles with critical comments and discussion. Through critical analysis of the literature, gap of this study is created which is presented in Section 2.2. In Section 2.3, problem formulation of this research thesis is explained. Finally, Section 2.5 highlights the main contributions of this dissertation.

2.1   Literature Survey

The anticipated growth in aerospace vehicles around the globe has incited many researchers and organizations to identify unexplored challenges that must be resolved to fulfill the needs of safe integration of UASs into global airspace. Despite the tremendous growth in aerospace vehicles, a very limited number of articles have been published so far that propose channel characterization for aircraft-to-ground (A2G) and ground-to-aircraft (G2A) communication links as compared to terrestrial channels. Most of these research articles provide channel models between

14

aircraft and satellite [9–11] which are mostly related to aeronautical communications. Moreover, a considerable effort has also been devoted in the literature to characterize the propagation behavior of radio signals in A2G communication environments [1, 2, 10–34]. In every realistic radio communication environment, multipath is one of the major causes of fading that limits the achievable capacity. In A2G/G2A radio propagation environments, the scatterers around ground station (GS) or aircraft station (AS) also create multipath propagation environment and produce small-scale fading in the received signal [2, 12, 14, 21]. Moreover, the high-mobility of aircrafts in multipath environments spreads the frequency spectrum which further creates time variations in channel characteristics. Hence, it is essential to analyze the characteristics of fading channel that limits the achievable capacity of A2G/G2A radio links and in turn degrades their performance.

The elementary work of characterizing multipath propagation phenomenon between aircraft and satellite/ground terminals was carried to improve the communication performance of the aeronautical communication systems. Various research studies have been performed in this regard; however, most of the published research articles in this domain focused only on characterizing communication link between a satellite and an aircraft. For more details about aeronautical channel modeling one can consult to [9–11, 24–27, 31, 35, 36] and the references therein. Various measurement-based studies have also been performed in [14, 21, 24, 25, 27, 31–34, 37, 38] to analyze the limiting behavior of A2G channel; however, these studies are limited to low-altitude airborne communication and are site specific. In [24], the authors presented a measurement-based multipath channel model for narrow band aeronautical telemetry communication links. Almost the same work was done in [14, 25] while considering a wideband channel model for aeronautical telemetry, where the authors conducted a measurement campaign to observe the power delay profile of the channel, which was further used to evaluate the delay spread of the channel and multipath losses. In [15], spatial and temporal characteristics of A2G channel for V/UHF band were investigated, where (Add some sentences here). In [16], the authors modeled A2G propagation environment by using a tapped-delay filter and analyzed communication performance of A2G

channel in terms of Bit-Error-Rate (BER). A2G communication system employing multiple antenna arrays was investigated in [17], where both statistical and geometrical models were used to describe the time-space dispersion of the channel. It was concluded that the topography of earth degrades the performance of multi-antenna systems. In [29, 39–41], the capacity and performance of A2G communication links employing multi-input-multi-output (MIMO) antennas was investigated and their use in increasing the channel capacity of A2G communication environment was suggested. In A2G communication, signals coming from the aircraft develop a unique multipath environment after their reflections from the topography of the earth. To observe the impact of earth's topography in generating a multipath scattering environment, considerable measurement-based research efforts have been made in [19, 22, 28, 32–36, 42, 43] characterizing multipath environment over land, forest, and mountainous and oceanic regions. For more measurement-based studies of A2G wireless link in different propagation scenarios using high-altitude platforms (e.g. Air balloon, Quad-copter, or Aircraft), one can consult to [14, 21, 29, 41, 44–61]. In some of the above-cited measurement campaigns were conducted over C and L bands [32, 34, 42, 43, 47–50, 62], while the rest of the cited measurement studies were performed at different frequencies ranging from 0.9 GHz to 18 GHz. In wireless communication, the radio propagation environment poses severe challenges for a transmitted signal and attenuates its power due to several environmental-impediments. The amount of the attenuated power of the received signal in comparison to the transmitted signal is termed as path loss. Measurement-based path-loss models can be used to predict an appropriate distance or range of AS to remain in contact with the GS. In the above-cited measurement campaigns, the authors in [21, 32, 42, 43, 46–51, 62] observed the behavior of signal propagation path-losses and developed path-loss models for different A2G communication environments. Time dispersive nature of the propagation environment is usually observed through root-mean-square (RMS) delay spread, which provides the extent in which a transmitted signal spreads over time after reception. Characterization of multipath nature of A2G communication environments was made in [14, 32, 41–43, 46–51, 62], where the authors used the

power delay profiles (PDPs) of the transmitted signal to evaluate the root-mean-square (RMS) delay spread of the channel. From the results, it was observed that RMS delay spread in urban or suburban A2G channel environment is larger than the RMS delay spread observed in open space, mountainous, forest and over water or sea [42, 43, 48]. Although, measurement-based studies provide accurate knowledge of a specific A2G communication environment with substantial use of resources; however, the results obtained through measurement campaigns cannot be generalized for all environments. Studies of the above mentioned articles show that the terrain topography severely affects the profile of doppler-delay spread spectrum and influences uniquely the A2G channel characteristics on the basis of terrain topography. Therefore, an accurate modeling of A2G channel necessitates the consideration of the infrastructure around ground station (GS) that acts as the cluster of scatterering object.

In time-varying propagation environments, the Doppler spread occurs due to the motion of the transmitter, the receiver or of the scattering objects present in between the transmitter and the receiver. In A2G/G2A communication environments, the Doppler shift solemnly depends upon the speed and altitude of the aircrafts. Usually, high Doppler shifts are experienced when the aircraft is close to the GS; however, the rate of change in Doppler shifts is significantly reduced when the aircraft is at high altitude and far away from the GS. This is due to the fact that at higher altitudes the angular spread decreases, while it increases at low altitudes [2]. Doppler shift generates offset in carrier frequency and degrade the performance of the communication link. Various research studies have been published in the literature [2, 19, 27, 41, 45, 46, 50, 63–68] to model and characterize the Doppler spread in A2G communication environments. In [2], the characterization of the Doppler spectrum and second order fading statistics for A2G communication environments were presented by considering uniformly distributed scatterers around GS. Moreover, the characteristics of Doppler shift and angular spread were also analyzed by considering the mobility of aircraft, the altitude of aircraft and the height of ground terminal. In [27, 63], simulations were performed to observe the Doppler effects at different phases of aircraft flight at

airport. In [19], the authors discussed a three-dimensional A2G doppler spread spectrum in rich scattering environment. Doppler spread in multipath environment in orthogonal frequency division multiplexing (OFDM) was discussed in [64–66]. For more details about modeling and characterization of Doppler spectrum in A2G communication environments, one can consult to [41, 45, 46, 50, 67–69], and the references therein.

To analyze the characteristics of a propagation environment, a model depicting an explicit representation of some part of reality is usually developed to perceive the restrictions of the environment and to exploit the necessary countermeasures for the best utilization of the channel. Geometrical channel modeling is the well-known channel modeling technique that describes the spatial distribution of the received multipath signals by assuming randomly distributed scatterers within a specified geometrical shape in which two communicating units may reside. For the exploitation of the spatial nature of communication environment in designing, analysis and implementation of wireless systems, various research studies have been published in the literature covering different applications with different geometric channel models. For more details about geometrically-based stochastic channel models, one can consult to [2, 20, 70–80] and the references therein. The initial work for the representation of air-to-ground (A2G) channels through geometrical channel modeling was proposed in [13], where the authors presented a three-dimensional ellipsoidal geometry based A2G geometric channel model to analyze the temporal and spatial characteristics of A2G communication environment. This work was further extended in [2, 20, 70] by providing an analysis of the multipath shape factors in A2G communication environment. Although, geometric channel models help in analyzing a propagation environment; however, the use of a specific distribution delineating geographical/scattering regions is unrealistic.

RADAR Cross-Section (RCS) is one of the important parameters of RADAR systems that reveal the presence of intended targets in their range of coverage. Quantitatively, it is a fictitious surface area that gives a measure to observe the intensity of the received EM wave reflected from a target object in order to exploit its visibility. In the literature various electromagnetic techniques have been presented

to predict RCS of an object that can be classified into two large families: rigorous techniques and asymptotic techniques. The rigorous techniques, such as the method of moments (MoM) [81], the finite difference time domain (FDTD) [82], finite element method (FEM) [83], Transmission Line Matrix (TLM) [84], fast multipole methods (FMM) and multilevel fast multiple method (MLFMM) [85] work on the basis of discretization of the geometry of an object and require high computational resources. On the other hand, asymptotic techniques, such as Physical Optics (PO) [86], Geometric Optics (GO) [87], Physical Theory of Diffraction (PTD) [88] and Geometrical Theory of Diffraction (GTD) [89] increase the accuracy of the result with an increase in frequency while keeping the computational cost constant. Hence, these approaches are more suitable to analyze electrically large bodies such as aircrafts or ships. In [90], the authors compared and verified the results of PO with the measurements taken in an anechoic chamber. The results show a good suitability between the measurements and numerical resultsof PO. In [91], the authors obtained statistical parameters of aircraft's RCS measurements and deduced strong dependency of statistical parameters on radar operating frequency, the geometry of aircraft and aspect angles. Moreover, it was concluded that the average value of RCS highly influence the detection probability of a target as compared to the normalized value of RCS. In [92], the authors monitored RCS of commercial aircrafts over different flying routes and inspected the effect of RCS fluctuations due to the change in aspect angles and their dependence in aircraft classification. In this study, the wire model of Boeing 747-200 is developed to calculate RCS with the help of Numerical Electromagnetic Code (NEC). From the results, it was concluded that the change in aspect angles strongly affect RCS measurements and in result provides fluctuations in RCS measurements. In [93], the authors presented an implementation procedure of measuring RCS of aircrafts and highlighted some important tradeoffs between computational cost and the accuracy in modeling and simulation of RCS related applications. In this article, the authors compared the accuracy of various interpolation techniques in generating continuous samples of RCS and recommended spline interpolation method with

less interpolation error. In order to increase the computational efficiency of monostatic RCS, various interpolation techniques have also been proposed in the literature [94–98] to reduce the time-memory requirement of RCS calculations. In [99], the authors highlighted interdependence between RCS and spatial reflection coefficient (SRC) and formulated a relationship between them. This relationship was supposed to be useful in using both terms interchangeably. In order to facilitate RCS-based analyses, a number of open-access RCS simulation packages have been introduced in the literature, such as FDTD-RCS [100] code, MoM-based NEC2 [101] code and PO-based POFACET [102, 103] code. The FDTD-based RCS package works by discretizing the targeting object into a number of Yee cells; NEC2 utilizes wire-grid model; while POFACET utilizes facet-based triangulation information of the intended object. Among these simulation packages, POFACET estimates are found more accurate in specular direction providing best results for electrically large bodies [104]. In this research, POFACET based RCS estimates are utilized for G2A communication channel modeling.

A radio propagation environment is naturally susceptible to various channel impediments that may change over time in some unpredictable ways due to the movement of transmitter, receiver or the environment between them. Path loss (PL) gives an insight of communication link and provides a measure to represent dissipated amount of power radiated by a transmitter on its way to the receiver. In this regard, various research studies have been proposed in the literature considering aeronautical, G2A or A2G communication environments. In recent studies, the authors in [32, 47], conducted measurement campaigns at 900 MHz and 5 GHz frequency bands with drones flying at an altitude ranging between 500 m to 2 km. However, in this study, height dependency of UAVs was not assessed which is much likely to be used by commercial drones in near future. In [105], the authors performed measurements with a stationary balloon at 1900m altitude and presented a modified two-ray model that shows variations in path loss exponent. To highlight the dependency of path loss exponent on UAV altitude, the authors in [106] observed measurements at 800 MHz and concluded with a discussion that PL exponent decreases with an increase in the UAV altitude. In [107], the authors

comprehensively analyzed the channel measurements of air vehicles and provided the design guidelines to establish link budget of the UAV communication, taking account of propagation losses, shadowing and signal fading. In [108], the authors investigated the impact of an interfering node in UAVs network considering LoS and NLoS communication links. In presence of interfering node, closed-form expression of outage probability is derived and optimal heights of UAVs are determined. Moreover, it was concluded that NLoS environments could be better than LoS environments when the average received power of the interference is much higher than that of the main signal link. For more details and discussion, the readers may consult to [21, 42, 43, 47, 58, 109, 110] for PL estimates using log-distance models, [53, 111] for path loss modeling considering shadowing for NLoS paths, [30, 32, 48, 62] for two-ray path loss models and the references therein. Although, various research studies contribute to PL modeling for A2G and aeronautical communication links; however, none of the existing research studies specifically reported G2A path loss modeling. G2A and A2G communication scenarios posses different signal propagation environments and thus can not be considered the same.

It is well evident from the literature that a transmitted radio signal when received at the receiver carries not only the direct line of sight component but a series of delayed replicas of the same transmitted signal [112]. The delayed copies are in fact the result of reflection, diffraction, refraction or scattering from the surrounding objects located in-between the transmitter and the receiver end. The same methodology also applies to the aeronautical communication, where the flying aircrafts act as scatterers and re-radiate interfering signals that may degrade the communication performance of the desired link. The concept of reflection or scattering of radio signals due to the presence of aircrafts in the propagation environment can be legitimized by analyzing the work presented in [99, 113, 114]. In [113], the authors quantitatively measured the interference to an ILS-localizer due to reflection/scattering of radio signals from large-size aircrafts like Airbus® and Boeing® aircrafts while taxing on airport. In this study, bistatic RCS results are used to assess the disturbing influence of reflections from the aircrafts.

From the results, it was observed that both aircrafts under study provided significant interference to ILS-localizer; however, the aircraft A380 significantly provided large disturbing influence as compared to the aircraft B747. In [115], the authors used computational models of three commercial aircrafts, the Boeing 747-200®, the Airbus A320® and the Boeing 737-200®, in MoM-based NEC2 simulation package. From the results, it was observed that the flight routes influence RCS signatures and thus, accurate knowledge of the aircraft's flight route is needed for aircraft identification. Airplane flutter phenomena usually observed on the ground over terrestrial TV sets is also caused by the reflected or scattered multipath waves from the airplanes. In [114], the authors proposed a model of fluttering to produce signal fluctuations as a result of multipath scattering from airplane due to the airplane flutter phenomena. Simulations results are validated with the measurements at 60.75 MHz and 208.75 MHz. For more details and understanding, the reader may consult to [116–119] and the references therein. The degradation of the received signal at the aircraft from the neighboring aircrafts is a similar phenomenon which will be discussed in detail in the proposed research.

In recent years, the demand of in-flight internet connectivity (IFIC) for onboard passengers has increased tremendously and is expected to boost up more dynamically in the coming years. To address this demand of acquiring IFIC, various airlines companies have either installed or planned to install the IFIC system in the coming years. According to a report published in 2018, currently 82 airlines offer in-flight internet to its passengers worldwide with 17% increase since the start of 2017 [120]. Moreover, in coming years, IFIC is supposed to become an important factor for airlines to gain the interest of passengers and could become a vital resource of revenue generation. The IFIC market is envisioned to grow from \$5.03B in 2018 to \$7.65B by 2023, with a compound annual growth rate of 8.72% from 2018 to 2023 [121]. A survey of Honeywell [122] reports that the availability of in-flight internet highly influences a passengers' selection of flights and it was observed that around 66% of the passengers selected flights based on IFIC availability. According to a recent Inmarsat survey [123], it was observed that IFIC plays a major role in changing customer's loyalty and satisfaction with airlines.

The analysis reveals that 81% of the passengers aspired to use Wi-Fi if available, 74% of the business travelers felt it crucial, and 67% wanted to rebook their flight with an airline having IFIC. Therefore, the commercial aviation industry should grab attention of the passengers by providing them freedom to stay connected to the world whenever and wherever they want.

The high demand of in-flight internet connectivity (IFIC) directed the interest of academia and development organizations to find alternate ways of providing seamless in-flight internet connectivity to onboard passengers at favorable cost. In recent developments, IFIC can be provided through cellular-based direct air-to-ground communication (DA2GC) or satellite-based communication (SC). Provision of in-flight internet through satellite-based communication link is the one globally accepted solution for transcontinental flights; however, due to long transmission latency and cost-inefficiency, it cannot be assumed an optimal solution for data-rate hungry real-time applications. The transcontinental commercial flights carry significant share of the airline market because among 34.8 million worldwide commercial flights, 40% flights were reported to be international in 2015 [124]. Currently, SC is the only global solution that provide IFIC to transcontinental flights. On the other hand, DA2GC system exploits its ground stations equipped with upward-directed radio transmitters for providing IFIC using cellular communications. The DA2GC system connects with flying aircrafts via a direct link and provides IFIC in the same way as a connection for a regular terrestrial mobile user. Ground stations (GSs) are similar to cellular towers; however, these are placed far away from each other covering an approximate radius of 50 to 150km [125]. The DA2GC system has an edge of easy and low-cost installation of GSs; however, it only provides coverage over the ground. Therefore, provision of worldwide IFIC necessitates the use of satellites, especially over the sea where DA2GC cannot operate. A hybrid system with combination of DA2GC and SC can also be used for global coverage and efficiency.

In 2008, the GoGo Inc. built the cellular based air-to-ground network and inaugurated its functioning on first commercial aircrafts. The IFIC in U.S and Canada is provided through a large number of ground stations (around 225) employed with

Ev-DO CDMA 2000 standard operating at 800 MHz frequency. With growing demand of bandwidth, GoGo engineering team upgraded their DA2GC system to second generation system, named as ATG-4, that provides a peak speed of 9.8 Mbps [126]. With the passage of time, the company still suffered with low bandwidth, and hence planned to launch a series of satellites to achieve high data rates, i.e. Ku-Satellite (Max. data rate of 30Mbps) in 2013, 2Ku-Satellite (Max. data rate of 70Mbps) in 2016, HTS-Ku Satellites (Max. data rate of 100 Mbps) and HTS-LEO Satellites (Max. data rate of 200Mbps) expected in 2018 [127]. Further, in 2018, Inmarsat and Deutsche Telekom collectively launched global IFIC with their technology partner Cobham SATCOM and Nokia, named as European Aviation Network (EAN). The EAN is a hybrid IFIC network that covers all the 28 European Union member states with a setup of S-band satellites and 300 LTE-based ground stations providing IFIC up to 75 Mbps/cell. In the network, S-band satellites are operated by Inmarsat and LTE-based ground network is operated by Deutsch Telekom [128, 129].

In [130], authors presented a satellite-based IFIC mechanism for aircraft passengers and cabin crew; however, incorporating satellites in this complex framework made this mechanism inefficient. In order to provide cost effective solution for IFIC, an improved framework utilizing ad-hoc network was proposed in [131]. A multi-hop ad-hoc wireless network design of aircrafts is presented in [132], in which the system utilizes space-time division multiple access scheme to communicate and deliver data to neighboring aircrafts. In this study, a practical air-to-air experiment was conducted to observe the transmission characteristics between aircrafts and the PL characteristics of the propagation channel were derived. For good performance, it was observed that the proposed system required dense network of aircrafts which is seldom a case in a typical coverage region. In [133], the authors introduced a mesh network based model of aircrafts for the delivery of IFIC to aircrafts flying across oceans. In this model, an aircraft flying in the coverage range of coastal ground stations acts as a relay node and delivers data to its neighboring aircrafts of the mesh network. In order to optimize the capacity of A2G communication link, a Geographic Load Sharing Routing (GLSR) was also introduced.

However, it is quite perceptible that a data relaying aircraft (around coastal regions) may become a bottleneck of the network which may deteriorate network performance as a result of network congestion. In [134] as a remedial measure, a link scheduling constraint mechanism was presented to combat congestion in the GLSR. In [1], the authors planned to develop dedicated G2A links by exploiting already laid submarine optical fiber cables to provide IFIC to aircrafts flying over remote oceanic regions through stationed ships connected with submarine optical fiber cables.

In [41], the authors conducted a measurement campaign to examine the suitability of Multi-Input-Multi-Output (MIMO) antennas for A2G communication. It was concluded that the spatial properties of the A2G communication channel support the implementation of MIMO technology in DA2GC system. For more details and discussion about the use of MIMO technology in A2G communication system, the reader may consult to [29, 39, 40] and the references therein. In [14, 21, 24, 25, 27, 31–34, 37, 38], measurement-based studies have been presented to analyze the performance-limiting characteristics of A2G channel; however, these studies are only limited to low-altitude airborne communication and are also site-specific. For more measurement-based studies of A2G wireless link in different propagation scenarios using high-altitude platforms (e.g. Air balloon, Quad-copter, or Aircraft), one may consult to [14, 21, 29, 41, 44–61]. A large number of works characterizing multipath environment over land, forest, mountains and oceans are presented in [19, 22, 28, 32–36, 42, 43], where the impact of earth's topography in generating multipath environment is also observed. The initial work of characterizing temporal and spatial characteristics of A2G communication environment through geometric-based channel modeling was presented in [13], where, the authors assumed a three-dimensional ellipsoid covering all possible scatters around the ground station while keeping communication units at its focal points. This work was later continued in [2, 20, 70], where the authors characterized the Doppler spectrum, level crossing rate, spatial spread and second order statistics of the A2G multipath communication channel. In these articles, the vicinity of ground station is assumed to be surrounded with effective scatterers; whereas, the

vicinity of AS is considered as a scatterers-free region which is an unrealistic assumption. Nevertheless, no concrete channel characterization was done so far for G2A communication link.

2.2   Gap Analysis

Since, G2A communication systems are solemnly designed for dedicated coverage to flying aircrafts; therefore, such systems are generally equipped with directional antennas for directional signal transmission or reception. Directive antenna patterns benefit in increasing range and signal strength while limiting interfering signals coming from the scatterers or the sources not of interest (SNOI). Thus, in such scenarios the scatterers around the GS may not act as scatterer because the directive patterns may provide nulls towards SNOI, when equipped with smart antenna systems. In the literature as discussed earlier, various articles have been published covering A2G/G2A collectively; however, with the best of our knowledge, G2A propagation channel modeling with directive beam patterns is yet to be investigated. Therefore, it is pertinent to examine signal propagation of upward directed G2A communication links in wide-beam and narrow-beam scenarios and to characterize these links in multipath environments.

2.3   Problem Formulation

As discussed above, most of the research literature supposedly model G2A channels interchangeably in the same way as that of land mobile communication links. G2A communication systems are specifically designed for dedicated coverage to flying aircrafts utilizing upward directed radio beams. In such scenario, the infrastructure around GS may not act as scatterers because the directive radio pattern may not incorporate the signals coming through those scattering objects. Hence, it is necessary to examine conscientiously the distinctive characteristics of G2A communication environments with directive radio beam patterns. Moreover, the G2A

communication links are usually thought to be a line of sight (LoS) communication; however, in reality apart from direct waves, the intended aircraft may receive a number of multipaths as a result of reflections from proximate aircrafts. Such phenomenon may induce a multipath fading environment between ground station and the intended aircraft that may decrease communication performance due to constructive or destructive addition of signals. To the best of our knowledge, G2A channel model with directive radio beams has not been introduced yet incorporating the multipath phenomenon of the transmitted signal. Hence, it is essential to develop a G2A channel model that provides a clear insight of the propagation mechanism for the complete performance analysis of the G2A communication link in wide-beam and narrow-beam scenarios.

2.4   Research Methodology

In order to develop G2A multipath channel model for performance analysis, our line of action is three fold. In the first stage, we intend to focus on estimating the aircraft reflecting properties. To achieve this purpose, we introduce a new term named as Spatial Reflection Coefficient (SRC) and establish a concrete relationship of the interdependence between RCS and SRC. The proposed relationship is then used to extract the reflective information of the body of an aircraft on the basis of the observed RCS. A facet-based model of the aircraft A380® and a simulation tool POFACET® is used to obtain bistatic RCS results. At the second stage, we explore the existence of multipaths in G2A communication environment due to the presence of proximate scattering aircrafts around the intended aircraft and develop a multipath channel model for G2A communication links. Utilizing the proposed G2A multipath channel model and the observed reflective properties of the aircraft, the intended research objectives i.e. channel characterization, interference modeling and performance analysis of G2A communication link are achieved at the third stage. Organizing the research presented in the above-mentioned three stages accomplishes the primary concept of this dissertation, i.e., Modeling and Characterization of Ground-to-Air Communication Channel.

2.5 Thesis Contributions

The main contributions of this dissertation are summarized as follows.

1. A concrete relationship is established between Radar Cross-Section (RCS) and spatial reflection coefficient (SRC) for the two proposed scenarios, i.e., Satellite-to-Aircraft and Ground-to-Aircraft. Geometrical models of these two scenarios are presented for the evaluation of correct incident angles of impinging waves on the surface of aircraft and their RCS observations.

2. Existing work on A2G/G2A channel is critically reviewed and properly commented wherever needed.

3. G2A propagation channel is analyzed by differentiating its attributes from those of A2G communication link and the existence of a multipath environment around the intended aircraft is explored.

4. A geometrically-based G2A multipath channel model is proposed by introducing a three dimensional prolate spheroid assuming single-bounce multipath geometry. This model can be modified for any G2A multipath propagation scenario with an appropriate choice of semi major and semi minor axis in accordance with the population of proximate aircrafts around the intended aircraft.

5. Analytical expressions of the signal received at the intended aircraft are formulated for two scenarios; wide-beam communication link and narrow-beam communication link. The model suitably justifies its existence and provides an insight to analyze multipath multiuser G2A communication link scenarios. The model is also equally applicable to analyze the performance of high data-rate communication link to the network of passenger aircrafts, flocks of jet fighters and mesh of UAV drones. Moreover, it can be viewed as an alternative simulations for generating tapped-delays of several propagation scenarios for G2A communication systems.

6. A performance analysis of G2A channel model established in chapter 4 of this thesis is presented. Power delay profiles (PDPs) of G2A communication channel are generated to observe its time-dispersive nature.

7. A closed-form utilizing G2A channel model proposed in chapter 4, and the theory of BRCS, expression for the total power received at the intended aircraft is developed. For numerical computations of BRCS, physical optics (PO) based simulation software POFACET® and a facet-based aircraft A380® model are used.

8. A quasi-realistic G2A propagation environment is formulated in Matlab® for time-dispersive analysis of G2A communication system.

9. Statistics of the developed power delay profiles (PDPs) are evaluated and the expected data rates of the designed scenario are predicted.

10. A visual demonstration of the interference in wide-beam and narrow-beam communication scenarios is presented.

Chapter 3

Reflection Phenomenon in G2A Communication Link

In this chapter, reflection phenomenon of Ground-to-Air (G2A) communication link is analyzed. Section 3.2 presents methodology to develop a relationship between the RADAR Cross Section (RCS) and Spatial Reflection Coefficient (SRC). To evaluate correct incident angles of impinging Electromagnetic (EM) waves on the aircraft's body, the proposed geometry is implemented in Section 3.3 for two scenarios, satellite-to-aircraft and ground-to-aircraft. Section 3.4 gives the details of simulation tool and the description of aircraft's facet-based model. In Section 3.5, simulation results of each incident angle evaluated in Section 3.3 are presented and analyzed in detail. Moreover, the behavior of the relationship between the RCS and SRC is also discussed and analyzed in the Section 3.5.

3.1 Introduction

RADAR (RAdio Detecting And Ranging) is a device that reveals the presence of a target within its range of coverage. The post-processing capability of a RADAR on the received reflected Electromagnetic (EM) waves (echos or radar returns) extracts the information of the target's direction, range, velocity, orientation and

other classifying characteristics. When the radar's transmitted EM waves impinge on target's surface, the reflecting surface of the object radiates energy in all directions. The radiated energy depends upon the target size, physical shape, orientation and reflecting properties of the surface. These all can be put together to specify target's identification parameter known as Radar Cross Section (RCS). Quantitatively, it can be termed as a fictitious surface area which explains the intensity of EM wave reflected back to the radar's receiver antenna. The RCS is a measure of an object's reflecting ability which exploits the visibility of the intended target towards the RADAR. Due to high sensitivity and long range capability in modern RADARs, RCS is considered as one of the most important factors in the performance evaluation of stealth technology and for airborne weapon systems [135, 136]. In the designing of modern fighter aircraft, the performance of stealth technology and the visibility of an aircraft highly depend on the results and measurements of RCS. In order to accurately predict the RCS of a target, it is necessary to analyze the factors that affect its behavior, such as material, incident angle, radar signals wavelength, size of the target, radar operating frequency and target's orientation.

3.2 Relationship of Spatial Reflection Coefficient and RCS

3.2.1 Radar Cross Section

In radar systems, RCS is a measure which defines amount of scattered or reflected energy from the surface of a target towards the receiver antenna. If the locations of both the transmitter and receiver are identical then it is referred as monostatic RCS; however, in the cases when the locations are non-identical it is interpreted as Bistatic RCS (BRCS). Both the terms are identical in scattering methodology except the inclusion of bistatic angle in BRCS which makes it more complex than

monostatic RCS. In terms of complex electric field amplitudes, the RCS (σ_{B}) is defined as follows [137, 138].

$$\sigma_{\mathrm{B}}(\theta_i, \phi_i, \theta, \phi,) = \lim_{R \to \infty} 4\pi R^2 \frac{|E_s(\theta, \phi)|^2}{|E_i(\theta_i, \phi_i)|^2} \qquad (3.1)$$

where, R is the distance between the target and the receiver antenna, and E_s and E_i are the complex amplitudes of the incident and the scattered electric fields respectively. Spherical angle coordinates (θ_i, ϕ_i) and (θ, ϕ) represents incident angles of incoming wave and reflected wave respectively.

3.2.2 Spatial Reflection Coefficient

In electromagnetic wave theory, reflection of a signal is one important phenomenon which occurs when the wave impinges on a reflective surface having a large dimension compared to its wavelength. When a signal reaches the receiver through different propagation paths, such environment is known as multipath environment. The relation between reflected and incident field is usually described by Fresnel equations, which depends upon the permittivity, conductivity of the surface and frequency, incident angle, polarization of the incident wave. Reflection of a radio wave possesses directional property which can be further categorized into two types of reflections, specular reflection and diffuse reflection. In specular reflections, the angle of the reflected path is relatively constant to the angle of the incident wave; however, the diffuse reflections have random phase relative to the angle of the incident wave due to irregularities of the surface. In both the cases, the induced path loss varies on the basis of reflection coefficients which depends upon the dielectric characteristics of the reflective surface. For specular reflections, the path loss is obtained by using Fresnel equations while for diffused/scattered reflections a diffused scattering coefficient is multiplied with specular reflection coefficient [5–7], as explained in chapter 1. The scattered reflections possess a unique spatial properties based upon reflecting angles of the wave from the scattering surface. Based upon the spatial characteristics of the scattered waves, we introduce a new

parameter SRC as an addition to earlier terms elaborating reflection phenomenon of radio waves. SRC is defined as the ratio of the complex electric field intensity of the incident wave to that of the reflected wave electric field intensity in a specific direction [139].

$$\Gamma = \frac{E_s}{E_i} \tag{3.2}$$

This can also be represented as

$$\Gamma = \rho_0 e^{-j\theta} \tag{3.3}$$

where $\rho_0 = |\Gamma|$ represents magnitude of the spatial reflection coefficient and varies between $0 \leq \rho \leq 1$, θ is the phase angle of the reflection which presents phase change of the reflection and varies between $-\pi \leq \theta \leq \pi$. The amplitude value of the reflection coefficient is considered as a composite representation of three independent factors i.e reflection coefficient of smooth surface, roughness coefficient and diffusion factor. These three terms highly influence the scattering properties of a surface and compositely defines the nature of a reflection coefficient [140].

3.2.3 Relationship of Spatial Reflection Coefficient and RCS

Since Radar Cross Section and the spatial reflection coefficient are inter-dependent on each other; therefore, a relationship can be easily made between these two terms. Both RCS and SRC depend on the incidence angle, material properties, signaling frequency, polarization and observation angle. In order to develop a relation between RCS and SRC, we have assumed a typical bistatic geometry of signal reflection from the surface of an aircraft towards another aircraft present in the surroundings. As illustrated in Fig. 3.1, the aircraft (A_1) located at radial distance d_1 from radar transmitting antenna reflects the intercepted signal towards an aircraft (A_2) present at distance d_2. Referring Fig. 3.1 the received power
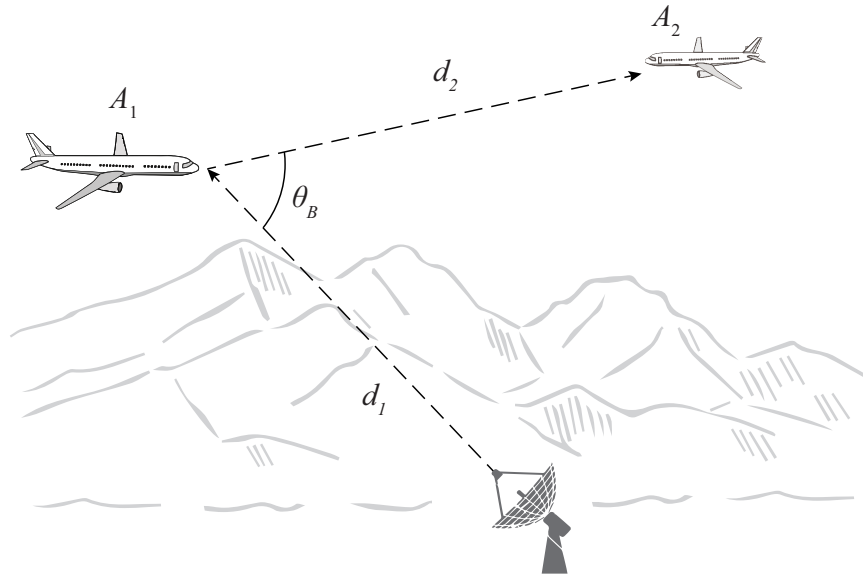
FIGURE 3.1: An illustrative geometry of bistatic signal reflection from the surface of aircraft A_1 on to aircraft A_2.

density at distance d_1 is calculated as

$$P_d = \frac{P_t G_t}{4\pi d_1^2} \tag{3.4}$$

where P_t denotes peak transmitted power and G_t is the gain of the radar transmitting antenna. Considering the methodology of bistatic radar cross section, the total reflected/scattered power received at aircraft (A_2) can be calculated as [4]

$$(P_r)_{\text{ref}} = \frac{P_t G_t A_e \sigma_{\text{B}}(\phi_i, \theta_i, \phi, \theta)}{(4\pi)^2 d_1^2 d_2^2} \tag{3.5}$$

where A_e is the effective aperture of the receiver antenna, σ_B is the bistatic RCS of the aircraft A_1 and d_2 is the distance/range of aircraft A_2 from A_1. In terms of spatial reflection coefficient denoted by Γ, the total reflected/scattered power received at aircraft A_2 can be written as [5, 6].

$$(P_r)_{\text{ref}} = \frac{P_t G_t A_e \Gamma^2(\phi_i, \theta_i, \phi, \theta)}{4\pi(d_1 + d_2)^2} \tag{3.6}$$

Both the expressions presented in Eq. (3.5) and Eq. (3.6) are equivalent in nature and thus can be compared to formulate a relation between the RCS and SRC. Solving both expressions yields a final look of the relationship between the magnitude of spatial reflection coefficient (SRC) and RCS.

$$|\Gamma(\phi_i, \theta_i, \phi, \theta)| = \frac{(d_1 + d_2)}{d_1 d_2} \sqrt{\frac{\sigma_{\mathrm{B}}(\phi_i, \theta_i, \phi, \theta)}{4\pi}} \qquad (3.7)$$

From the expression, it is notable that SRC is directly proportional to the square root of the RCS multiplied by a constant multiple based upon the path lengths of incident and reflected path.

3.3   System Model

3.3.1   Satellite-to-Aircraft Scenario

Communication through satellites is a one effective resource of relaying radio signals between two different points on the earth, whether on the ground, at oceans or in the air. In recent years, satellites have become a vital part in many fields with a variety of applications like navigation, communication, weather and earth observation etc. Moreover, satellite communication plays an important role to fulfill human needs of requiring in-flight TV and internet access during their on-the-air spare time. A signal transmitted through satellite to an aircraft may get reflected/scattered from aircraft's surface with a fractional decrease in incident signal's power depending upon the properties of aircrafts surface. The reflected signal may reach to aircraft's neighboring signal receivers (i.e. satellites, radars or aircrafts), which may degrade their communication performance due to interfering reflected signals. In order to evaluate RCS/SRC of EM signals, a satellite-to-aircraft scenario is assumed. Due to high bandwidth and coverage over a large geographical area, geostationary satellites are considered which usually travel at an altitude of approximately 35800 Km.

In order to obtain incident angle of the striking wave on the aircraft, a geometrical
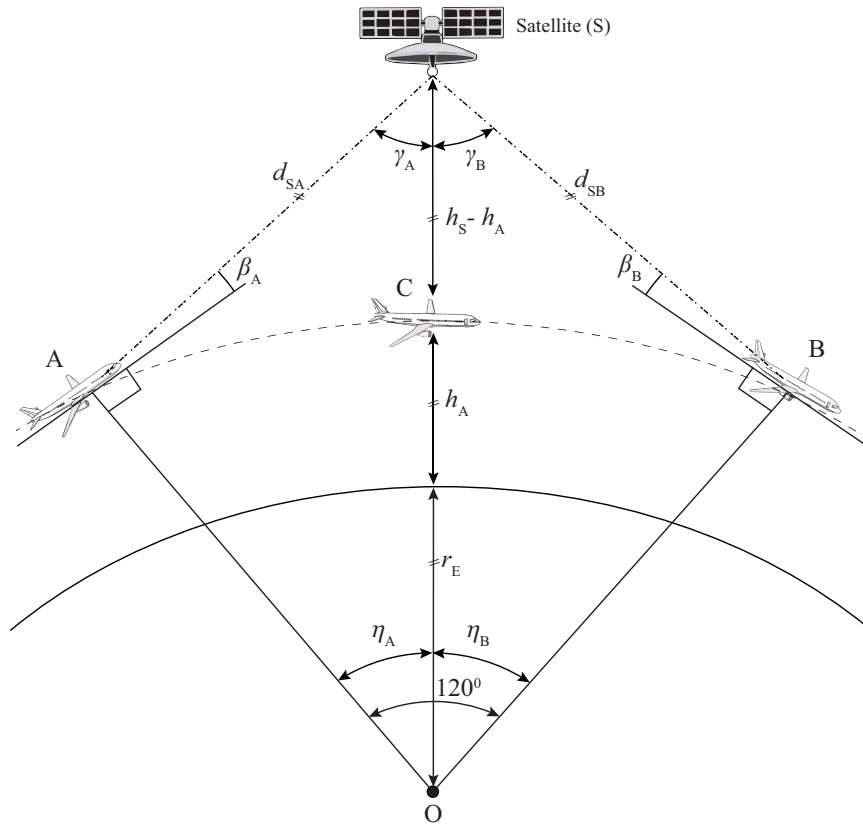
FIGURE 3.2: An illustrative geometry of signal incidence on aircraft through satellite.

model of Satellite-to-aircraft scenario is presented in the Fig. 3.2. Depending upon application's requirement, the number of satellites may vary; however, for simplicity, three satellites are assumed at latitudes separated with 120 degree of central angle to cover the whole geographical region of the earth. Consider a satellite S at the equator with an altitude h_S from the surface of the earth making angle γ_A and γ_B with aircrafts at position A and B respectively. Let h_A, r_E, d_{SA}, d_{SB} denotes the altitude of the flying aircrafts, the radius of the earth, propagation distance from satellite to aircraft at position A and B respectively. The incident waves make angles β_A and β_B with the axis of aircrafts A and B respectively. By using cosine rule, the lengths of propagation paths d_{SA} and d_{SB} can be calculated as follows.

$$d_{SA} = \sqrt{(h_S + r_E)^2 + (h_A + r_E)^2 - 2(h_S + r_E)(h_A + r_E)\cos\eta_A} \qquad (3.8)$$

$$d_{SB} = \sqrt{(h_S + r_E)^2 + (h_A + r_E)^2 - 2(h_S + r_E)(h_A + r_E)\cos\eta_B} \qquad (3.9)$$

by using sine rule, the angles γ_A and γ_B in reference to the equator can be obtained as

$$\gamma_A = \sin^{-1}\left(\frac{(r_E + h_A)\sin\eta_A}{d_{SA}}\right) \tag{3.10}$$

$$\gamma_B = \sin^{-1}\left(\frac{(r_E + h_A)\sin\eta_B}{d_{SB}}\right) \tag{3.11}$$

by utilizing the geometry of the triangle SOA and SOB, the incident angles are obtained as follows

$$\beta_A = \frac{\pi}{2} - \eta_A - \gamma_A \tag{3.12}$$

$$\beta_B = \frac{\pi}{2} - \eta_B - \gamma_B \tag{3.13}$$

Hence, by setting $h_A = 10$km, $h_S = 35796$km, $r_E = 6378.137$km, $\eta_A = 60°$, $\eta_B = -60°$, the incident angles of striking waves on aircrafts at position A and B are obtained as $21.921°$ and $158.079°$ respectively. It is worth noting that the incident angle of incoming waves will experience variable angle depending upon the location of the aircraft. The EM waves will strike perpendicularly to the surface of aircraft located on the equator and will form an incident angle $\beta_C = 90°$ with aircraft's horizontal axis.

3.3.2 Ground-to-Aircraft Scenario

In order to observe scattering properties of a signal transmitted towards aircraft through ground wireless terminal/radar, a ground-to-aircraft scenario is assumed and presented in the Fig. 3.3. The Fig. 3.3(a) explains the limitation of LoS communication link due to spherical geometry of the Earth's surface. For clarity, a zoomed-in look of signal incidence and their corresponding angles with aircraft surface is illustrated in Fig. 3.3(b). In this scenario, a wireless transmitter with three aircrafts having the same altitude (h_A) present at three different positions are considered. The coverage range of a transmitter is denoted by a dotted circular ring in which an aircraft is considered to be detectable or could receive communication
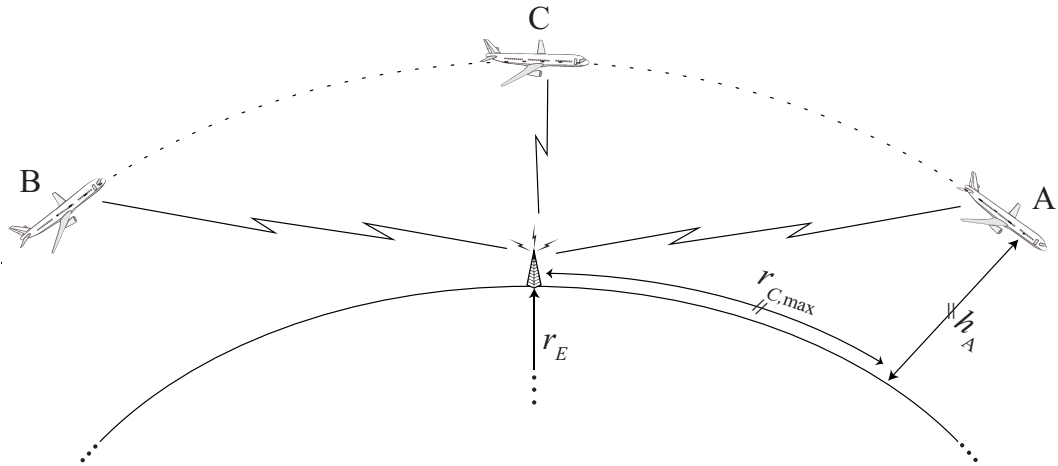
(a) LoS G2A communication geometry on earth sphere.
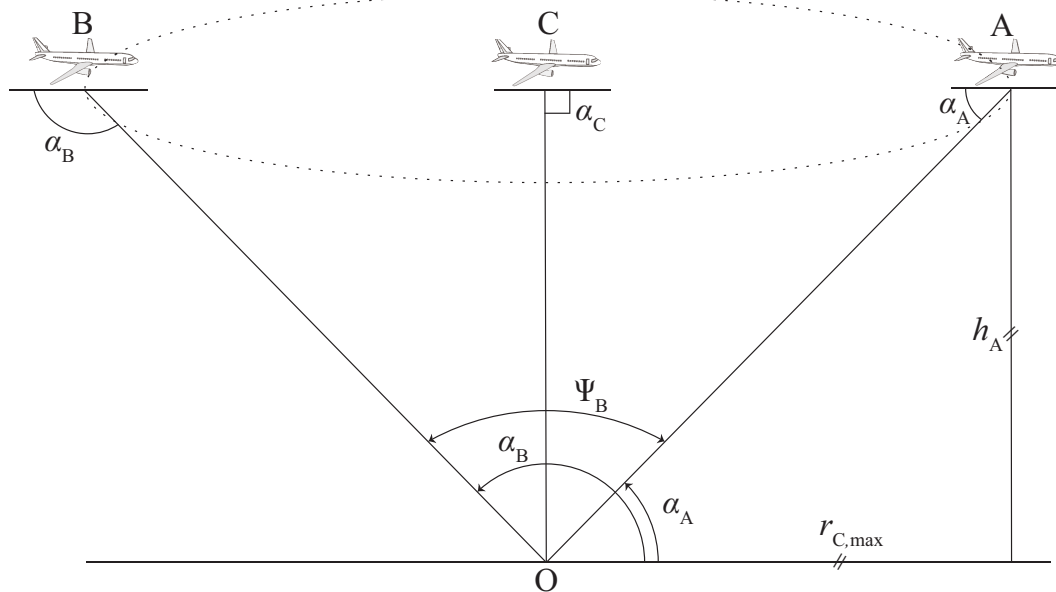
(b) A zoomed-in look of signal incidence on aircrafts.

FIGURE 3.3: A ground-to-aircraft geometry of signal incidence on aircraft.

signals from ground transmitter. The aircrafts at position A and B are located at extreme/edge of the coverage range of the radar or ground transmitter while the aircraft at position C is assumed to be located at the middle of the coverage range which is exactly above the transmitter. Maximum spread of the beamwidth can be obtained by knowing the altitude of the aircraft and the maximum radius $r_{\mathrm{C,max}}$ of the coverage region. The angular spread of the beamwidth can be evaluated as follows [141].

$$\Psi_{\mathrm{B}} = 2\tan^{-1}\left(\frac{r_{\mathrm{C,max}}}{h_{\mathrm{A}}}\right) \tag{3.14}$$

where

$$r_{\mathrm{C,max}} = \cos^{-1}\left(\frac{r_{\mathrm{E}}}{r_{\mathrm{E}} + h_{\mathrm{A}}}\right) \tag{3.15}$$

The maximum angular span Ψ_{B} of beamwidth can then be evaluated as $176.8951°$, by substituting $r_{\mathrm{E}} = 6378.137$ km and $h_{\mathrm{A}} = 10$ km in Eq. (3.15) and (3.14). By utilizing the geometry presented in Fig. 3.3(a), the incident angles α_{A} and α_{B} of EM waves impinging on aircraft A and B respectively are obtained as $1.5525°$ and $178.45°$. Since, the aircraft A is located on the edge of the maximum coverage region; therefore, the angle α_{A} formed with the aircraft's surface is the minimum threshold angle below which the ground transmitter could not maintain a line of sight with the aircraft.

3.4 Description of Simulation Tool and Aircraft A380 Facet-based Model

In order to estimate RCS of aircraft, the simulation tool POFACET® is chosen due to its open source availability and verified authenticity with the measurement results [90]. Physical Optics (PO) is a one commonly used RCS prediction approach which provides best possible RCS results in specular direction for electrically large complex bodies. It is a high-frequency simulation approach which is applicable in the situations when the wavelength of the incident wave is much smaller than the dimension of targeted body. In order to analyze scattering properties of incident EM waves on the surface of aircrafts, MATLAB-based Physical optics simulation tool POFACET® 4.2 is used. In this tool, the RCS of a complex object is usually approximated by utilizing a large number of triangular meshes (facets) that collectively represents the continuous surface of the complex object. The total RCS of the object is then evaluated by the superposition of the square root of the magnitude of each individual facet's RCS. For our modeling, we choose A380® the world's largest commercial aircraft as an example. For the designing of aircraft A380®, AutoCAD® model (.dwg file) of aircraft A380® is obtained [142, 143] within accuracy of 10cm. The AutoCAD® software provides an opportunity to
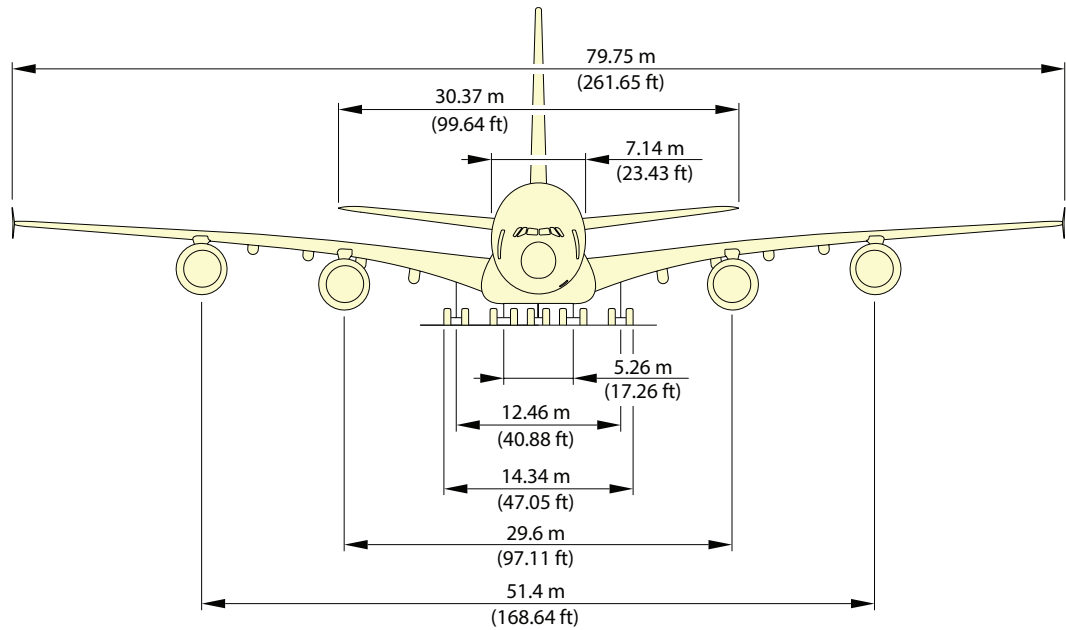
(a) Front view.
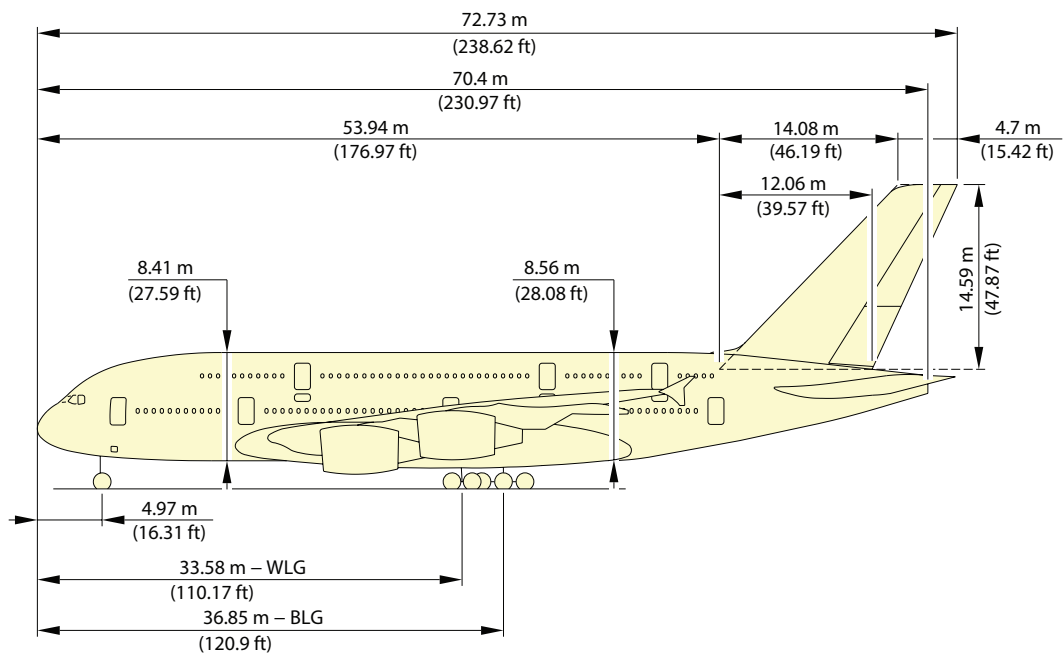
(b) Side view.

FIGURE 3.4: Aircraft A380 detailed dimensions [142].

create a blueprint of any design to view it realistically before the continuation of design process. A detailed description of aircraft A380® dimensions are shown in Fig. 3.4. Since, the POFACET® [144] simulation tool requires a facet-based model to predict RCS, therefore, AnyCAD® software is used to generate facet-based model of aircraft A380®. The facet-based representations of aircraft A380®

are demonstrated in Fig. 3.5. Fig. 3.5(a) and Fig. 3.5(b) show top and bottom look of facet-based aircraft A380® which is the main requirement our proposed model, while Fig. 3.5(c) presents a side view of the aircraft. The steps of the gradational procedure involved in the calculation of the scattering properties of the aircraft are listed in Table 3.1. In case when RCS profiles of UAVs are required, the same procedure will be followed as listed in Table 3.1. The RCS measurements of UAVs and aircrafts would be significantly different from each other due to their size and geometry specification. In POFACET®, the simulation procedure will only differ in designing of facet-based model of air vehicles.

TABLE 3.1: Gradational procedure for the calculation of bistatic RCS

Gradational Algorithm Procedure:
1.Create an arbitrary aircraft model (aircraft.stl file format)
2. Run pofacet.m // GUI of POFACET® will be shown
3. Select Calculate Bistatic RCS // Options: Design Model Manually,
// Design Model Graphically,
// Calculate Monostatic RCS,
// Calculate Bistatic RCS, Utilities
4. Select Angle for the calculation of bistatic RCS // Options: Angle & Frequency
5. Load file (airplane.stl) // Set view point if needed
6. Adjust incident angles range // (θ_i, ϕ_i)
7. Set observation angles range // $0° \leq \theta \leq 360°$ and $0° \leq \phi \leq 360°$
8. Adjust computational parameters // Taylor series parameters, incident polarization
// and frequency
9. Adjust surface roughness // If required
10. Press the button Calculate RCS
11. Select material type "R_s" // Options: Surface resistivity values (R_s) or Material data
12. Get the output

3.5 Simulation Results and Discussion

In this section, the RCS of aircraft A380® facet-based model is evaluated and analyzed for two scenarios: Satellite-to-aircraft and Ground-to-aircraft. For simulation process, three positions of aircrafts in both scenarios are considered to compute bistatic RCS for specific incident angles as explained in Fig. 3.2 and Fig. 3.3 of Sec. 3.3. The simulations of bistatic RCS are performed in spherical coordinates systems with incident angles (θ_i, ϕ_i) and observation angles (θ, ϕ). The incident angle is considered to be fixed because in bistatic RCS cases the
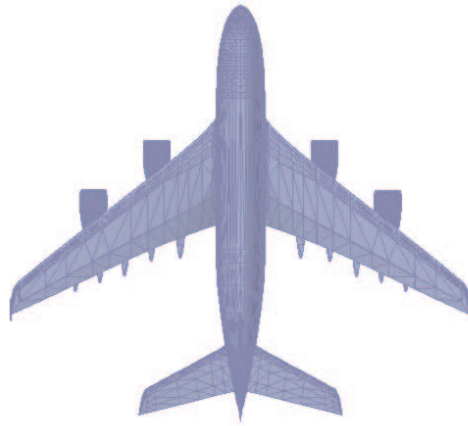
(a) Top view.
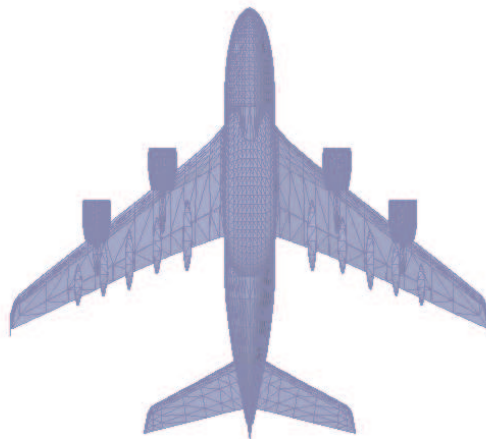
(b) Bottom view.
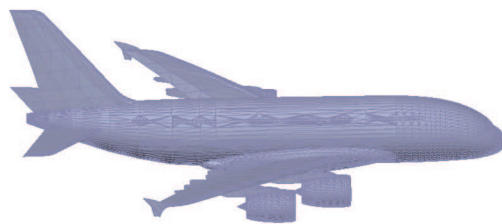
(c) Side view.

FIGURE 3.5: Facet-based representation of aircraft A380.

radar/transmitter is located at a fixed angle to the targeting aircraft while the observation angle may vary. Therefore, it is not necessary to calculate bistatic RCS for each incident angle. Although, the bistatic RCS can be observed for a wide range of observation angles equivalent to spherical geometry in the range $0 \leq \theta \leq \pi$ and $0 \leq \phi \leq 2\pi$; however, for simplicity only zero-azimuth plane (i.e $\phi_i = 0, \phi = 0$) is considered to approximate bistatic RCS for the range of observation angle $0 \leq \theta \leq \pi$. The measured values can be represented easily in terms of bistatic angles by keeping the incident angles as the reference instead of aircraft horizontal axis. In the scenario of Satellite-to-aircraft, only upper surface of the aircraft is considered for the evaluation of bistatic RCS, because a signal transmitted through satellite will encounter with only upper surface of the aircraft. The upper surface of the aircraft would be the main source of reflection and scattering of the signal towards the satellite or any other signal receiving entity. Similarly, in the scenario of ground-to-aircraft communication, the bottom surface of aircraft would be the main source of signal reflection/scattering at different observation angles towards the signal receiving units on the earth. In both the scenarios, the aircraft axis of motion (reflection plane) is considered as a reference for observation angles of bistatic RCS. The observation angles are measured in counter-clock wise rotation with reference to reflection plane on signal arrival side. For simulation, the number of Taylor series based polynomial is taken as 3, incident wave polarization mode is set at linear-vertical polarization, and the aircraft surface roughness is assumed as a smooth surface.

In satellite-to-aircraft communication link scenario, when both satellite and aircraft are present on the equator the signal transmitted through satellite will make a 90 degrees angle with aircraft upper body. In this case, the bistatic RCS fluctuations are obtained and plotted in Fig. 3.6 with respect to observation angle (θ). The results are measured in counter-clock direction by keeping the horizontal axis of aircraft motion as a reference axis. The RCS values are observed only at upper half region ($0° \leq \theta \leq 180°$) of the observation angels because in this region the reflections would be prominent with high power gain. In the figure, a high peak is envisioned at angle 92.5° which is basically a specular reflection from the aircraft
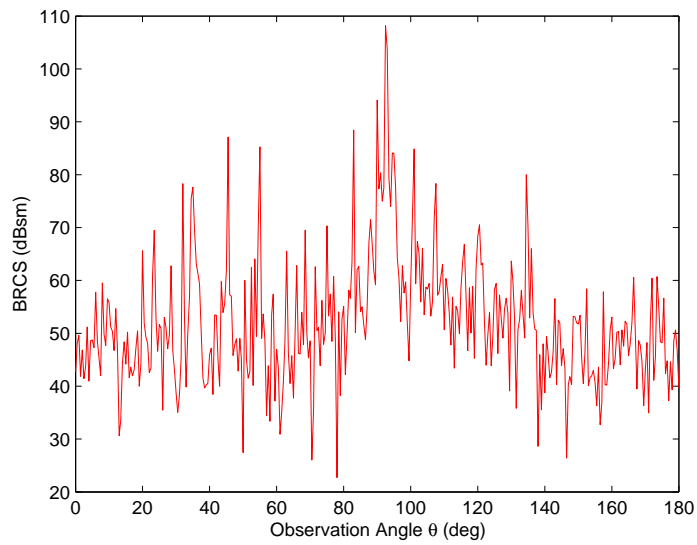
(a) Linear Plot.
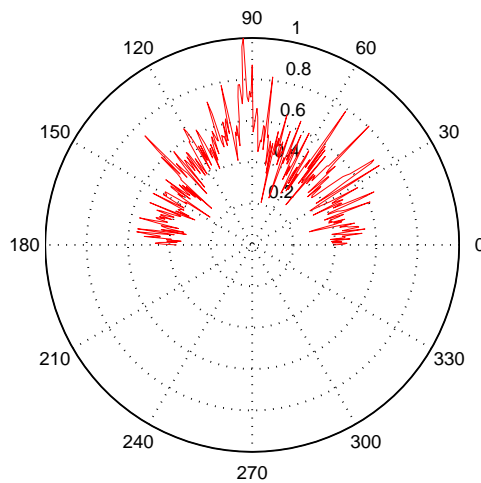
(b) Polar Plot.

FIGURE 3.6: RCS observation of signal incidence at $\beta_C = 90°$ in Satellite-to-aircraft communication scenario.

surface. Hence, at observation angles on which the BRCS is high, the reflecting surface of aircraft will possibly provide strong interference to satellites or aircrafts located at these observation angles.

In Fig. 3.7, the angular bistatic scattering response of aircraft at incident angle $\beta_A = 21.921°$ is shown with both linear and normalized poler plots in Fig. 3.7(a) and Fig. 3.7(b) respectively. The impact of signal incidence at angle β_A shows
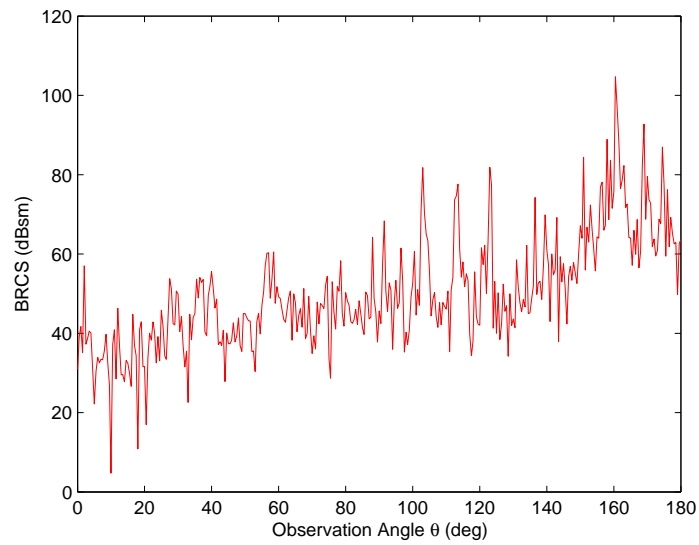
(a) Linear Plot.
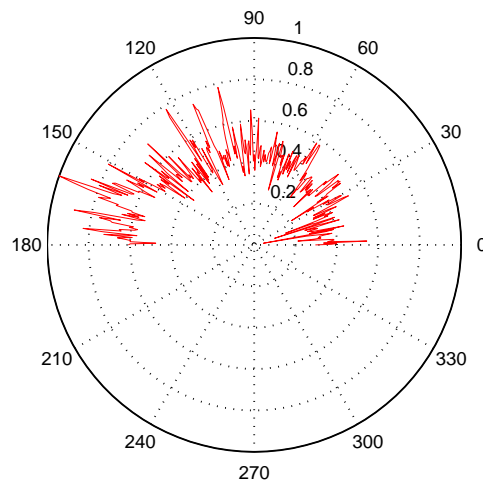
(b) Polar Plot.

FIGURE 3.7: RCS observation of signal incidence at $\beta_A = 21.921°$ in satellite-to-aircraft communication scenario.

that the aircraft upper body scatters signal power in all direction with different power amplitudes. The specular reflection of aircraft is obtained at angle 158.079° with a power gain of 104.7 (dBsm). Fig. 3.8 presents scattering behavior of aircraft surface for an incident angle of 158.079° with both linear and normalized polar graphs in Fig. 3.8(a) and Fig. 3.8(b) respectively. The results shows that at this particular incident angle the aircraft metallic surface and its curved structure

scatters signal power in all directions with different amplitude levels according to the observation angles θ. Specular reflection of the signal is observed at an angle of 22° with a power gain of 98.29 (dBsm). From the simulation results, it can be concluded that in Satellite-to-aircraft communication links the aircraft metallic surface and its curved shape may provide interference to its surrounding receivers (satellite/aircrafts) due to signal reflections from its surface. In this situation, the performance of the surrounding receivers may get degraded based upon the interfering signal power level received at the receiver end. Hence, these simulation results provides a way to observe interfering signal reflections from flying aircrafts during the communication between satellites and aircrafts. In Fig. 3.9, bistatic RCS of an aircraft by impinging a signal at incident angle $\alpha_C = 90°$ to its lower body is evaluated and shown in both linear and polar plots. In the scenario of ground-to-aircraft, angular bistatic RCS observation are calculated by considering only the lower surface of aircraft. This is due to the fact that in this case the lower body of the aircraft would be the main source of signal reflection with high amplitude of scattering power as compared to aircraft's upper surface. Moreover, it is quite realistic to assume that in this scenario, the transmitted signals will not strike on the upper surface of the aircraft. By keeping aircraft's axis of motion as a reference, angular bistatic RCS values are evaluated with respect to observation angles of range 0° to 180° in $\phi = 0$ plane, which is the lower half region of the aircraft in which the signal will scatter and carry the high scattering power. The observation angles are measured in counter clock direction by keeping the aircraft's axis of motion as a reference axis, as shown in Fig. 3.9(b). From the figure, it is worth notable that the lower part of the complex structure of aircraft constitutes good reflecting properties and generates signal reflection at every observation angle which are considered in this simulation. In the figure, the highest peak of bistatic RCS is observed at 131.5° with 90.29 dBsm amplitude, however, the specularly reflected RCS amplitude value is obtained as 87.72 dBsm at angle 87.5°. The high peaks other than the specularly reflected power occur due to the complex curved structure of the aircraft's metallic body which reflects/scatters incident wave towards these particular observation angles and as a result gives
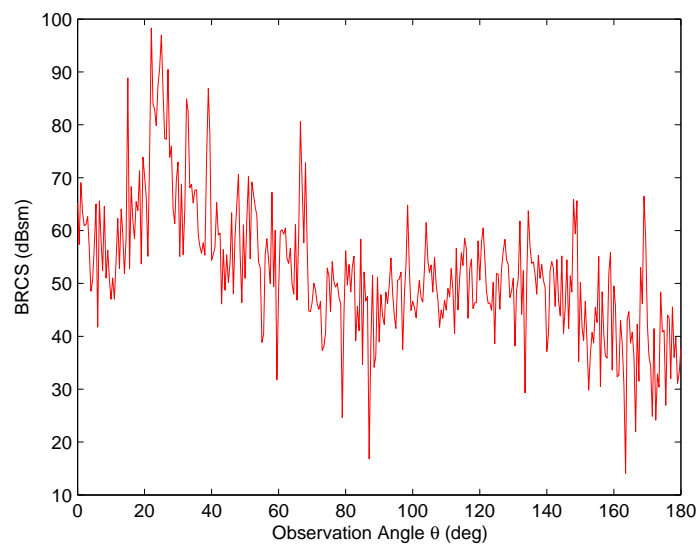
(a) Linear Plot.
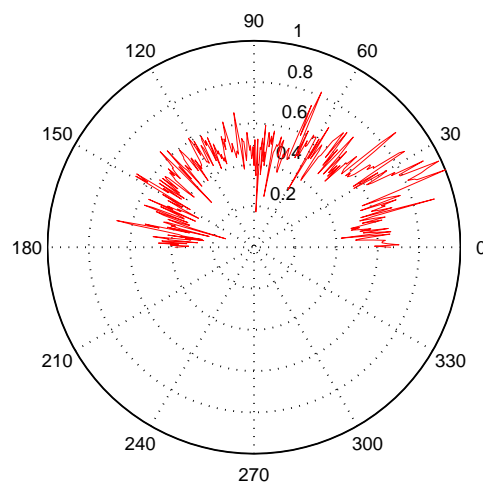
(b) Polar Plot.

FIGURE 3.8: RCS observation of signal incidence at $\beta_{\mathrm{B}} = 158.079°$ in satellite-to-aircraft communication scenario.

rise to bistatic RCS.

In Fig. 3.10, bistatic RCS of aircraft at incident angle $\alpha_{\mathrm{A}} = 1.5525°$ is presented with both linear and polar graphs in Fig. 3.10(a) and Fig. 3.10(b) respectively. The bistatic RCS shows specularly reflected behavior at an angle 179.5° with amplitude 87.21 dBsm. In Fig. 3.11, bistatic RCS of impinging wave having incident
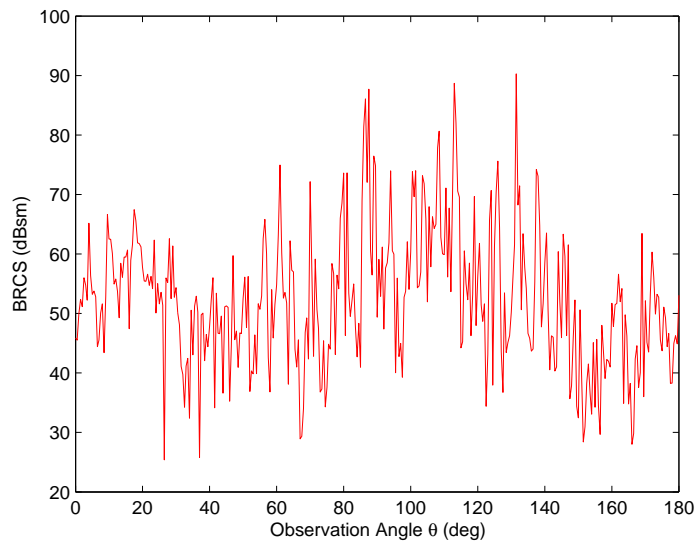
(a) Linear Plot.
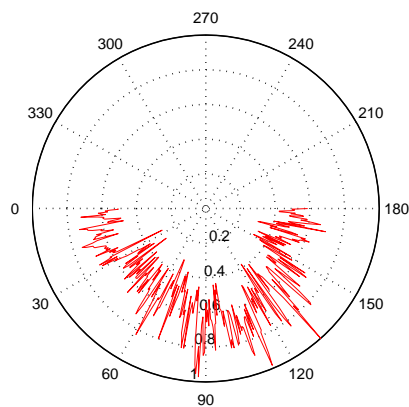
(b) Polar Plot.

FIGURE 3.9: RCS observation of signal incidence at $\alpha_C = 90°$ in ground-to-aircraft communication scenario.

angle $\alpha_B = 178.55°$ with respect to observation angles θ is presented. The maximum value of bistatic RCS is observed at angle $2°$ with amplitude 81.59 dBsm. Bistatic RCS observations at these incident angles give a way to envision the interfering reflected power from aircraft's surface which degrades the performance of neighboring receivers whether aircrafts or ground terminals. By keeping the knowledge of interfering signal power, counter-measures can be made for better performance and error avoidance.

Fig. 3.12 presents the behavior of spatial reflection coefficient as a function of
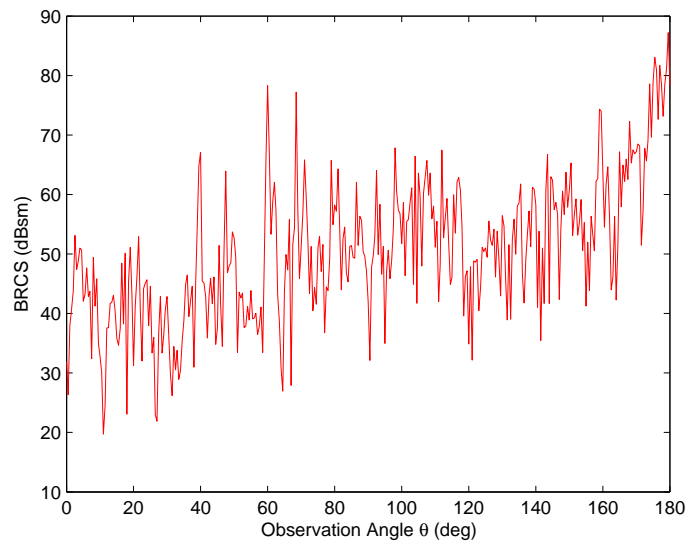
(a) Linear Plot.
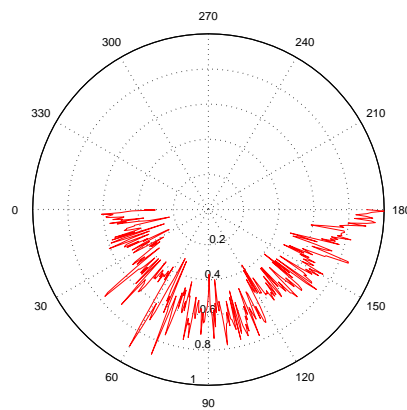
(b) Polar Plot.

FIGURE 3.10: RCS observation of signal incidence at $\alpha_A = 1.5525°$ in ground-to-aircraft communication scenario.

RCS, line-of-sight (LOS) distance d_1 and reflected signal distance (d_2). For simulation, bistatic RCS results obtained in satellite-to-aircraft scenario with 90° signal incidence are only used. Whereas, the LoS distance (d_1) and reflected signal distance (d_2) are taken as 35786 Km and 10 Km respectively. The result explains that how much power is reflected from the surface of the aircraft and as a result providing interfering signal reflection to its neighboring receivers. At 90° signal incidence from the satellite, the aircraft surface will provide a strong reflection to aircrafts/satellites which are present at 90° observation angle, however, it will
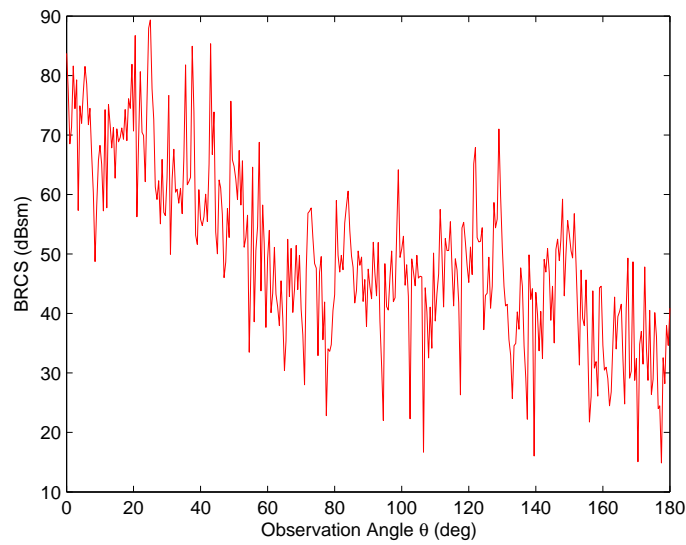
(a) Linear Plot.
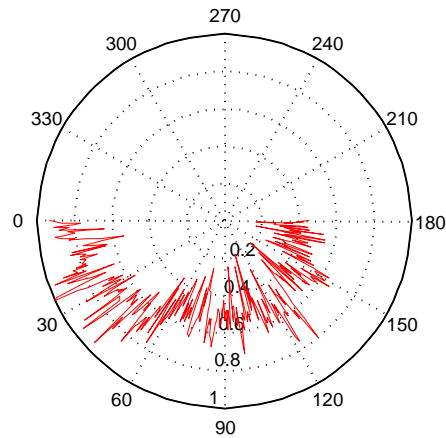
(b) Polar Plot.

FIGURE 3.11: RCS observation of signal incidence at $\alpha_B = 178.45°$ in ground-to-aircraft communication scenario.

provide quite ignorable interference at rest of the observation angles. Varying the distances of LoS (d_1) and reflected signal paths (d_2), the behavior of spatial reflection coefficient can be envisioned in Fig. 3.13. From the figure, it is observable that the amplitude of SRC decreases as the distance increases and increases when the distances decrease. The results shows a way to observe the scattering mechanism of a signal from flying aircrafts and strength of reflected interfering signal. A comparison between SRC and RCS is shown in the Fig. 3.14. Comparison between SRC and RCS shows that both the terms follows the same trend with a constant scaling factor based upon the propagation distances. From the analysis,
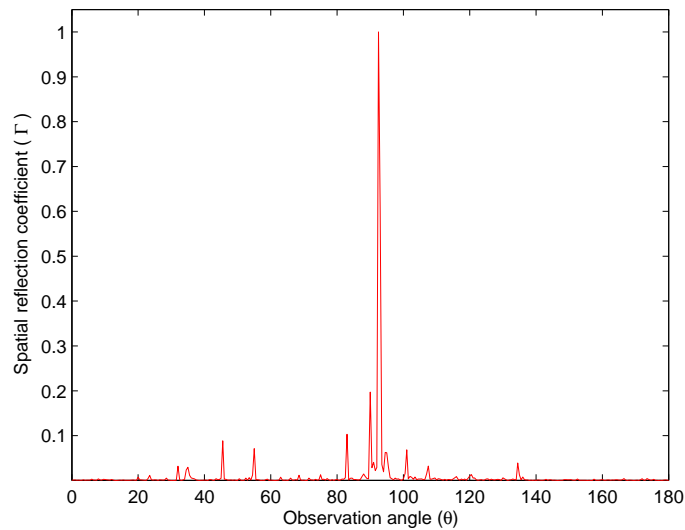
FIGURE 3.12: Plot of spatial reflection coefficient as a function of bistatic RCS formulated with 90° signal incidence in satellite-to-aircraft scenario.

it is observed that SRC and RCS follows the same scattering behavior and can be used interchangeably to analyze a communication system model. In wireless communication systems, multipath environment is a propagation phenomenon which occurs due to reflection, diffraction, refraction or scattering of a signal through objects (scatterers) present between the transmitter and receiver. In such environments, the receiver receives multiple versions of phase shifted and attenuated signals which when combined results a faded signal of much less power. Thus, the RCS can be used interchangeably instead of reflection coefficient to validate and analyze any communication system model. From the design and simulation point of view, as POFACET [144] simulation tool works by utilizing a facet-based representation of a model; therefore, inaccurate facet-based modeling of a model may induce facetization error which may lead to inaccurate observation of the RCS. The facetization error usually occurs when a smooth continuous surface is represented by discrete facets having inappropriate size (i.e. large facets) as compared to the smoothness of the surface. Hence, to decrease the facetization error, an appropriate mesh size must be used to generate a tight fitting mesh representation of the model. On one hand, accurate calculations of bistatic RCS require a smooth facet-based model with small facet size, while on the other hand, this leads to
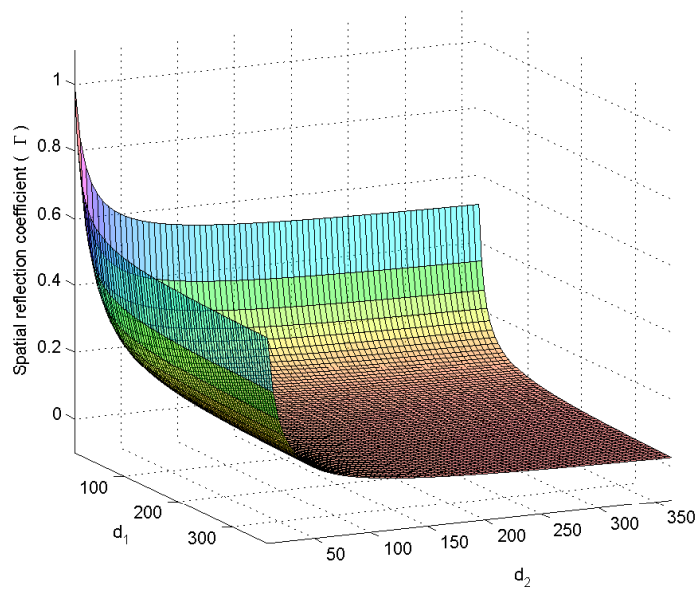
FIGURE 3.13: Reflection coefficient as a function of RCS, d_1 and d_2.
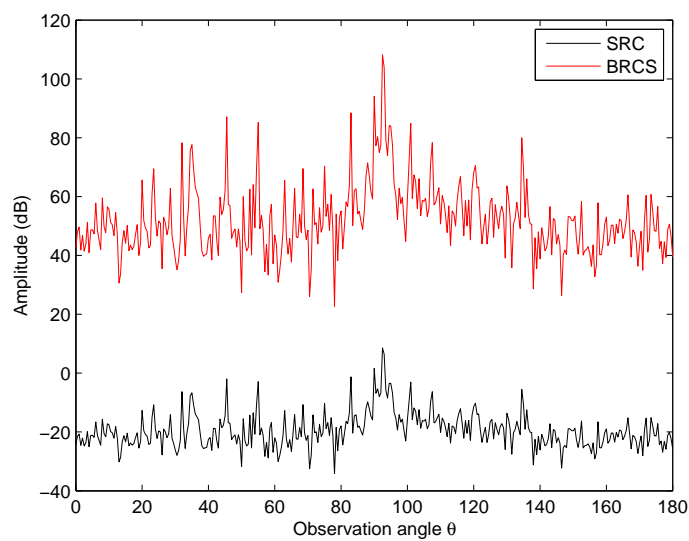
FIGURE 3.14: Comparison between SRC and BRCS.

high computations which is not always possible to perform on normal computers. Therefore, a machine having a high-processing capability may get more accurate RCS results with less facetization error.

Chapter 4

G2A Communication Channel Modeling

In this chapter, Ground-to-Aircraft (G2A) communication channel model is developed. In Section 4.2 geometrically-based physical G2A propagation model is explored with essential details regarding establishment of G2A propagation environment in its succeeding subsections. In Section 4.3, G2A multipath channel is modeled for two propagation scenarios: wide-beam communication link and narrow-beam communication link.

4.1 Introduction

The advancements in wireless mobile technology have significantly influenced the daily life of every human being through innovative ways of communication, despite one's physical location around the globe. The availability of data services on mobile devices has further enhanced the communication activity in a more suitable and inexpensive way by their integration with real-time applications. These applications facilitated people to stay connected to the world every where and at any time. Due to the growing potential of data-hungry real-time applications, the demand of high data-rate internet access is expected to grow more dynamically in

coming decades. This increase in demand is basically for the availability of uninterrupted wireless connectivity with high mobility and guaranteed performance. Rise in demand in recent years was not only seen from the mobile users on the ground but was also observed in the case of the passengers traveling in aircrafts around the globe. To address the demand of in-flight internet, satellite communication system is still one of the major global solutions for the provision of data services to flying aircrafts; however, it is not the best solution for real-time communication services due to its longer end-to-end delays. Therefore, in recent years, the exploration of new ways to provide high-speed seamless internet connectivity to aircraft passengers has gained the attention of the researchers and development organizations. Air-to-Ground (A2G) and Ground-to-Air (G2A) communication systems are the alternate feasible ways other than the satellite communication systems that can provide high-speed data services with less route delays for data-hungry real-time applications [1]. These links are also a prime requirement of Unmanned Aerial Vehicles (UAVs) to control their operations through ground terminals. The demand of UAV is anticipated to grow exponentially in future due to its immense use in various applications like internet provision, military operations, cargo delivery, weather monitoring, precision farming, firefighting, law enforcement, customs and border patrolling [1–3]. To achieve the progressive demands of A2G/G2A communication links, reliable understanding of the propagation environment in A2G/G2A is needed. Though, the researchers supposedly model A2G and G2A channels interchangeably in the same way [1, 2] as that of A2G links; however, the propagation environments in both links affects the link performance differently. In A2G channel environment, scattering objects are usually assumed to reside only around Ground Station (GS) which cannot be supposed conversely in G2A link. Due to distinct signal propagation geometry of A2G and G2A communication environments, the characteristics of A2G and G2A radio communication links would also be distinctive. Therefore, it is pertinent to examine conscientiously the distinctness of G2A and A2G communication environments. The objective of this study is to characterize G2A communication link in multipath environments.

4.2 Ground-to-Aircraft Multiuser Communication System Model

4.2.1 System Model

In order to design a spectrally-efficient communication system for ground-to-aircraft communication, a complete understanding of the radio signal propagation is required. In the literature, the Ground-to-Aircraft (G2A) link is usually perceived as a LoS communication link; however, in reality apart from the direct waves, the aircraft receiver may receive a number of reflected, diffracted and scattered waves from the proximate aircrafts via different propagation paths. In some cases, only a LoS condition may exist when there is no aircraft present in the proximity of the intended aircraft; however, surmising only LoS communication for G2A is not always a realistic assumption. Hence, reflections from the proximate aircrafts will construct a multipath fading environment between the ground station and the intended aircraft which may degrade communication performance due to constructive or destructive addition of signals. Consider a ground-to-aircraft communication scenario as depicted in the Fig. 4.1. Assume there are K number of aircrafts (including the aircraft of interest) flying in the coverage region of G2A communication link. The notation A_k represents the kth aircraft, where $k = 0, 1, 2, 3, \cdots, K$. In order to avoid collision among them, flying aircrafts maintain a safe separation distance among them which leads to the uniqueness of the signal propagation paths. There could be some cases in which the lengths of propagation paths may get equal due to the orientation of aircrafts in space. For instance, if the aircraft is above the communication link then aircrafts lying in the tier of the same separation distance may provide multipath signals with the same propagation delay. An intended aircraft (say A_0) may observe $K - 1$ multipath signals from flying aircrafts with delay $\tau_k = \frac{d_k}{c}$, where d_k be the length of the signal propagation path via aircraft A_k and c is the speed of light. Signals having shorter propagation path will arrive quite earlier, while the signal copies following longer routes will arrive later with more delays. Since, each multipath
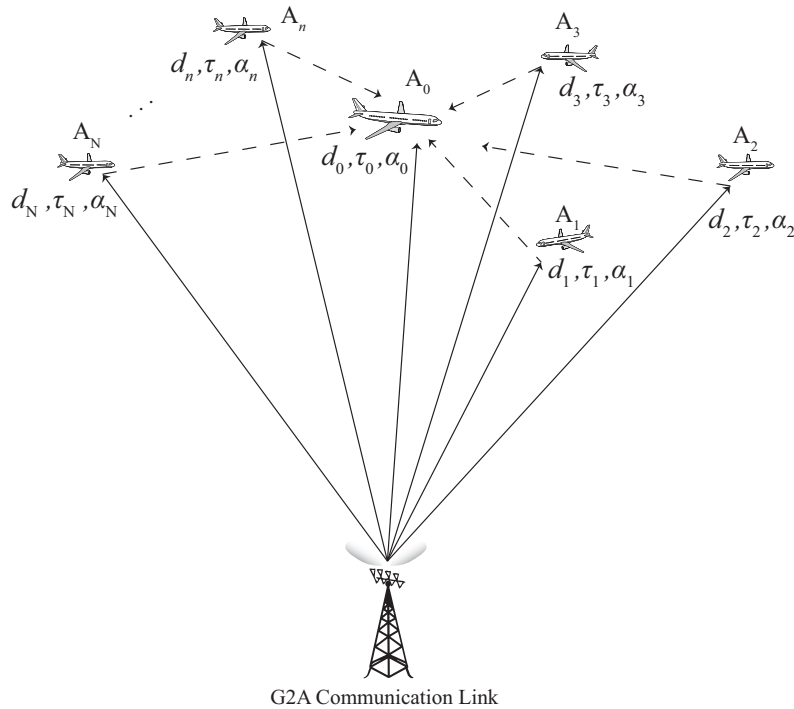
FIGURE 4.1: Ground-to-Aircraft wave propagation in a multipath scattering environment due to the presence of aircraft in the surrounding.

will undergo a specific fading phenomenon, therefore, the attenuation factor of the path k can be denoted by α_k.

4.2.2 Finding Suitable Shape for Physical G2A Propagation Scenario

In order to find the exact locus of the scattering aircrafts and their corresponding delays, we need to develop the physical G2A propagation model. Multipath nature of the radio propagation environment imposes unavoidable constraints on the performance of communication systems. To analyze the communication performance, it is necessary to quantify the limiting effects of the channel wherefore their proper counter measures could be established to increase the limiting performance bound. From signal propagation aspects, it is essential to develop a method of channel characterization that provides a clear insight of the propagation mechanism for the complete performance analysis of a communication system. In ground-to-aircraft (G2A) communication environment, transmitted radio signals undergo reflection,
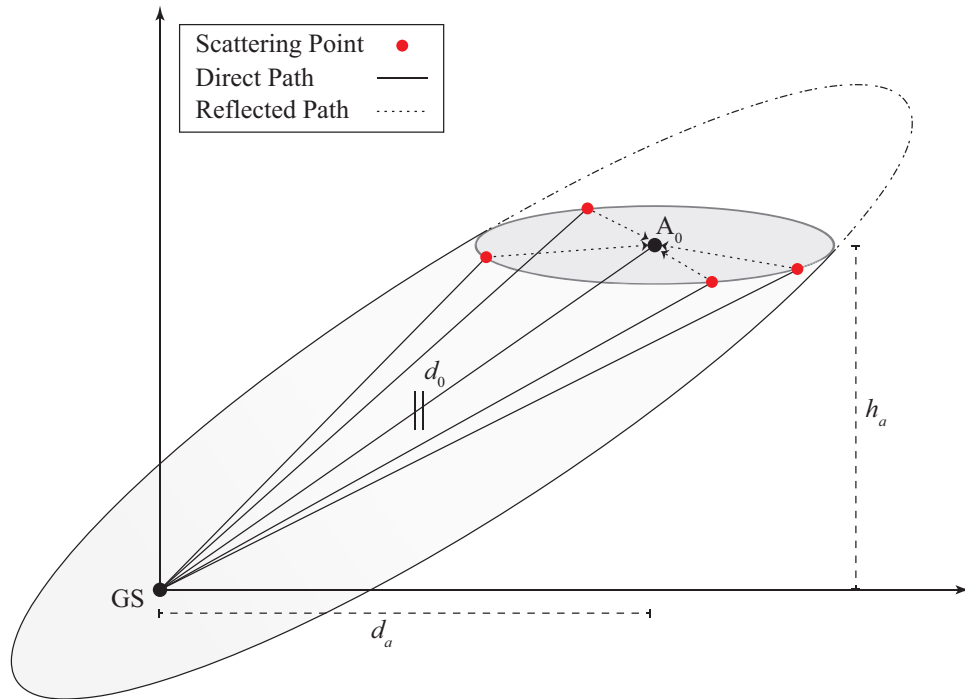
FIGURE 4.2: Geometrical representation of G2A multipath components arriving at the intended aircraft via proximate aircrafts located on prolate spheroid with same propagation delay.

diffraction or scattering mechanisms and arrive at the aircraft receiving unit with random amplitudes and arrival times. In the proximity of the intended aircraft, the radio waves are likely to be reflected from the surface of the proximate aircrafts. The time delays, amplitudes and carrier phases of the received signals solemnly depend upon the spatial location of the scattering aircrafts (A_k) and their orientation in the propagation environment. The resulting multipath environment may thus generate a frequency-selective fading environment which certainly affect the communication performance of the G2A link of the intended aircraft.

Consider an aircraft station A_0 flying at an altitude h_a is communicating with ground station (GS), as illustrated in the Fig. 4.2. The radial distance from GS to A_0 is denoted by d_0 and the horizontal distance between GS and the A_0 is represented by d_a. It is quite evident from the preceding discussion that in G2A communication scenario multipath signals may exist due to the presence of proximate aircrafts, acting as scatterers, in the vicinity of the intended aircraft. The scattering aircrafts that will provide multipath signals with the same propagation delay can be presumed on the same prolate spheroid, where AS and GS are to
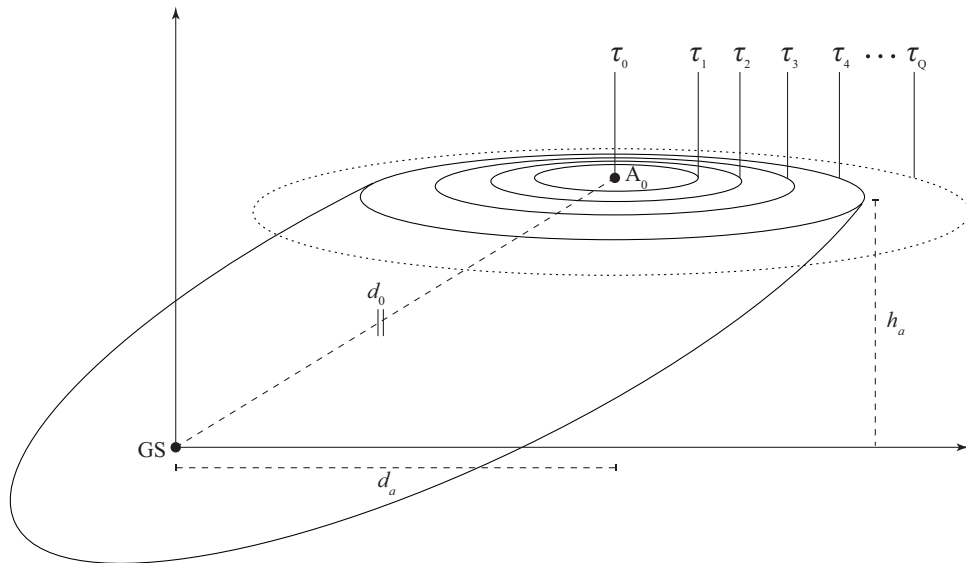
FIGURE 4.3: Geometry of confocal prolate spheroids representing series of elliptical regions as a result of horizontally plane cross-section.

be located on its focal points. Prolate spheroid is basically a surface of revolution obtained by rotating an ellipse along its major axis and hence it follows all the elliptic properties. In geometry, a prolate spheroid is the set of all points in three-dimensional space, such that the sum of the distances from any point on the prolate spheroid to the two focal points is a positive constant. Hence, considering the case of communication link between GS and AS, the signals arriving through aircrafts lying on the surface of a defined prolate spheroid with GS and AS as its focal points will reach with the same time delay. It is pertinent to note that all the scattering aircrafts with the same altitude (h_a), causing multipaths of the same propagation length can be found to be located on the boundary of the elliptic region developed as a result of cross-section of the prolate spheroid with a horizontally-parallel plane at its focal point as highlighted in the Fig. 4.2.

4.2.3 Formation of Confocal Prolate Spheroids

The lengths of propagation paths may vary with time according to the motion of the intended aircraft (A_0) and the motion of the proximate aircrafts (A_k). Moreover, the propagation lengths of the arriving signals and their respective times of

arrival also suggest the intrinsic physical location of the scatters with respect to the focal points either GS or AS. However, when the times of arrival of two signals become the same, it becomes impossible to differentiate between their spatial locations; hence, in such situation the angular direction of arriving signals must be considered. If we assume single-bounced-scattering-scenario, then all the scattering aircrafts with identical path lengths can be located on a particular prolate spheroid with a constant delay as illustrated in Fig. 4.3. In the figure, a series of concentric ellipses can be envisioned which are basically the result of horizontally-parallel planes cutting confocal prolate spheroids at their common focal point where AS is located. Thus multiple confocal prolate spheroids can be used to generate a tap-delay channel model to address the possible channel effects that degrade communication performance. The multipaths coming through scattering aircrafts located on a specific prolate spheroid collectively sum up in-phase providing combined power of the wave at the receiving antenna at a corresponding propagation delay. The propagation delay of each wave of qth prolate spheroid in the scattering zone of G2A communication environment can be written in terms of a differential propagation delay ($\Delta\tau$) and the LoS propagation delay (τ_0).

$$\tau_q = \tau_0 + q\Delta\tau, \qquad q = 0, 1, 2, \cdots, Q \tag{4.1}$$

The precision of the G2A propagation model using prolate spheroid can be improved if K is increased or $\Delta\tau$ is made infinitesimally small. Propagation delays of all the multipaths in the G2A environment are confined to the interval $[\tau_0, \tau_{\max}]$, where, $\tau_{\max}$ is the maximum propagation delay which is selected in such a way that energy contribution of the multipath signals with propagation delays greater than $\tau_{\max}$ are negligible and can be ignored.

4.3 Ground-to-Aircraft Channel Model Development

In this section, we intend to develop an appropriate depiction of radio signal propagation from GS towards flying aircrafts. In reality, G2A communication environment is time-dispersive in nature which introduces multipath fading at the receiver. A repeated pulse-sounding experiment can be used to observe the amplitudes and relative delays of the dispersive replicas of the transmitted signal. Since, the states of the time-dispersive channel in G2A communication link are difficult to be estimated correctly; therefore, it is appropriate to analyze its fading phenomenon statistically. For this purpose, we concentrate on two major G2A communication scenarios; i.e. wide-beam communication link and narrow-beam communication link.

4.3.1 General Modeling Assumptions

Before establishing G2A channel model parameters, we first introduce some prevalent modeling assumptions, as follows:

1. For simplicity, all aircrafts in the coverage region of GS are assumed to fly at the same altitude h_a.

2. Scattering aircrafts are positioned on the boundary of the elliptical-shaped scattering region, which is the result of plane cross-section of prolate spheroid as discussed in sec. 4.2 in detail. Although, considering countless scattering regions may refine G2A propagation model; however, it becomes impractical because multipaths via longer route delays experience greater path loss and reach at the receiver with negligible power [73].

3. To avoid collision among aircrafts, concentric circular rings (circular rings of mandatory minimum separation distances) around the intended AS are assumed with multiple of 10 km radii difference. Hence, intersection points

between circular rings and the plane cross-sectioned ellipses are the conceivable locations of scattering aircrafts at which they are assumed to be located during their flight while maintaining the minimum safe separation distance.

4. The dimension of each confocal prolate spheroid is obtained by means of possible delays developed by line-of-sight (LoS) and diffused components.

5. Each scattering aircraft is considered as an omnidirectional reradiating element; however, the reradiating scattering properties depend upon the spatial locations of the aircrafts and their orientations in three dimensional space. The spatial locations of the aircrafts will define the incidence and reflection angles of the multipaths towards the intended aircraft station.

6. For simplicity, single-bounced multipath geometry is considered and it is assumed that the received signal at the antenna of the intended aircraft A_0 undergoes no more than one reflection by proximate aircrafts when transmitted by GS to the AS.

7. The GS is located at the origin of the three-dimensional space with coordinates $(0, 0, 0)$. Hence, the location of any aircraft A_k can be represented in the system by Cartesian coordinates (x_k, y_k, z_k) or equivalently in polar coordinates by (r_k, θ_k, ϕ_k).

4.3.2   Plane Cross-Section of Prolate Spheroid

It is well evident from the literature [145, 146] that a plane cross-section of an arbitrarily-oriented ellipsoid at any specific angle forms an ellipse except when the plane is perpendicular to its major axis. The ellipse formed by the plane cross-section of ellipsoid can be introduced as an intersection ellipse. A triaxial ellipsoid is called a prolate spheroid when its two minor axes are equal in length while the major axis is greater than its minor axes. The equation of the prolate spheroid with its minor axis $a_p = b_p$ and major axis $c_p > a_p$ can be written as

$$\frac{x^2 + y^2}{a_p^2} + \frac{z^2}{c_p^2} = 1 \tag{4.2}$$

where, the eccentricity of prolate spheroid can be defined as

$$e_p = \sqrt{\frac{c_p^2 - a_p^2}{c_p^2}} = \frac{\sqrt{c_p^2 - a_p^2}}{c_p} = \sqrt{1 - \frac{a_p^2}{c_p^2}}$$

By adjusting dimensions of prolate spheroid and the corresponding cross-section angle θ of plane, the following expressions yield the length of the semi-major (a_{cs}) and the semi-minor (b_{cs}) axes of the plane cross-sectioned ellipse, respectively.

$$a_{cs} = \frac{c_p a_p^2}{c_p^2 \cos^2(\theta) + a_p^2 \sin^2(\theta)} \tag{4.3}$$

and

$$b_{cs} = \frac{b_{E_0}}{a_{E_0}} \sqrt{a_{E_0}^2 - z'^2} \tag{4.4}$$

where,

$$a_{E_0} = \frac{c_p}{2a_p} \sqrt{4a_p^2 - (r_1 - r_2)^2 \cos^2(\theta)}$$

$$b_{E_0} = \frac{\sqrt{4a_p^2 - (r_1 - r_2)^2 \cos^2(\theta)}}{2}$$

$$z' = \frac{2\sqrt{c_m^2 - a_m^2} + r_1 \sin(\theta) - r_2 \sin(\theta)}{2}$$

$$r_1 = \frac{a_p^2}{c_p + \sin(\theta)\sqrt{c_p^2 - a_p^2}}$$

$$r_2 = \frac{a_p^2}{c_p + \sin(\theta + \pi)\sqrt{c_p^2 - a_p^2}}$$

The coordinates of the center of the cross-sectioned ellipse can be obtained as follows.

$$C = \left(\frac{r_1 \cos(\theta) - r_2 \cos(\theta)}{2}, \frac{2\sqrt{c_m^2 - a_m^2} + r_1 \sin(\theta) - r_2 \sin(\theta)}{2} \right) \tag{4.5}$$

For more details about the derivation of the intersection ellipse, the reader can see Appendix 10.

4.3.3 Intersection of the Ellipse Formed by Plane Cross-Sectioned Prolate Spheroid at an Angle θ_{Beam} and a Circle of an Arbitrary Radius r_0

The ellipse formed by the plane cross-section of a prolate spheroid and the circle of separation distance may intersect at either none or two or four points. The intersecting points may become infinite in a special case when the intersection ellipse coincides with the circle of separation distance. This case occurs when the aircraft of interest is rightly above the GS making an angle of 90^0. Three different situations are shown in Fig. 4.4 according to their points of intersection while considering inner and outer cases of the circle of separation distance. It can be observed that the situations 1 and 2 would rarely occur while the situation 3 occurs quite frequently and becomes the case of our general consideration. Since, the geometry of the aircraft channel model depends upon multiple intersection ellipses with different major and minor axes and circles of different radii; therefore, the geometrical G2A channel model would thus be a combination of these scenarios depending upon the radius of circle, and the major and minor axes of the intersection ellipse.

Considering the situation 3 as a general case, the points of intersection between
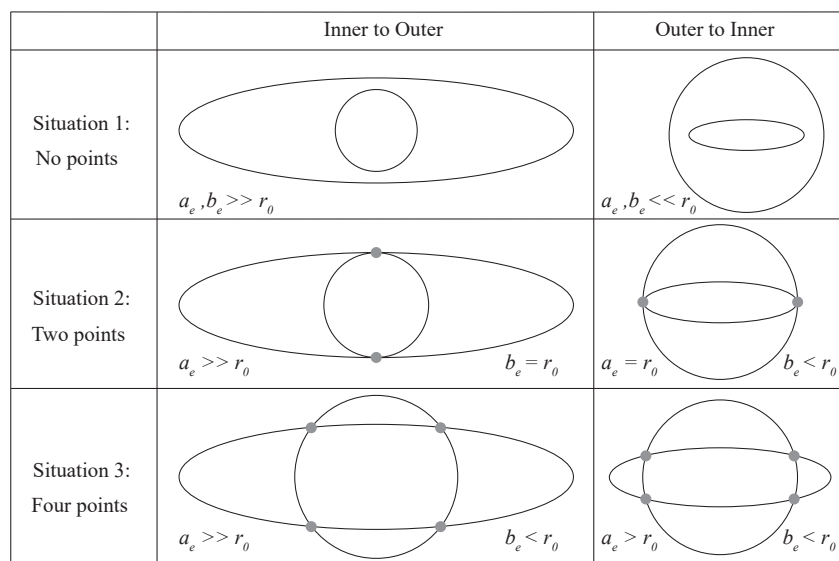
FIGURE 4.4: Intersection scenarios of ellipse and circle.

p^{th} circle of an arbitrary separation distance r_p and the qth plane cross-sectioned ellipse while both enjoying a common center (x_c, y_c), can be calculated as

$$
\begin{aligned}
x_{pq} &= x_c \pm a_{eq} \sqrt{\frac{r_p^2 - b_{eq}^2}{a_{eq}^2 - b_{eq}^2}} \\
y_{pq} &= y_c \pm b_{eq} \sqrt{\frac{b_{eq}^2 - r_p^2}{a_{eq}^2 - b_{eq}^2}}
\end{aligned}
$$

where, r_p is the radius of the pth circle of separation distance while a_{eq} and b_{eq} are the lengths of major and minor axes of qth plane cross-section ellipse.

4.3.4   Ground-to-Aircraft Multipath Channel Model

A perspective geometry of the 3D G2A system model is depicted in Fig. 4.5. Being on the foci of the prolate spheroid, the intended aircraft station (AS) is represented by A_0 while the ground station is mentioned as G. The aircraft A_0 flying at an altitude h_a makes an angle θ_{Beam} with the GS. The radial distance between A_0 and the G is denoted by d_0 while the horizontal distance of A_0 from GS is mentioned with D_0. The same parameters A_0, d_0 and D_0 can be modified for their onward use in the system model to define any scattering aircraft A_k with d_k and D_k around A_0, where $k = 1, 2, 3, \cdots, K-1$. Elliptical rings of varying dimensions which surround a common point A_0 are basically the result of horizontal plane cross-section of confocal prolate spheroids at an altitude h_a, as shown in Fig. 4.5. Concentric circular rings around A_0 are the conceivable boundary/locations of scattering aircrafts over which they can fly by maintaining the minimum safe separation distances to avoid collision with other aircrafts. Having the above information in mind, one can visualize the proposed G2A communication system model as a combination of multiple plane cross-sectioned ellipses and concentric circles with varying radii. Concentric circles cover all the proximate aircrafts around A_0 that may induce multipath scattering; whereas, the confocal prolates and their resulting plan cross-sectioned ellipses depict the phenomena of arrivals of signals with equal delays from the
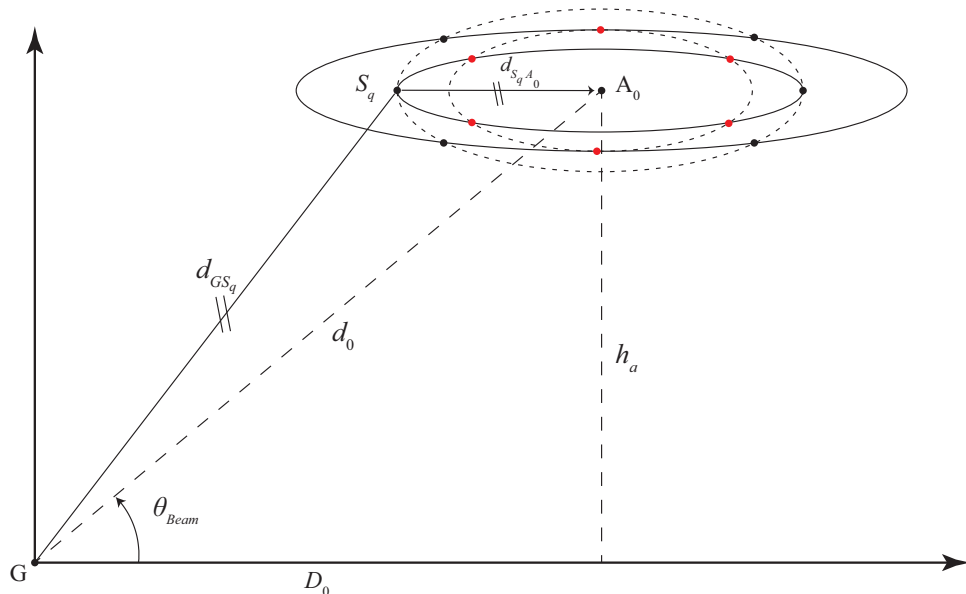
FIGURE 4.5: System model.

proximate aircrafts and their consequent constructive or destructive fading. Intersecting points of intersection among concentric circles and cross-sectioned ellipses are the only feasible locations at which the proximate aircrafts around A_0 can be assumed to be located, as highlighted in the figure. For clarity, only one scattering point is mentioned by S_a which is one possible location of scattering aircraft. Distance from GS to scattering aircraft S_a and from S_a to A_0 are denoted by d_{GS} and d_{SA} respectively, as shown in the Fig. 4.5. Let r_p is the radius of the pth circle while a_{eq} and b_{eq} are the major and minor axis of qth plane cross-section ellipse, where $p = 1, 2, \cdots, P$ and $q = 1, 2, \cdots, Q$. The innermost concentric circle is of radius r_1 which is the minimum safe-separation distance bound to fulfill the requirement of collision avoidance, i.e. $r_1 = \min(r_1, r_2, \cdots, r_P)$. Due to the characteristics of any multipath propagation environment, multiple copies of the same transmitted signal are received at the receiver with different time delays and path losses. Since, the prolate spheroid follows the properties of the ellipse; therefore, the multipath components coming from any proximate scattering aircraft A_k located on the same elliptic ring (say q^{th} elliptic ring) will arrive at the receiver antenna of A_0 with identical delay τ_q traversing the same distance $d_{GS_q A_0}$ such that $d_{GS_q A_0} = d_{GS_q} + d_{S_q A_0}$, as shown in Fig. 4.5. Therefore, these multipaths will add up in-phase. If a LOS propagation path exists between G and A_0, which

is conceivably a definite case in G2A communication environment, then the first signal component will arrive at the receiver with delay $\tau_0 = d_0/c$, where c is the speed of light and d_0 is the LOS distance between A_0 and G.

Following the properties of prolate spheroid, the distances d_{GS_q}, d_{S_qA} and the length of major axis of qth prolate spheroid $2c_{pq}$ together satisfy the condition as

$$d_{GS_q} + d_{S_qA_0} = 2c_{pq} \tag{4.6}$$

Since, $\tau_q = \frac{d_{GS_qA_0}}{c}$, therefore, in terms of delay τ_q, this can be written as

$$d_{GS_q} + d_{S_qA_0} = c\tau_q \tag{4.7}$$

Combining Eq. (4.6) and Eq. (4.7) the delay of scattering aircraft S_q lying on q^{th} elliptic ring can be obtained as

$$\tau_q = \frac{2c_{pq}}{c} \tag{4.8}$$

Hence, the lengths of semi-major axis c_{pq} and semi-minor axis a_{pq} of the qth prolate spheroid can be written as

$$
\begin{aligned}
c_{pq} &= \frac{c\tau_q}{2} \\
a_{pq} &= \frac{1}{2}\sqrt{4c_{pq}^2 - d_0^2}
\end{aligned}
\tag{4.9}
$$

Whereas, the eccentricity of the qth prolate spheroid can be defined in terms of the radial distance d_0 and the delay τ_q of multipath signal via proximate aircraft located on the qth prolate spheroid.

$$e_q = \frac{d_0}{c\tau_q} \tag{4.10}$$

4.3.5   G2A Multipath Channel Model

A reliable performance analysis of G2A communication link needs a realistic G2A channel modeling, which further necessitates a detailed interpretation of G2A

physical channel environment. In reality, a radio signal when reflected by a scattering object reaches at the receiver in the form of a cluster of numerous components having approximately the same mean power, angle and delay [147]. We term this cluster as a single multipath of the transmitted signal with a specific delay. In this channel model, $L - 1$ number of multipaths are considered to be coming from $K - 1$ proximate scattering aircrafts located around A_0, as shown in Fig. 4.5. A real-valued passband transmit signal $\widetilde{x}(t)$ with carrier frequency f_c along with a baseband transmit signal $x(t)$ can be written as

$$\widetilde{x}(t) = \Re\left[x(t)e^{j2\pi f_c(t)}\right] \tag{4.11}$$

The transmitted signal passes through scattering environment of $L - 1$ different propagation paths other than the LOS path. Relative movement of the aircraft in the environment introduces doppler frequency shifts to the incident waves. The doppler shifts for lth plane wave arriving at the receiver antenna with angle θ_l is denoted as

$$f_{d_l} = f_m \cos(\theta_l) \tag{4.12}$$

where, $f_m = \frac{v}{\lambda}$ is the maximum doppler frequency shift with aircraft speed v and wavelength λ. Due to the high mobility of aircrafts, the reflected components would suffer with doppler effects causing shift in the carrier frequency. The passband received signal passing through L different propagation paths can be expressed as

$$\widetilde{y}(t) = \Re\left[\sum_{l=0}^{L-1} \alpha_l(t)e^{j2\pi(f_c+f_{d_l})(t-\tau_l)}x(t-\tau_l)\right] \tag{4.13}$$

where f_c is the radio carrier frequency and α_l, τ_l and f_{d_l} are the attenuation, delay and the doppler shift associated with the lth received signal component coming through l^{th} propagation path. The delay $\tau_l = \frac{d_l}{c}$ is the propagation time required for the signal coming through the lth propagation path, where d_l represents the length of the lth path and c is the speed of light. The path length d_l depends upon the physical properties of the aircraft scattering geometry, as explained earlier in the above section.

Similar to Eq. (4.11), the received bandpass signal $\widetilde{y}(t)$ can also be expressed in

combination with baseband signal $y(t)$ as

$$\widetilde{y}(t) = \Re\left[y(t)e^{j2\pi f_c(t)}\right] \tag{4.14}$$

where the received complex envelope is given by

$$y(t) = \sum_{l=0}^{L-1} \alpha_l(t)e^{j\phi_l(t)}x(t-\tau_l) \tag{4.15}$$

where

$$\phi_l(t) = 2\pi\{f_{d_l}t - (f_c + f_{d_l})\tau_l\}$$

The corresponding time-variant channel impulse response of G2A multipath propagation environment having L propagation paths can be written as

$$h(t,\tau) = \sum_{l=0}^{L-1} \alpha_l(t)e^{j\phi_l(t)}\delta(\tau - \tau_l(t)) \tag{4.16}$$

where $\delta(.)$ is the dirac delta function. The attenuation factor $\alpha_l(t)$, depends on the path-loss of the propagation path and the cross-sectional area of the reflecting surface through which the reflected signal is reradiated towards the receiver. By analyzing the dependency of ϕ_l over doppler frequency and the delay, this can be concluded that it will vary with time as the doppler frequency and the delay changes. An equivalent representation of channel model in terms of direct LOS ray and indirect diffused rays from the scattering aircrafts can be expressed as

$$h(t,\tau) = h_{LOS} + h_{NLOS} \tag{4.17}$$

where,

$$h_{LOS} = \alpha_0(t)e^{j\phi_0(t)}\delta(\tau - \tau_0)$$
$$h_{NLOS} = \sum_{l=1}^{L-1} \alpha_l(t)e^{j\phi_l(t)}\delta(\tau - \tau_l(t))$$

4.3.5.1 Wide-Beam Communication Link

In wide-beam communication link scenario, the G2A transmitter radiates EM waves towards all aircrafts by generating a fixed directed wide-beam towards the sky that covers a large geographical airspace and provides coverage to K number of aircrafts (i.e. A_0 and $K - 1$ scattering aircrafts). An illustration of wide-beam communication link scenario is depicted in Fig. 4.6. The fundamental objective of a multiuser communication system is to provide the ability of accommodating many subscribing units over the same channel with minimal mutual interference. Code Division Multiple Access (CDMA) is one globally-accepted multiplexing technique that works on the principle of Multi-user Detection (MUD) and multiplexes the data of various users by their unique signature sequences (distinct PN sequences). In CDMA-based communication systems, entire bandwidth is assigned to each user over a common radio frequency. The same working principle can be employed to design a communication system for G2A communication.

Consider that a CDMA-based G2A base station is communicating with K number of aircrafts A_k flying in coverage region of GS, where $k = 0, 1, 2, \cdots, K - 1$.
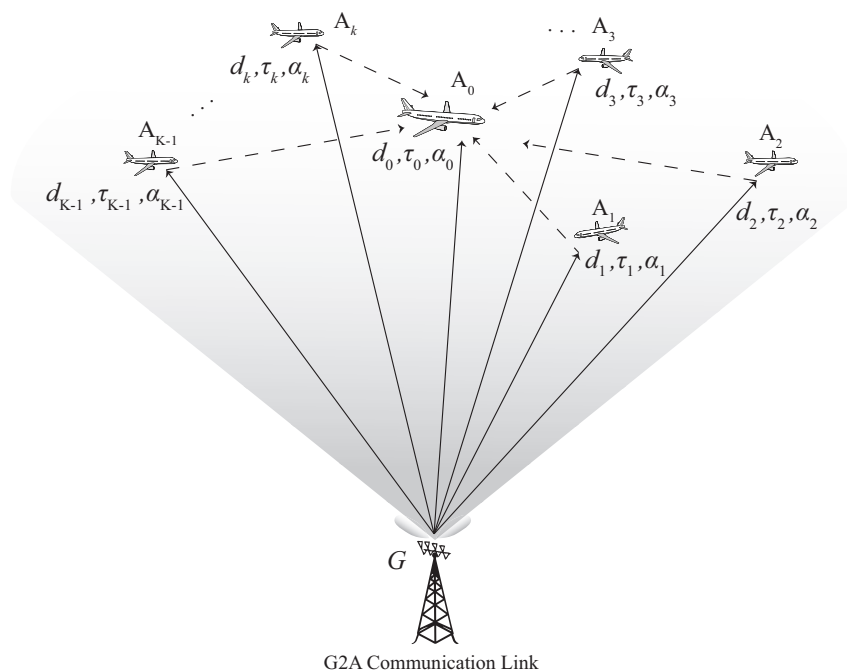
FIGURE 4.6: G2A wide-beam based communication link scenario.

An illustration of wide-beam based communication scenario is shown in Fig. 4.6. Unique signature sequence of length K and duration T_s is assigned to each aircraft to extract its information symbols from the composite signal transmitted by GS, where K is the spreading gain of the PN sequence and T_s is the symbol duration. The composite baseband CDMA signal vector of all the aircrafts can be written as

$$\mathbf{x}(t) = \sum_{k=0}^{K-1} b_k \mathbf{c}_k(t) \tag{4.18}$$

where, b_k is the information symbols transmitted to the kth aircraft and $\mathbf{c}_k$ is the spreading code sequence vector of the kth aircraft. The signal received at the intended aircraft A_0 will be a composite signal carrying information of all the aircrafts A_k connected with the same GS. In order to extract the symbol information from the composite received signal, the aircraft A_0 correlates composite signal with its own signature sequence c_0. Similarly, with the same procedure, each aircraft A_k in the system can extract its information symbol separately.

As discussed earlier in the above subsections, the proximate scattering aircrafts around the intended aircraft A_0 form a multipath environment; therefore, the received signal at the aircraft A_0 would be a combination of LOS component and delayed multipaths components. Following single-bounced multipath geometry, the received baseband signal having L multipath components can be written as

$$\mathbf{y}(t) = \sum_{l=0}^{L-1} \alpha_l(t) \mathbf{x}(t - \tau_l) + \mathbf{n}(t) \tag{4.19}$$

This expression can also be written as

$$\mathbf{y}(t) = \sum_{l=0}^{L-1} \sum_{k=0}^{K-1} \alpha_l(t) b_k \mathbf{c}_k(t - \tau_l) + \mathbf{n}(t) \tag{4.20}$$

From the expression, it can be conveniently observed that L multipath components of composite signal including LoS component are received at A_0 in which each component carries the desired information of A_0 along with interfering content of the $K - 1$ multiuser interferers (i.e. of $K - 1$ proximate aircrafts).

4.3.5.2   Narrow-Beam Communication Link Scenario

In narrow-beam communication link scenario, it is assumed that the ground station (G) is equipped with smart antenna system and is capable of radiating separate directed radio beams through its advanced spatial-processing capability towards each aircraft A_k present in the coverage region of G. Spatial Division Multiple Access (SDMA) based communication is the most sophisticated utilization of physical communication channel with only angular separation among users in a multiuser system. An illustrative representation of narrow-beam based communication link scenario is shown in Fig. 4.7. SDMA-based communication system accommodates various users by assigning separate spatial signatures on the basis of their physical location in view of the transmitter. Through sophisticated utilization of space, it can increase the capacity of the system by reusing frequency, with simultaneous transmissions. The same working methodology of SDMA -based communication system can be employed to design a narrow-beam communication system for G2A communication.
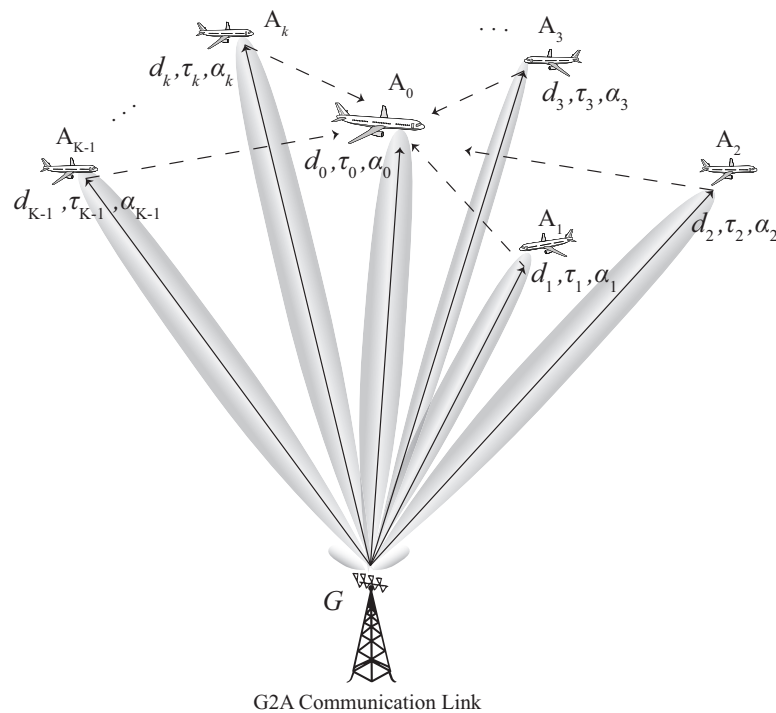
FIGURE 4.7: G2A Narrow-beam communication link scenario.

Consider an SDMA-based G2A base station (G) is communicating simultaneously with K number of active aircrafts A_k flying in the coverage region of G, where $k = 0, 1, 2, ..., K - 1$. Moreover, it is assumed that ground station G is equipped with adaptive planar antenna arrays with $M \times N$ antenna elements and is capable of radiating highly directional narrow beams towards aircrafts A_k while tracking their precise location in the space. An illustrative scenario of narrow-beam based G2A communication system is presented in Fig. 4.7. The ground station G separates the data streams of each connected aircraft A_k by assigning associated beamforming matrices $\mathbf{W}_0, \cdots, \mathbf{W}_{K-1}$ of dimension $M \times N$ to all the connected aircrafts A_k over the same channel. Hence, the signal received at the intended aircraft A_0 can be written as follows

$$y(t) = \sum_{l=0}^{L-1} \sum_{k=0}^{K-1} \sum_{m=0}^{M} \sum_{n=1}^{N} w_{mn}^k a_{mn}(\theta_l, \phi_l) \alpha_l(t) s_k(t - \tau_l) + n(t) \qquad (4.21)$$

where, w_{mn}^k is the mn^{th} entry of kth beamformer for aircraft A_k, $a_{mn}(\theta_l, \phi_l)$ is the response of mn^{th} antenna element of planar antenna to a path in direction (θ_l, ϕ_l), $\alpha_l(t)$ is the fading coefficient associated with l^{th} signal propagation path in G2A communication link, $s_k(t)$ is the information symbol of the nth aircraft and $n(t)$ is an additive white gaussian noise. From the above expression, it can be clearly observed that L multipath components of composite transmitted signal received at A_0 carry desired information of A_0 as well as the interfering content of the $K - 1$ multiuser interferers connected with G2A communication link.

4.4 Model Limitations

Though the proposed geometric ground-to-air model encompasses all the physical parameters of the channel and reflecting/scattering surfaces; however, there are some limitations of the proposed model. Those can be listed as under.

1. The model does not address multi-altitude G2A multipaths geometry. Only those multipath components are accommodated that arrive to the intended

aircraft via proximate scattering aircrafts flying at the same altitude of the intended aircraft. multipaths coming

2. The model does not encounter time-variations of the G2A multipath propagation environment.

Chapter 5

G2A Channel Characterization and Multi-Aircraft Interference Modeling

This chapter characterizes G2A channel model and models multi-aircraft interference in presence of proximate aircrafts around the intended aircraft. Section 5.1 provides a brief introduction to the fundamental parameters of the G2A communication channel model and develops an expression for total signal power received at the intended aircraft coming from the ground station. In section 5.2, simulation procedure is explained in detail and results are presented. A visualized interpretation of interference caused in wide-beam and narrow-beam G2A communication link scenarios is discussed in Section 5.3.

5.1 G2A Communication Channel Model

5.1.1 RADAR Cross Section (RCS)

In RADAR systems theory, RADAR Cross-Section (RCS) of scattering object is defined as the ratio between the power density of the radio waves impinged on a

scattering object and the power density scattered in the direction of the radar's receiving antenna. Eq. (3.1), presents the BRCS (σ_B) in complex electric field amplitudes. In situations, when both the transmitter and receiver antennas are placed at different locations by maintaining a considerable distance, the RADARs are known as bistatic radars whereas the RCS is termed as Bistatic RADAR Cross Section (BRCS). The formation of RCS collectively depends upon incident angle of impinging wave, bistatic angle, reflection and absorption properties of the reflecting surface, geometry of the object and the polarization of electromagnetic wave at the reflecting object and the receiver. These terms compositely make it complex to evaluate RCS of a scattering object. The geometry of the bistatic radar based scenario for our proposed model is demonstrated in Fig. 5.1, where a bistatic signal is illustrated to be received at the aircraft A_2 as a result of the reflection from aircraft A_1 making bistatic angle θ_B. In the figure, d_1 represents the distance of target aircraft A_1 from the transmitter and d_2 represents the distance between aircrafts A_1 and A_2. One counterpart of RCS is the spatial reflection coefficient (SRC) that represents the same information while being used in different field of research [99]. The interdependence relation between RCS (σ_B) and SRC (Γ) is given in Eq. (3.7).
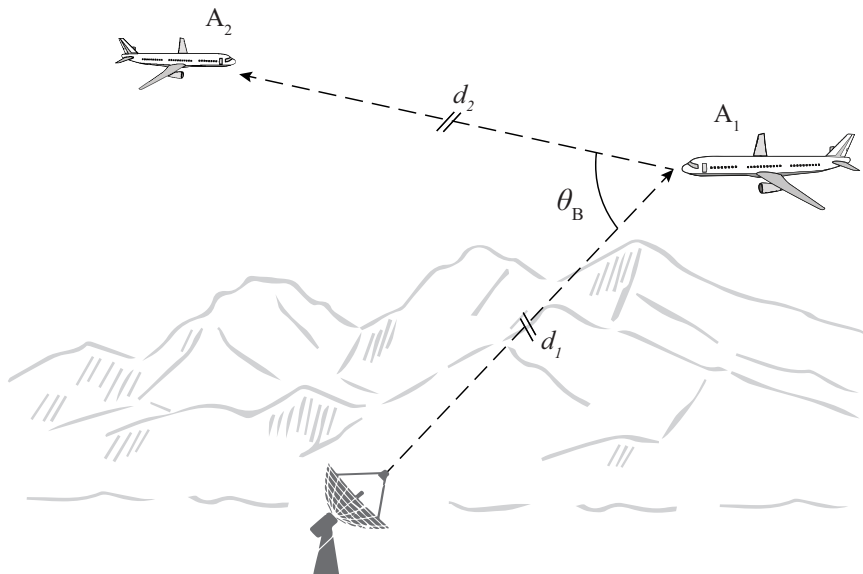

FIGURE 5.1: A demonstrative scenario of bistatic signal reflection from the surface of aircraft A_1 on to A_2.

5.1.2 Aircraft Free-Space Radio Propagation Model

In this section, we intend to develop received signal model for the proposed G2A propagation channel presented in chapter 4 of this thesis. In this model, the Frii's free-space equation is used to express the total amount of power received at the intended aircraft (A_0) coming from the ground station via multiple paths. The Frii's free space propagation model is usually used to express the received signal strength when there is no obstructor between transmitter and receiver. It predicts the decay of the received power as a function of separation distance between a transmitter and a receiver raised to some power i.e. a power law function. Ground-to-Air (G2A) communication can be considered as a free-space propagation with a direct line-of-Sight (LoS) present at most of the time. Consider a G2A wireless communication scenario, as illustrated in Fig. 5.2. For simplicity, only one scattering aircraft other than the intended aircraft is considered. let $d_{\mathrm{GA_0}}$, $d_{\mathrm{GA_1}}$ and $d_{\mathrm{A_1A_0}}$ denote distance from ground station (GS) to the intended aircraft A_0, GS to scattering aircraft A_1 and aircraft A_1 to A_0 respectively, as shown in the figure. Assume the G2A wireless transmitter radiates electromagnetic waves in the transmitting direction with peak power output P_t and directive transmit gain G_t. Consider that the scattering aircraft A_1 re-radiates part of the received power to the intended aircraft A_0, as shown in Fig. 5.2. The received power density at aircraft A_1 with distance $d_{\mathrm{GA_1}}$ from a transmitting antenna can be represented as

$$P_r^{\mathrm{A_1}} = \frac{P_t G_t}{4\pi d_{\mathrm{GA_1}}^2} \tag{5.1}$$

Depending upon the cross sectional size of the aircraft A_1, the surface of the aircraft may intercept some part of the radiated power and re-radiates it in all possible directions. The measure of the intercepted power depends upon the size, orientation, physical shape and material of the aircraft. Since, BRCS specifies the ability of reflecting electromagnetic signals towards a specific direction; therefore, all the above-mentioned factors can be lumped together in one target-specific parameter, BRCS discussed in Sec. 5.1.1. It is the ratio of the reflected power to the incident power intercepted by the aircraft. The RCS of the scattering aircraft
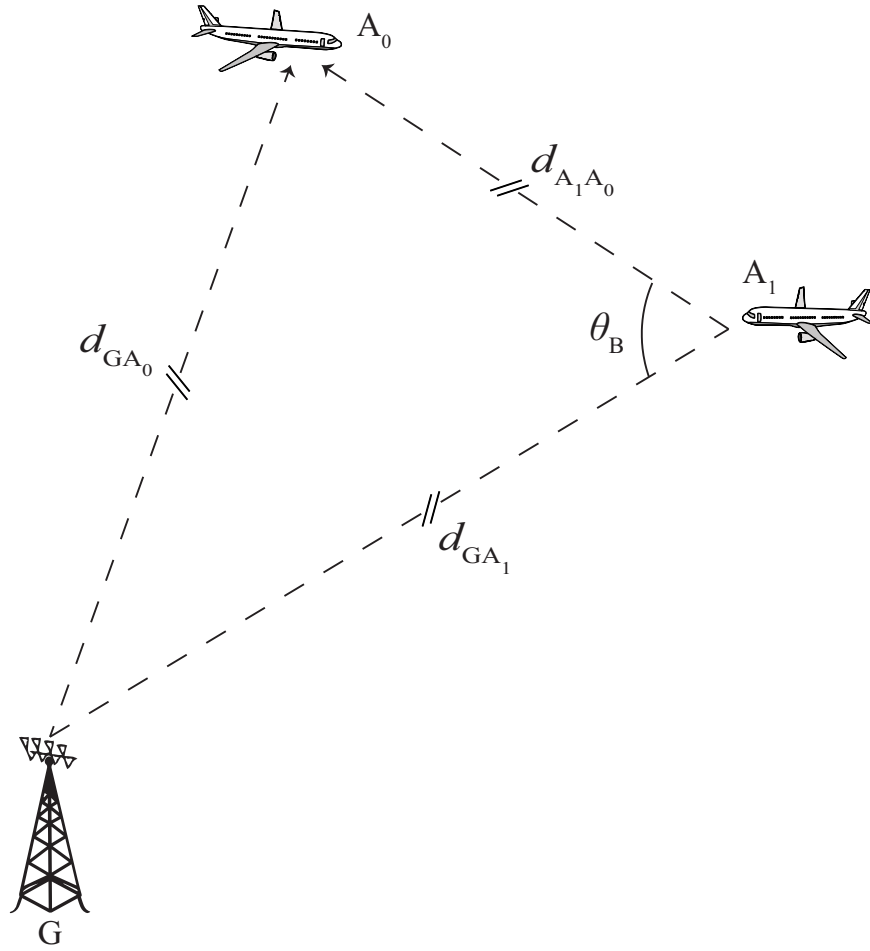
FIGURE 5.2: An illustration of G2A signal propagation geometry.

A_1 can be defined as

$$\sigma(\theta_i, \phi_i, \theta, \phi) = \frac{P_{\text{ref}}}{P_r^{A_1}} \quad \text{m}^2 \tag{5.2}$$

which implies that

$$P_{\text{ref}} = \sigma(\theta_i, \phi_i, \theta, \phi) P_r^{A_1} \tag{5.3}$$

where P_{ref} is the total amount of power reflected from the surface of the aircraft A_1 and $P_r^{A_1}$ is the amount of power density received by the aircraft A_1. Thus, the total power density received by the intended aircraft A_0 via scattering aircraft A_1 can be expressed as

$$P_r^{A_1 A_0} = \frac{P_{\text{ref}}}{4\pi d_{A_1 A_0}^2} \tag{5.4}$$

by substituting the expression of P_{ref}, the equation becomes

$$P_r^{\text{A}_1\text{A}_0} = \frac{\sigma(\theta_i, \phi_i, \theta, \phi)P_r^{\text{A}_1}}{4\pi d_{\text{A}_1\text{A}_0}^2} \tag{5.5}$$

by incorporating Eq. (5.1) in Eq. (5.5), the total power received at the receiver antenna of aircraft A_0 having an effective aperture A_e is

$$P_r^{\text{A}_1\text{A}_0} = \frac{P_t G_t A_e \sigma_{\text{B}}(\theta_i, \phi_i, \theta, \phi)}{(4\pi)^2 d_{\text{GA}_1}^2 d_{\text{A}_1\text{A}_0}^2} \tag{5.6}$$

utilizing expression $A_e = \frac{G_r \lambda^2}{4\pi}$, the total power received at the intended aircraft A_0 via aircraft A_1 can be expressed as follows:

$$P_r^{\text{A}_1\text{A}_0} = \frac{P_t G_t G_r \lambda^2 \sigma_{\text{B}}(\theta_i, \phi_i, \theta, \phi)}{(4\pi)^3 d_{\text{GA}_1}^2 d_{\text{A}_1\text{A}_0}^2} \tag{5.7}$$

In addition to the power received by A_0 via A_1, the aircraft A_0 also receives signal power directly from the ground communication link as,

$$P_r^{\text{GA}_0} = \frac{P_t G_t G_r \lambda^2}{(4\pi)^2 d_{\text{GA}_0}^2} \tag{5.8}$$

Hence, the total power received at the aircraft A_0 can be expressed as follows

$$P_{\text{r}} = \frac{P_t G_t G_r \lambda^2}{(4\pi)^2 d_{\text{GA}_0}^2} + \frac{P_t G_t G_r \lambda^2 \sigma_{\text{B}}(\theta_i, \phi_i, \theta, \phi)}{(4\pi)^3 d_{\text{GA}_1}^2 d_{\text{A}_1\text{A}_0}^2} \tag{5.9}$$

5.2   Simulation Results and Discussion

In order to analyze the proposed G2A communication channel model a quasi-realistic simulation scenario is developed in this section. For this purpose, the simulation procedure consists of three steps with the ultimate goal of generating power delay profile (PDP) of G2A communication environment. At first, multipath components of the transmitted signal in the proposed G2A propagation environment are generated using the proposed geometry discussed in chapter 4 of this thesis. Secondly, the bistatic RCS (BRCS) of each scattering aircraft is

estimated that provides one of the afore-mentioned NLoS multipaths as a result of reflection from the surface of the aircraft. Finally, PDP of the proposed model is generated by combining the power from all the multipaths with their respective delays.

5.2.1   Environment Description and Ray-Tracing

In this section, we intend to form a quasi-realistic G2A propagation environment in Matlab® for the time dispersive analysis of the G2A communication system. The model gives an insight of real G2A communication environment by incorporating safe-separation distance and prospective scatterers around the intended aircraft, as presented in Fig. 5.3. This model is further used to extract the parametric information of G2A communication channel. For simulation purpose, the intended aircraft and the proximate scattering aircrafts are assumed to be located at a constant altitude of 30 km from the ground while maintaining a safe-separation distance of 10 Km from each other. For simplicity, only two circular rings of radius 10 and 20 Km are considered, which are the conceivable boundary/locations of the proximate scattering aircrafts at which they can fly by keeping the minimum safe separation distance. Although, some more scattering aircrafts can be accommodated on the second circular ring; however, the reflected signals coming via those aircrafts will reach with larger delays and negligible power. As shown in the figure, the positions of the scattering aircrafts are the intersecting points between the circular and elliptical rings as explained in Sec. 4.3.4. Depending upon the assumed scenario, a total of 12 scattering aircrafts can be placed around the intended aircraft, among them 6 aircrafts reside on first circular ring and the other 6 reside on the second circular ring. Hence, in the designed scenario, a total of 12 multipath components excluding LoS component may arrive at the receiver of the intended aircraft. Three elliptic rings are shown in the figure, which are the result of the cross section of the plane and the prolate spheroid at its focal point where the intended aircraft is located. The details of plane cross sectioned ellipse are given in the chapter 4 of this work. For better understanding, the top view of
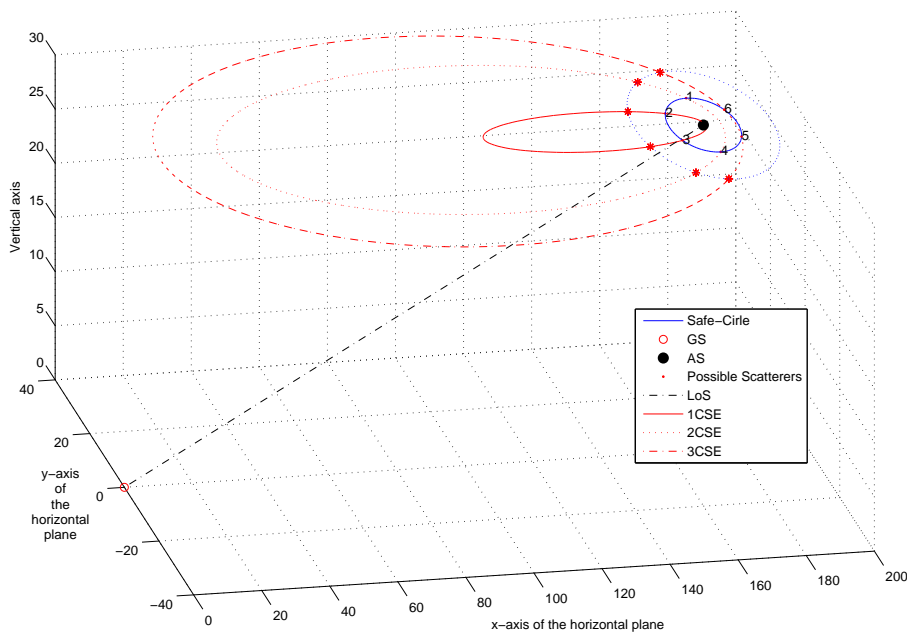
FIGURE 5.3: Ground-to-Aircraft 3D propagation model.

G2A propagation model is shown in Fig. 5.4. From the figure, it can be observed that among the 6 scattering aircrafts, 2 reside on the first elliptic ring, 2 on the second and 2 on the third elliptic ring. The same is the case for aircrafts located on the outer circular ring. In Fig. 5.5(a) and Fig. 5.5(b), formation of propagation paths having identical path lengths via scattering aircrafts residing on inner and outer circles is shown. From the figures, it can be seen that some paths have the same propagation path lengths. Fig. 5.5(a) shows that the three unique path lengths that emerge due to the signals coming via the 6 aircrafts present on the inner circle are 174.3174, 183.0523 and 191.3670. Likewise, the same propagation path lengths 174.3174, 183.0523 and 191.3670 are also experienced by the signals coming via aircrafts located on the outer circle. As discussed in chapter 4 of this research work, prolate spheroid follows the same properties of the ellipse; therefore, multipath components coming through scattering aircrafts located on the same elliptic ring will reach at the receive antenna of the intended aircraft with identical delay (τ) traversing the same distances. In short, the equidelay multipaths will add up in-phase at the receiver as shown in Fig. 5.6, where all possible multipaths
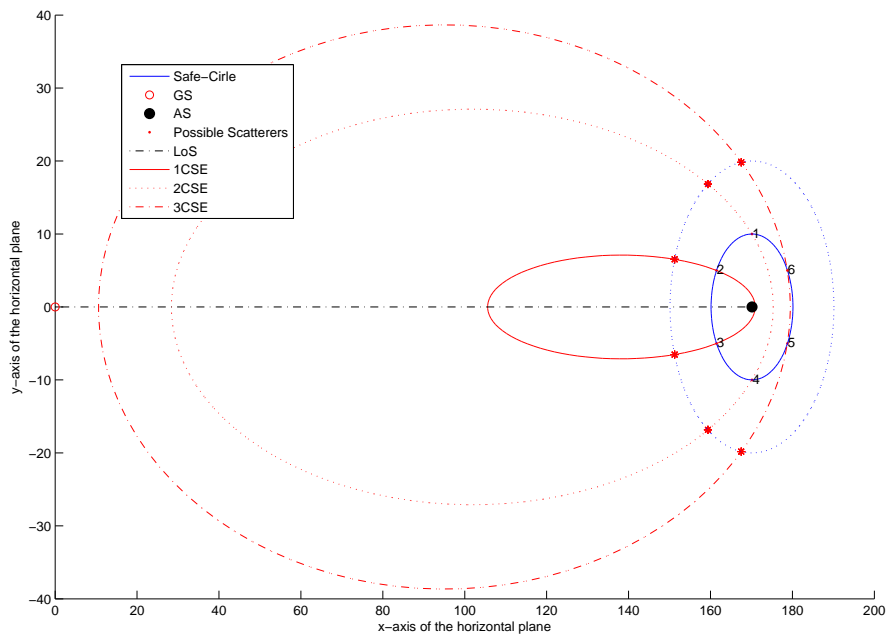
FIGURE 5.4: Top view of the G2A 3D propagation model.

along with line-of-sight (LoS) signals are shown with their respective frequency of occurrence. Uniting all the multipaths of the proposed scenario, Fig. 5.6 gives a precise information of the number of occurrence about all multipaths with different equidelay stems. The figure also explains that all scattering aircrafts associated with the same path lengths are located on the same prolate spheroid with the transmitter and receiver at its focal points. It is also worth observing that all 12 proximate scattering aircrafts form three unique equidelay multipaths. However, the number of equidelay multipaths depends upon the location of the scattering aircrafts, with respect to the intended aircraft and the ground station.

5.2.2   BRCS Approximation of Scattering Aircrafts

As discussed earlier in subsection 5.1.1, RCS and reflection coefficients have inter-dependence on each other; therefore, RCS can be used interchangeably to extract the reflective properties of scattering aircrafts. Therefore, in order to observe
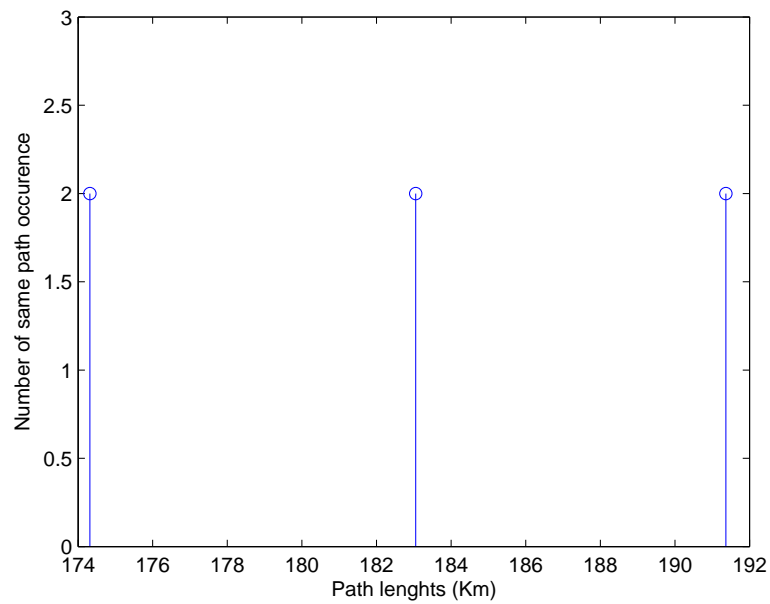
(a) Inner Circle.
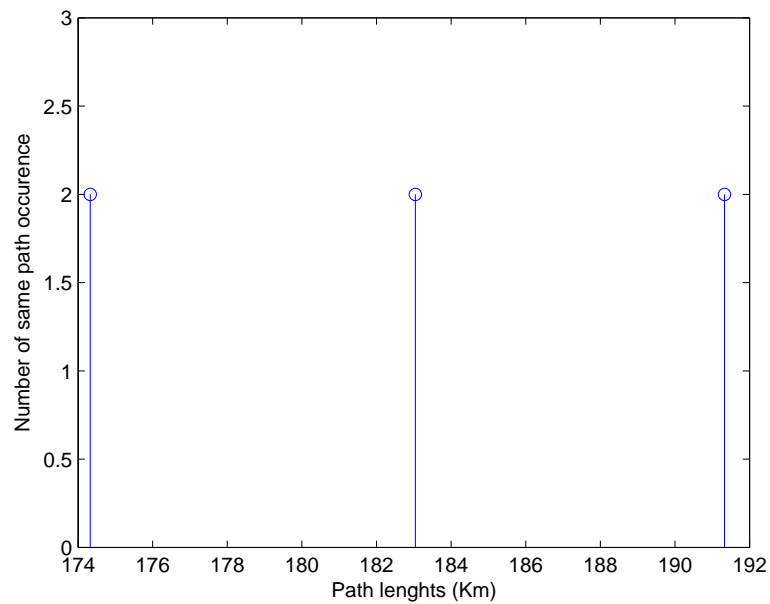
(b) Outer Circle.

FIGURE 5.5: Frequency of occurrence of the propagation path lengths of the signals coming via scattering aircrafts located on inner and outer circles.

the reflection properties of the scattering aircrafts in our proposed G2A propagation scenario, RCS of scattering aircrafts is required. For this purpose, scattering/reflection properties of the incident electromagnetic (EM) waves from the surface of the scattering aircrafts are acquired using a facet-based model of aircraft
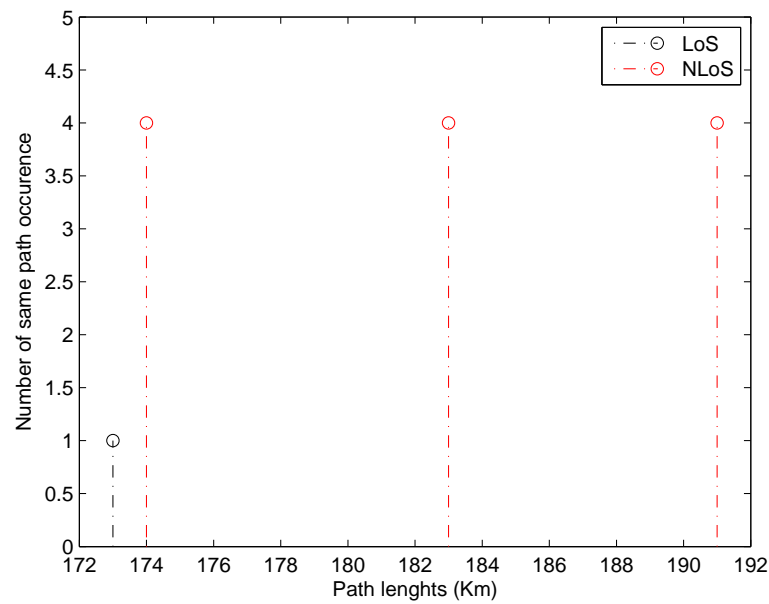
FIGURE 5.6: Propagation path lengths of signals coming from scattering aircrafts and their occurrences.
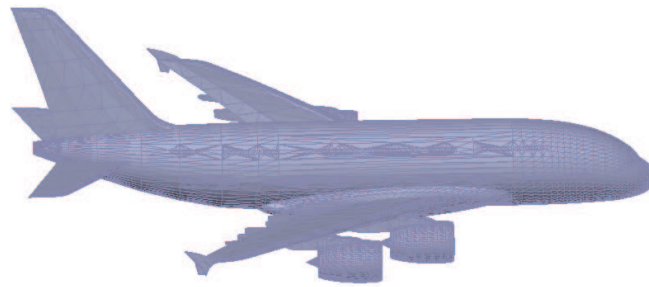
FIGURE 5.7: Facet-based model of aircraft A380®.

A380® and a MATLAB-based physical optics simulation tool POFACET®. For more details about Facet-based modeling and POFACET® the reader may consult to [99, 102, 103]. Since, POFACET® requires a facet-based model of A380® to predict its RCS; therefore, AnyCAD® software is used to generate its facet-based representation, as shown in Fig. 5.7. The simulations are performed in spherical coordinate system using incident angles (θ_i, ϕ_i) and observation angles $(\theta, \phi,)$, where θ is elevation angle and ϕ is azimuth angle. As the proposed model is considered to be static; therefore, the incident angles of the transmitted signal on the surface

of aircraft would be fixed. Though, BRCS can be evaluated over a wide range of observation angles equivalent to spherical geometry in the range $0 \leq \theta \leq \pi$ and $0 \leq \phi \leq 2\pi$. However, since all the aircrafts are presumed to be steady with fixed height; therefore, BRCS only at zero-elevation plane (i.e. $\theta = 0°$) is needed to be estimated with observation angles ranging from $0 \leq \phi \leq 2\pi$. Following the geometry of the proposed G2A communication model, incidence angles of radio signals impinged on the surface of aircrafts can be measured. For instance, the incident angles pertaining to a particular scattering aircraft positioned at (170.1385,10,30) are $\theta_i = 260.0169°$ and $\phi_i = 183.3637°$ and its corresponding observation angle at the intended aircraft in azimuth plane is $\phi = 270°$. The estimated BRCS (σ_B) related to the above-mentioned incident angle in azimuth plane are shown in the Fig. 5.8 and the BRCS observed at the intended aircraft for $\phi = 270°$ is 52.07 dBsm. In the same manner, BRCS observations of each scattering aircraft with its respective incident and observation angles can be estimated at the intended aircraft. Table. 5.1 gives a summary of the parameters involved in the calculation of BRCS i.e. the positions of aircrafts, POFACET incident angles, and observation angles with respect to the intended aircraft along with their resulting BRCS observed at the intended aircraft.
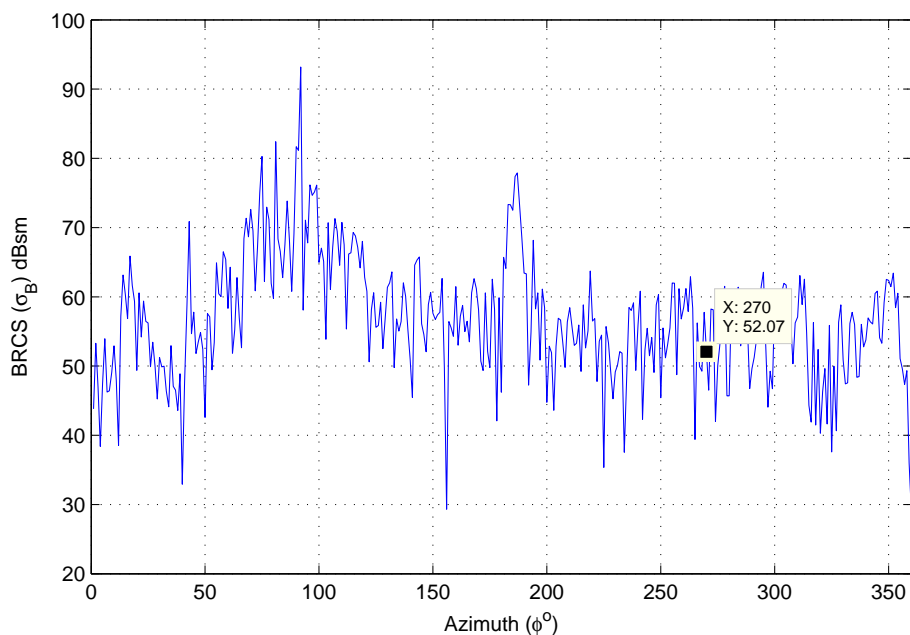

FIGURE 5.8: BRCS of a scattering aircraft in azimuthal plane.

TABLE 5.1: Summary of the parameters involved in the calculation of BRCS, along with their resulting BRCS observed at the intended aircraft.

Position of aircraft (*x,y,z*)	POFACET Incident angles ($\theta_i^\circ, \phi_i^\circ$)	Observation Angle ϕ°	BRCS(dBsm) $\sigma_B(\theta_i, \phi_i, \theta, \phi)$
(170.1385,10,30)	(260.0169,183.3637)	270	52.0704
(161.4782,5,30)	(259.4803,181.7735)	330	56.0249
(161.4782,5,30)	(259.4803,178.2265)	30	59.6778
(170.1385,-10,30)	(260.0169,176.6363)	90	60.8729
(178.7987,-5,30)	(260.4789,178.3982)	150	60.6082
(178.7987,5,30)	(260.4789,181.6018)	210	50.5264
(151.2395,6.5205,30)	(258.7905,182.4687)	340.9647	51.1834
(151.2395,-6.5205,30)	(258.7905,177.5313)	19.0353	53.5233
(159.3688,16.843,30)	(259.3969,186.0329)	302.5954	52.5196
(159.3688,-16.843,30)	(259.3969,173.9671)	57.4046	60.0943
(167.5154,19.8213,30)	(259.9155,186.7482)	277.5385	40.9153
(167.5154,-19.8213,30)	(259.9155,173.2518)	82.4615	67.8923

5.2.3   Power Delay Profile of G2A Communication Channel

Multipath propagation in wireless communication channel causes severe degradation of the transmitted radio signal at the receiver due to destructive interference. The time dispersive nature of the channel is usually determined through power delay profile also known as multipath intensity profile. This indicates the expected degree of time-dispersion and gives a distribution of average power of various paths associated with a specific multipath delay. In G2A wireless communication environment, a signal transmitted by GS may arrive at the receiver of the intended aircraft via various multipath as a result of reflections or scattering from the proximate scattering aircrafts. Utilizing the geometry of the proposed G2A communication model and acquiring signal reflection properties of the surface of the aircraft, the power delay profile of the model can be estimated. Fig. 5.9 presents a normalized power delay profile of the G2A communication channel pertaining to the given example scenario. Here, the excess delay and average received power is normalized by the delay and power of the first path (i.e LoS path). In

the Figure, there are four rays, one for the direct path with zero delay (i.e. $\tau = 0$) and the remaining three paths are the reflections from the proximate scattering aircrafts with delay $\tau_q > 0$, where $q = 1, 2, 3$. In this model, the mean excess delay ($\overline{\tau}$) and RMS delay spread (σ_τ) are measured to be 0.00212 ms and 0.0103 ms respectively. These are the effective channel parameters that give a basis for the performance comparative analysis of various multipath radio channels and provide guidance in designing a wireless communication system. It is worth mentioning here that if the delay spread exceeds a symbol duration (T_s) the received signal gets contaminated with inter symbol interference (ISI). In general, coherence BW (B_c) is considered inversely-proportional to the RMS delay spread (σ_τ); however, no exact relationship exists between them [112]. As a rule of thumb, the coherence bandwidth with a correlation level of 0.9 is defined as $B_c \approx \frac{1}{50\sigma_\tau}$, that yields $B_c = 1.9448$ kHz in our G2A communication channel case. A common rule of thumb representing flat fading is when $T_s \geq 10\sigma_\tau$ and frequency selective fading when $T_s < 10\sigma_\tau$ for a correlation level of 0.7 approximately. In that case, $B_c \approx \frac{1}{10\sigma_\tau}$ yields B_c equals to 9.7238 kHz. Hence, the system may guarantee $R_s = 9.72$ ksps with a symbol duration of $T_s = 0.1028$ ms without an equalizer and any higher rate beyond this limit will require an equalizer. However, if equalizers are avoided higher data rates can be achieved by intelligently selecting efficient modulation schemes with respect to the time-variations of the channel conditions. In such cases, $R_b = kRs$, where R_b is the achievable bit rate of the G2A communication link and k is the number of bits per symbol.

5.3 Interference Visualization

Interference is a fundamental phenomenon of a wireless propagation environment that limits the performance of wireless systems. It is basically the result of unwanted signals received at the same time when the desired signal arrives. To observe and analyze the interference caused in a communication system, it is essential to understand and visualize the signal propagation mechanism and have a deep understanding of the technique employed for the transmission and reception
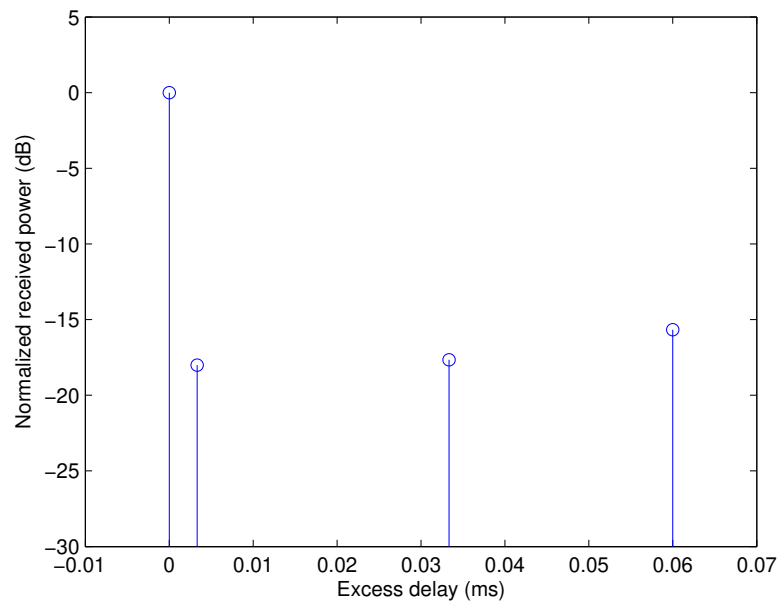
FIGURE 5.9: Normalized power delay profile of the proposed G2A communication system model.

of the signal. Here, we intend to give a visual understanding of the interference caused in both cases of G2A communication environments discussed in chapter 4 of this research i.e. wide-beam communication link and narrow-beam communication link. The visual interpretation represents signal power of the intended aircraft, interference power from $K-1$ proximate scattering aircrafts and AWGN noise levels at each excess delay. Considering, the channel models of both scenarios presented in chapter 4 of this research work, the received signal power can be fragmented as follows.

$$P_r = P_0 + P_I + P_n \tag{5.10}$$

where, P_0 is the desired signal power of the intended aircraft A_0, P_I is the sum of the interference powers, $P_I^{(k)}; k = 1, 2, \cdots, K$, caused by $K-1$ proximate scattering aircrafts and P_n is the thermal noise power. Although, the expression of the received power in both scenarios is the same; however, both scenarios possess different proportions of the signal power, interference power, and the thermal noise in each multipath received signal. Fig. 5.10, gives a visual demonstration of a CDMA signal power received at different instants of time. CDMA system methodology accommodates multiple users by utilizing unique orthogonal codes for each
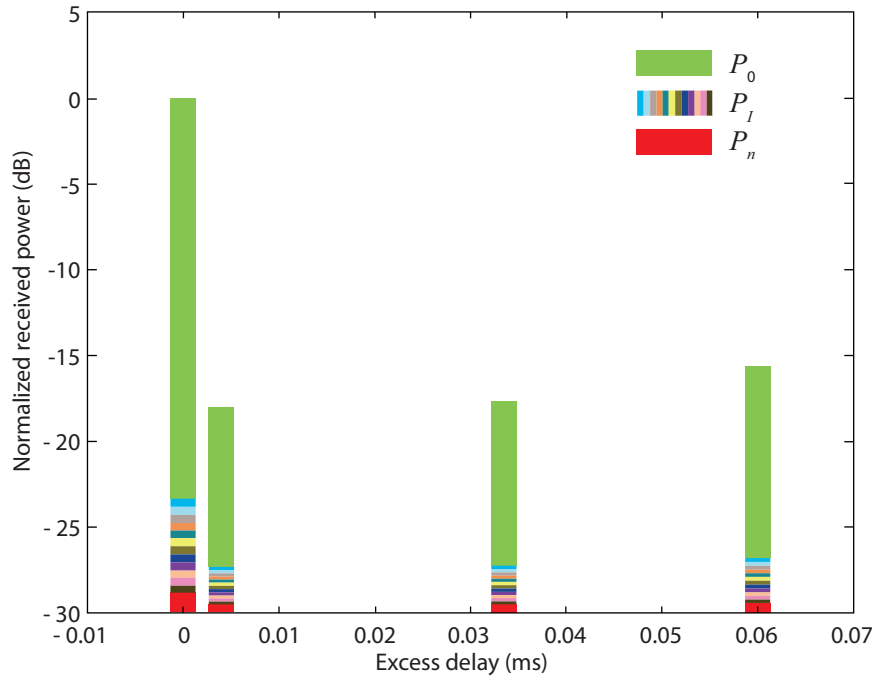
FIGURE 5.10: Wide-beam interference power visualization.

user in the system and makes it possible to share the entire bandwidth with all users. The system treats all users equally and provides them balanced opportunities of communication over the same bandwidth. Thus, the proportion of the transmitted signal power for the intended aircraft would be the same as those for the other proximate aircrafts connected with the same G2A communication link. After despreading the received signal at the intended aircraft would thus include a major portion of the desired signal, a portion of Multiple Access Interference (MAI) depending upon the received correlations of the signatures and the noise power. In the figure, the interfering contributions of proximate aircrafts to the intended aircraft are lumped together as a single interfering entity. If the orthogonality among spreading codes is maintained then MAI would become negligible and the intended aircraft will behave as single user present in the system. It is pertinent to note here that each multipath is a source of interference for the intended aircraft and a properly designed RAKE receiver can serve this purpose efficiently. However, in reality, spreading codes lose their orthogonality in multipath propagation environment and may result in rising MAI that reduces system capacity and bit-error-rate (BER) performance. On the other hand, in narrow-beam commu-
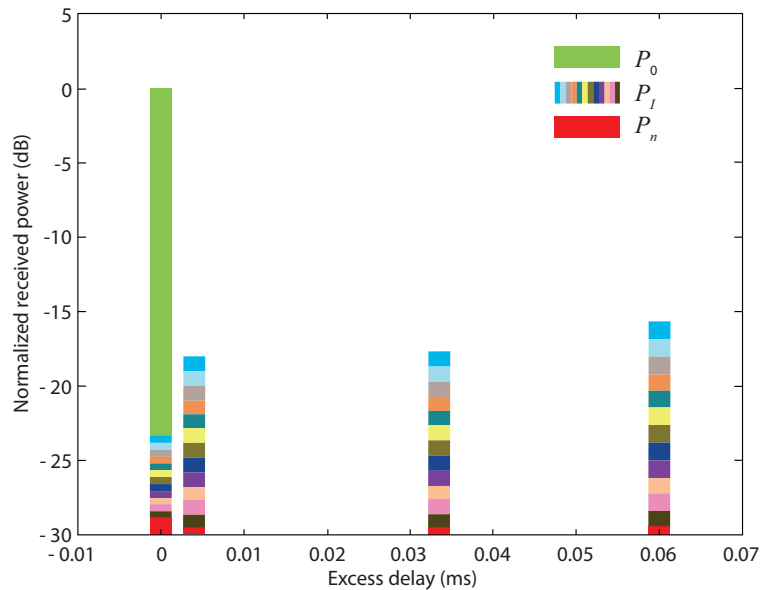
FIGURE 5.11: Narrow-beam interference power visualization.

nication link scenario, the G2A station equipped with smart antenna technology exploits the spatial separation of the aircrafts in airspace and accommodates multiple aircrafts to operate on the same carrier simultaneously. The system enhances transmission quality by directing narrow beams towards the intended aircraft while steering nulls towards other proximate aircrafts of no interest that may become a source of interference. The employed system permits frequency reuse, improves signal-to-inference ratio and reduces transmission power levels. In addition, the deleterious effects of the multipath propagation and co-channel interference can be mitigated by steering nulls towards the multipath generating sources. The system treats each aircraft equally depending upon its physical location in the geographical airspace and tries to maintain optimal transmission power level for it that may result in reducing interference to the proximate aircrafts. Thus, the intended aircraft receives a major part of its information signal from the dedicated radio beam exclusively generated for it through its unique spatial signatures depending upon its position in the airspace. It is pertinent to mention here that in this scenario, the intended aircraft may receive the interfering signals due to the existence of proximate scattering aircrafts around it; however, these signals will be of negligible power and can thus be neglected. Fig. 5.11, presents a visual demonstration of SDMA signal power received at different instants of time. In the figure, the

interfering contributions from proximate scattering aircrafts are mentioned with a single interfering entity.

Chapter 6

Conclusion and Future Work

In this thesis, existing literature on A2G/G2A channel models have been intensively reviewed and appropriate critical comments are given wherever needed. From the literature, it has been observed that most of the published articles supposedly model G2A channels interchangeably in the same way as that of land mobile communication and G2A communication is generally thought to be a line-of-sight (LoS) communication. In this regard, G2A multipath channel has been profoundly analyzed by thoroughly differentiating its attributes from A2G communication link. Moreover, signal propagation mechanism in G2A communication has been conscientiously examined to highlight the existence of multipath environment due to the presence of scattering aircrafts in the vicinity of the intended aircraft. Utilizing all the necessary information, a geometrically-based physical G2A multipath channel model has been proposed. The proposed model is developed on the basis of three-dimensional confocal multipath prolate spheroids following the assumption of single-bounced multipath geometry, where air station and ground station are assumed to be located on their focal points. Moreover, it has been observed that all the scattering aircrafts with the same altitude, causing multipaths of the same propagation length can be assumed to be located on the boundary of the equi-delay elliptic region as a result of cross-section of the prolate spheroid with a horizontally-parallel plane at its focal point. This proposed model can be modified for any G2A multipath propagation scenario with appropriate choice of semi

major and semi minor axes in accordance with the positions of scattering aircrafts around the intended aircraft. The proposed model suitably justifies the existence of multipath scattering environment around the intended aircraft and provides an insight to analyze multiuser G2A communication in the presence of multipath scattering in wide-beam and narrow-beam communication link scenarios. Analytical expressions for the received signal power at the intended aircraft have been formulated for both wide-beam and narrow-beam communication link scenarios. Furthermore, an expression for the total power received at the intended aircraft has been developed and time-dispersive nature of the proposed G2A channel has been analyzed. For time-dispersive analysis of the channel, power delay profiles (PDPs) of the G2A wireless channel have been formulated utilizing multipath propagation geometry of the G2A communication link. For numerical computations, a quasi-realistic G2A propagation environment has been developed in Matlab®. The intensities of the reflected/scattered signals received at the intended aircraft from the surface of proximate scattering aircrafts are predicted with the help of bistatic radar cross section (BRCS). Numerical computations of BRCS have been performed by incorporating a facet-based model of aircraft A380® with physical optics-based simulation software POFACET® platform. Statistics of PDPs have then been calculated and the expected data rates of the designed G2A communication scenario have been envisioned. Moreover, a visualized interpretation of the interference caused in wide-beam and narrow-beam communication link scenarios have also been developed and illustrated. The proposed model is equally applicable to analyze the performance of high data-rate communication link in the network of passenger aircrafts, flocks of jet fighters and mesh of UAV drones. This model can also be visualized as an alternative of generating tapped-delays of several propagation scenarios for G2A communication systems. The proposed model can not only be used to improve the analytic prediction of signals received at the intended aircraft in the presence proximate scattering aircrafts but also can be seen as a way to realistically simulate the exact scenario of G2A propagation environment. The model can only stand valuable if it is used with proper channel characteristics to accurately capture the salient features of the G2A propagation

environment. This aspect of channel characterization is required to be explored in future studies. The proposed research can also be utilized for performance analysis of high data-rate communication links with high mobile speeds over sparsely distributed multipath channels. As a future work, the proposed model can easily be extended to cater to multi-altitude multi-ray scenarios for aircrafts, unmanned aerial vehicles (UAVs) and micro air vehicles (MAVs). The proposed model can be verified by measurement results, obtained in rigorous measurement campaigns which were not possible at our end.

Bibliography

[1] S. J. Nawaz, N. M. Khan, M. I. Tiwana, N. Hassan, and S. I. Shah, "Airborne internet access through submarine optical fiber cables," *IEEE Transactions on Aerospace and Electronic Systems*, vol. 51, no. 1, pp. 167–177, 2015.

[2] S. Gulfam, S. Nawaz, A. Ahmed, M. Patwary, and Q. Ni, "A novel 3D analytical scattering model for air-to-ground fading channels," *Applied Sciences*, vol. 6, pp. 207–1–207–21, Aug. 2016.

[3] U.S. Dept. Transportation, "Unmanned aircraft system (UAS) service demand 2015-2035: literature review and projections of future usage," technical report. v.1.0, dot-vntsc-dod-13-01, Feb. 2014.

[4] B. R. Mahafza, *Introduction to radar analysis.* CRC press, 2017.

[5] O. Landron, M. J. Feuerstein, and T. S. Rappaport, "In situ microwave reflection coefficient measurements for smooth and rough exterior wall surfaces," in *43rd IEEE Vehicular Technology Conference*, pp. 77–80, 1993.

[6] O. Landron, M. J. Feuerstein, and T. S. Rappaport, "A comparison of theoretical and empirical reflection coefficients for typical exterior wall surfaces in a mobile radio environment," *IEEE Transactions on Antennas and Propagation*, vol. 44, no. 3, pp. 341–351, 1996.

[7] S. R. Bullock, *Transceiver and system design for digital communications.* SciTech Publishing Inc., 2009.

[8] S. Hayat, E. Yanmaz, and R. Muzaffar, "Survey on unmanned aerial vehicle networks for civil applications: A communications viewpoint," *IEEE Communications Surveys Tutorials*, vol. 18, no. 4, pp. 2624–2661, 2016.

[9] P. A. Bello, "Aeronautical channel characterization," *IEEE Transactions on Communications*, vol. 21, no. 5, pp. 548–563, 1973.

[10] J. H. Painter, S. C. Gupta, and L. R. Wilson, "Multipath modeling for aeronautical communications," *IEEE Transactions on Communications*, vol. 21, no. 5, pp. 658–662, 1973.

[11] A. Neul, J. Hagenauer, W. Papke, F. Dolainsky, and F. Edbauer, "Propagation measurements for the aeronautical satellite channel," in *37th IEEE Vehicular Technology Conference*, vol. 37, pp. 90–97, 1987.

[12] F. Dovis, R. Fantini, M. Mondin, and P. Savi, "Small-scale fading for high-altitude platform (HAP) propagation channels," *IEEE Journal on Selected Areas in Communications*, vol. 20, no. 3, pp. 641–647, 2002.

[13] W. G. Newhall and J. Reed, "A geometric air-to-ground radio channel model," in *IEEE Military Communications Conference*, pp. 632–636, 2002.

[14] W. Newhall, R. Mostafa, C. Dietrich, C. R. Anderson, K. Dietze, G. Joshi, and J. Reed, "Wideband air-to-ground radio channel measurements using an antenna array at 2 GHz for low-altitude operations," in *IEEE Military Communications Conference*, pp. 1422–1427, October 2002.

[15] B. Zheng, Q. H. Ren, Y. J. Liu, and Z. Y. Chu, "Simulation of two V/UHF air-to-ground communication channel models," in *International Conference on Wireless Communications, Networking and Mobile Computing*, pp. 1083–1086, Sept 2007.

[16] M. A. Zaman, S. A. Mamun, M. Gaffar, M. M. Alam, and M. I. Momtaz, "Modeling VHF air-to-ground multipath propagation channel and analyzing channel characteristics and BER performance," in *IEEE Region 8*

International Conference on Computational Technologies in Electrical and Electronics Engineering (SIBIRCON), pp. 335–338, July 2010.

[17] S. Blandino, F. Kaltenberger, and M. Feilen, "Wireless channel simulator testbed for airborne receivers," in *IEEE Globecom Workshops*, pp. 1–6, Dec 2015.

[18] M. Wentz and M. Stojanovic, "A MIMO radio channel model for low-altitude air-to-ground communication systems," in *IEEE 82nd Vehicular Technology Conference*, pp. 1–6, Sept. 2015.

[19] M. Ibrahim and H. Arslan, "Air-ground doppler-delay spread spectrum for dense scattering environments," in *IEEE Military Communications Conference*, pp. 1661–1666, Oct 2015.

[20] S. M. Gulfam, J. Syed, M. N. Patwary, and M. Abdel-Maguid, "On the spatial characterization of 3-D air-to-ground radio communication channels," in *IEEE International Conference on Communications (ICC)*, pp. 2924–2930, 2015.

[21] Y. S. Meng and Y. H. Lee, "Measurements and characterizations of air-to-ground channel over sea surface at c-band with low airborne altitudes," *IEEE Transactions on Vehicular Technology*, vol. 60, no. 4, pp. 1943–1948, 2011.

[22] K. Chamberlin, "The effect of tree cover on air-ground, VHF propagation path loss," *IEEE Transactions on Communications*, vol. 34, no. 9, pp. 958–962, 1986.

[23] R. W. Sutton, E. H. Schroeder, A. D. Thompson, and S. G. Wilson, "Satellite-aircraft multipath and ranging experiment results at L band," *IEEE Transactions on Communications*, vol. 21, no. 5, pp. 639–647, 1973.

[24] M. Rice, R. Dye, and K. Welling, "Narrowband channel model for aeronautical telemetry," *IEEE Transactions on Aerospace and Electronic Systems*, vol. 36, no. 4, pp. 1371–1376, 2000.

[25] M. Rice, A. Davis, and C. Bettweiser, "Wideband channel model for aeronautical telemetry," *IEEE Transactions on Aerospace and Electronic Systems*, vol. 40, pp. 57–69, Jan 2004.

[26] S. M. Elnoubi, "A simplified stochastic model for the aeronautical mobile radio channel," in *IEEE 42nd Vehicular Technology Conference*, pp. 960–963, 1992.

[27] E. Haas, "Aeronautical channel modeling," *IEEE Transactions on Vehicular Technology*, vol. 51, no. 2, pp. 254–264, 2002.

[28] Q. Feng, J. McGeehan, E. K. Tameh, and A. R. Nix, "Path loss models for air-to-ground radio channels in urban environments," in *IEEE 63rd Vehicular Technology Conference*, vol. 6, pp. 2901–2905, 2006.

[29] J. Chen, B. Daneshrad, and W. Zhu, "MIMO performance evaluation for airborne wireless communication systems," in *IEEE Military Communications Conference (MILCOM)*, pp. 1827–1832, 2011.

[30] D. W. Matolak, "Air-ground channels & models: Comprehensive review and considerations for unmanned aircraft systems," in *IEEE Aerospace Conference*, pp. 1–17, 2012.

[31] Q. Lei and M. Rice, "Multipath channel model for over-water aeronautical telemetry," *IEEE Transactions on Aerospace and Electronic Systems*, vol. 45, no. 2, pp. 735–742, 2009.

[32] D. W. Matolak and R. Sun, "Air-ground channel characterization for unmanned aircraft systems: the hilly suburban environment," in *IEEE 80th Vehicular Technology Conference*, pp. 1–5, 2014.

[33] D. W. Matolak and R. Sun, "Air-ground channel characterization for unmanned aircraft systems: The over-freshwater setting," in *IEEE Integrated Communications, Navigation and Surveillance Conference (ICNS)*, pp. K1-1–K1-9, 2014.

[34] D. W. Matolak and R. Sun, "Initial results for air-ground channel measurements & modeling for unmanned aircraft systems: Over-sea," in *IEEE Aerospace Conference*, pp. 1–15, 2014.

[35] D. W. Matolak, I. Sen, and W. Xiong, "The 5-GHz airport surface area channel–part I: Measurement and modeling results for large airports," *IEEE Transactions on Vehicular Technology*, vol. 57, no. 4, pp. 2014–2026, 2008.

[36] I. Sen and D. W. Matolak, "The 5-ghz airport surface area channel–part II: Measurement and modeling results for small airports," *IEEE Transactions on Vehicular Technology*, vol. 57, no. 4, pp. 2027–2035, 2008.

[37] Y. H. Lee, Y. S. Meng, and Y. H. Heng, "Experimental characterizations of an air to land channel over sea surface in c band," in *XXIXth URSI General Assembly, Chicago, IL, USA*, pp. 7–16, August 2008.

[38] Y. S. Meng and Y. H. Lee, "Multipath characterization and fade mitigation of air-to-ground propagation channel over tropical sea surface at c band," in *IEEE Antennas and Propagation Society International Symposium*, pp. 1–4, July 2010.

[39] C. Zhang and Y. Hui, "Broadband air-to-ground communications with adaptive MIMO datalinks," in *IEEE/AIAA 30th Digital Avionics Systems Conference*, pp. 4D4–1–4D4–10, Oct. 2011.

[40] X. Gao, Z. Chen, and Y. Hu, "Analysis of unmanned aerial vehicle MIMO channel capacity based on aircraft attitude," *WSEAS Transactions on Information Science and Applications*, vol. 10, no. 2, pp. 58–67, 2013.

[41] T. J. Willink, C. C. Squires, G. W. K. Colman, and M. T. Muccio, "Measurement and characterization of low-altitude air-to-ground MIMO channels," *IEEE Transactions on Vehicular Technology*, vol. 65, no. 4, pp. 2637–2648, 2016.

[42] R. Sun and D. W. Matolak, "Air-ground channel characterization for unmanned aircraft systems-part II: Hilly and mountainous settings," *IEEE Transactions on Vehicular Technology*, vol. 66, no. 3, pp. 1913–1925, 2017.

[43] D. W. Matolak and R. Sun, "Air-ground channel characterization for unmanned aircraft systems-part III: The suburban and near-urban environments," *IEEE Transactions on Vehicular Technology*, vol. 66, no. 8, pp. 6607–6618, 2017.

[44] L. Afonso, N. Souto, P. Sebastiao, M. Ribeiro, T. Tavares, and R. Marinheiro, "Cellular for the skies: Exploiting mobile network infrastructure for low altitude air-to-ground communications," *IEEE Aerospace and Electronic Systems Magazine*, vol. 31, no. 8, pp. 4–11, 2016.

[45] M. Simunek, F. P. Fontn, and P. Pechac, "The uav low elevation propagation channel in urban areas: Statistical analysis and time-series generator," *IEEE Transactions on Antennas and Propagation*, vol. 61, no. 7, pp. 3850–3858, 2013.

[46] W. Khawaja, I. Guvenc, and D. Matolak, "UWB channel sounding and modeling for UAV air-to-ground propagation channels," in *IEEE Global Communications Conference (GLOBECOM)*, pp. 1–7, Dec. 2016.

[47] D. W. Matolak and R. Sun, "Air-ground channel characterization for unmanned aircraft systems: The near-urban environment," in *IEEE Military Communications Conference*, pp. 1656–1660, Oct. 2015.

[48] D. W. Matolak and R. Sun, "Air-ground channel characterization for unmanned aircraft systems-part I: Methods, measurements, and models for over-water settings," *IEEE Transactions on Vehicular Technology*, vol. 66, no. 1, pp. 26–44, 2017.

[49] D. W. Matolak and R. Sun, "Antenna and frequency diversity in the unmanned aircraft systems bands for the over-sea setting," in *IEEE 33rd Digital Avionics Systems Conference (DASC)*, pp. 6A4–1–6A4–10, Oct. 2014.

[50] D. W. Matolak and R. Sun, "Air-ground channel measurements amp; modeling for UAS," in *Integrated Communications, Navigation and Surveillance Conference (ICNS)*, pp. 1–9, April 2013.

[51] N. Schneckenburger, T. Jost, D. Shutin, M. Walter, T. Thiasiriphet, M. Schnell, and U. C. Fiebig, "Measurement of the L-band air-to-ground channel for positioning applications," *IEEE Transactions on Aerospace and Electronic Systems*, vol. 52, no. 5, pp. 2281–2297, 2016.

[52] K. Takizawa, T. Kagawa, S. Lin, F. Ono, H. Tsuji, and R. Miura, "C-band aircraft-to-ground (A2G) radio channel measurement for unmanned aircraft systems," in *International Symposium on Wireless Personal Multimedia Communications (WPMC)*, pp. 754–758, Sept. 2014.

[53] F. Ono, K. Takizawa, H. Tsuji, and R. Miura, "S-band radio propagation characteristics in urban environment for unmanned aircraft systems," in *International Symposium on Antennas and Propagation (ISAP)*, pp. 1–4, Nov. 2015.

[54] N. Goddemeier, K. Daniel, and C. Wietfeld, "Coverage evaluation of wireless networks for unmanned aerial systems," in *IEEE Global Communications Conference (GLOBECOM) Workshops*, pp. 1760–1765, Dec. 2010.

[55] C. m. Cheng, P. h. Hsiao, H. T. Kung, and D. Vlah, "Performance measurement of 802.11a wireless links from UAV to ground nodes with various antenna orientations," in *15th International Conference on Computer Communications and Networks*, pp. 303–308, Oct. 2006.

[56] E. Yanmaz, R. Kuschnig, and C. Bettstetter, "Channel measurements over 802.11a-based UAV-to-ground links," in *IEEE Global Communications Conference (GLOBECOM) Workshops*, pp. 1280–1284, Dec. 2011.

[57] E. Yanmaz, R. Kuschnig, and C. Bettstetter, "Achieving air-ground communications in 802.11 networks with three-dimensional aerial mobility," in *IEEE International Conference on Computer Communications (INFOCOM)*, pp. 120–124, April 2013.

[58] N. Ahmed, S. S. Kanhere, and S. Jha, "On the importance of link characterization for aerial wireless sensor networks," *IEEE Communications Magazine*, vol. 54, no. 5, pp. 52–57, 2016.

[59] E. L. Cid, A. V. Alejos, and M. G. Sanchez, "Signaling through scattered vegetation: Empirical loss modeling for low elevation angle satellite paths obstructed by isolated thin trees," *IEEE Vehicular Technology Magazine*, vol. 11, no. 3, pp. 22–28, 2016.

[60] J. Romeu, A. Aguasca, J. Alonso, S. Blanch, and R. R. Martins, "Small UAV radiocommunication channel characterization," in *Fourth European Conference on Antennas and Propagation*, pp. 1–5, April 2010.

[61] H. T. Kung, C. K. Lin, T. H. Lin, S. J. Tarsa, and D. Vlah, "Measuring diversity on a low-altitude UAV in a ground-to-air wireless 802.11 mesh network," in *IEEE Global Communications Conference (GLOBECOM) Workshops*, pp. 1799–1804, Dec. 2010.

[62] R. Sun and D. W. Matolak, "Over-harbor channel modeling with directional ground station antennas for the air-ground channel," in *IEEE Military Communications Conference*, pp. 382–387, Oct. 2014.

[63] H. D. Tu and S. Shimamoto, "A proposal of wide-band air-to-ground communication at airports employing 5-GHz band," in *IEEE Wireless Communications and Networking Conference*, pp. 1–6, April 2009.

[64] Z. Wu, H. Kumar, and A. Davari, "Performance evaluation of ofdm transmission in UAV wireless communication," in *Thirty-Seventh Southeastern Symposium on System Theory*, pp. 6–10, March 2005.

[65] C. Bluemm, C. Heller, B. Fourestie, and R. Weigel, "Air-to-ground channel characterization for OFDM communication in C-band," in *7th International Conference on Signal Processing and Communication Systems (ICSPCS)*, Dec. 2013.

[66] V. Vahidi and E. Saberinia, "Orthogonal frequency division multiplexing and channel models for payload communications of unmanned aerial systems," in *International Conference on Unmanned Aircraft Systems (ICUAS)*, pp. 1156–1161, June 2016.

[67] R. Essaadali and A. Kouki, "A new simple unmanned aerial vehicle doppler effect RF reducing technique," in *IEEE Military Communications Conference (MILCOM)*, pp. 1179–1183, Nov. 2016.

[68] J. Yang, P. Liu, and H. Mao, "Model and simulation of narrowband ground-to-air fading channel based on markov process," in *International Conference on Network Computing and Information Security*, vol. 1, May 2011.

[69] M. Walter and M. Schnell, "The doppler-delay characteristic of the aeronautical scatter channel," in *IEEE Vehicular Technology Conference*, pp. 1–5, Sept. 2011.

[70] S. M. Gulfam, S. J. Nawaz, A. Ahmed, and M. N. Patwary, "Analysis on multipath shape factors of air-to-ground radio communication channels," in *Wireless Telecommunications Symposium (WTS)*, pp. 1–5, April 2016.

[71] P. Petrus, J. H. Reed, and T. S. Rappaport, "Geometrical-based statistical macrocell channel model for mobile environments," *IEEE Transactions on Communications*, vol. 50, no. 3, pp. 495–502, 2002.

[72] K. Mammasis and P. Santi, "A two-dimensional geometry-based stochastic model," *IEEE Transactions on Wireless Communications*, vol. 11, no. 1, pp. 38–43, 2012.

[73] N. M. Khan, M. T. Simsim, and P. B. Rapajic, "A generalized model for the spatial characteristics of the cellular mobile channel," *IEEE Transactions on Vehicular Technology*, vol. 57, no. 1, pp. 22–37, 2008.

[74] R. Janaswamy, "Angle of arrival statistics for a 3-D spheroid model," *IEEE Transactions on Vehicular Technology*, vol. 51, no. 5, pp. 1242–1247, 2002.

[75] K. N. Le, "On angle-of-arrival and time-of-arrival statistics of geometric scattering channels," *IEEE Transactions on Vehicular Technology*, vol. 58, no. 8, pp. 4257–4264, 2009.

[76] R. B. Ertel and J. H. Reed, "Angle and time of arrival statistics for circular and elliptical scattering models," *IEEE Journal on Selected Areas in Communications*, vol. 17, no. 11, pp. 1829–1840, 1999.

[77] K. Baltzis and J. Sahalos, "A simple 3-D geometric channel model for macrocell mobile communications," *Wireless Personal Communications*, vol. 51, no. 2, pp. 329–347, 2009.

[78] J. Hao, Z. Jie, and H. Kikuchi, "Angle and time of arrival statistics for a 3-D pie-cellular-cut scattering channel model," *Wireless Personal Communications*, vol. 78, no. 2, pp. 851–865, 2014.

[79] S. J. Nawaz, N. M. Khan, M. N. Patwary, and M. Moniri, "Effect of directional antenna on the doppler spectrum in 3-D mobile radio propagation environment," *IEEE Transactions on Vehicular Technology*, vol. 60, no. 7, pp. 2895–2903, 2011.

[80] R. B. Ertel, P. Cardieri, K. W. Sowerby, T. S. Rappaport, and J. H. Reed, "Overview of spatial channel models for antenna array communication systems," *IEEE Personal Communications*, vol. 5, no. 1, pp. 10–22, 1998.

[81] A. Ishimaru, *Electromagnetic Wave Propagation, Radiation, and Scattering: From Fundamentals to Applications.* John Wiley & Sons, 2017.

[82] A. Taflove, "Application of the finite-difference time-domain method to sinusoidal steady-state electromagnetic-penetration problems," *IEEE Transactions on electromagnetic compatibility*, no. 3, pp. 191–202, 1980.

[83] O. C. Zienkiewicz, R. L. Taylor, O. C. Zienkiewicz, and R. L. Taylor, *The Finite Element Method*, vol. 3. McGraw-hill London, 1977.

[84] L. Sevgi, "Target reflectivity and rcs interactions in integrated maritime surveillance systems based on surface-wave high-frequency radars," *IEEE Antennas and Propagation Magazine*, vol. 43, no. 1, pp. 36–51, 2001.

[85] W. C. Chew, E. Michielssen, J. Song, and J.-M. Jin, *Fast and Efficient Algorithms in Computational Electromagnetics*. Artech House, Inc., 2001.

[86] E. Mach, *The Principles of Physical Optics: An Historical and Philosophical Treatment*. Courier Corporation, 2013.

[87] Q. Xu, Y. Huang, X. Zhu, L. Xing, P. Duxbury, and J. Noonan, "Building a better anechoic chamber: A geometric optics-based systematic solution, simulated and verified [measurements corner]," *IEEE Antennas and Propagation Magazine*, vol. 58, no. 2, pp. 94–119, 2016.

[88] G. Apaydin, F. Hacivelioglu, L. Sevgi, W. B. Gordon, and P. Y. Ufimtsev, "Diffraction at a rectangular plate: first-order PTD approximation," *IEEE Transactions on Antennas and Propagation*, vol. 64, no. 5, pp. 1891–1899, 2016.

[89] M. Albani, G. Carluccio, and P. H. Pathak, "A uniform geometrical theory of diffraction for vertices formed by truncated curved wedges," *IEEE Transactions on Antennas and Propagation*, vol. 63, no. 7, pp. 3136–3143, 2015.

[90] Y. Bennani, F. Comblet, and A. Khenchaf, "RCS of complex targets: Original representation validated by measurements-application to ISAR imagery," *IEEE Transactions on Geoscience and Remote Sensing*, vol. 50, no. 10, pp. 3882–3891, 2012.

[91] J. D. Wilson, "Probability of detecting aircraft targets," *IEEE Transactions on Aerospace and Electronic Systems*, vol. AES-8, no. 6, pp. 757–761, 1972.

[92] A. David, C. Brousseau, and A. Bourdillon, "Simulations and measurements of a radar cross section of a boeing 747-200 in the 20–60 MHz frequency band," *Radio Science*, vol. 38, no. 4, pp. 3(1)–3(4), 2003.

[93] B. Persson and M. Norsell, "On modeling RCS of aircraft for flight simulation," *IEEE Antennas and Propagation Magazine*, vol. 56, no. 4, pp. 34–43, 2014.

[94] Z. W. Liu, D. Z. Ding, Z. F. Fan, and R. S. Chen, "Adaptive sampling bicubic spline interpolation method for fast calculation of monostatic RCS," *Microwave and Optical Technology Letters*, vol. 50, no. 7, pp. 1851–1857, 2008.

[95] Z. W. Liu, R. S. Chen, and J. Q. Chen, "Adaptive sampling cubic-spline interpolation method for efficient calculation of monostatic RCS," *Microwave and Optical Technology Letters*, vol. 50, no. 3, pp. 751–755, 2008.

[96] W. D. Li, H. X. Zhou, J. Hu, Z. Song, and W. Hong, "Accuracy improvement of cubic polynomial inter/extrapolation of mom matrices by optimizing frequency samples," *IEEE Antennas and Wireless Propagation Letters*, vol. 10, pp. 888–891, Aug. 2011.

[97] W.-D. Li, J.-X. Miao, J. Hu, Z. Song, and H.-X. Zhou, "An improved cubic polynomial method for interpolating/extrapolating mom matrices over a frequency band," *Progress In Electromagnetics Research*, vol. 117, pp. 267–281, 2011.

[98] Y. An, D. Wang, and R. Chen, "Improved multilevel physical optics algorithm for fast computation of monostatic radar cross section," *IET Microwaves, Antennas & Propagation*, vol. 8, no. 2, pp. 93–98, 2014.

[99] M.-Y. M. Mirza, N. M. Khan, A. Jamal, and R. Ramer, "Characterization of spatial reflection co-efficient for ground-to-aircraft and satellite-to-aircraft communication," *Applied Computational Electromagnetics Society Journal*, vol. 33, no. 1, pp. 56–68, 2018.

[100] L. Sevgi, *Complex Electromagnetic Problems and Numerical Simulation Approaches.* John Wiley & Sons, 2003.

[101] G. Burke and A. Poggio, "Numerical electromagnetic code-method of moments, part I: Program description, theory," *Technical Document*, vol. 116, 1977.

[102] E. E. J. Garrido and D. C. Jenn, "A matlab physical optics RCS prediction code." https://calhoun.nps.edu/handle/10945/37432, 2000. [Online; accessed 31-Aug.-2018].

[103] D. D. C. Jenn, "POFACETS." http://faculty.nps.edu/jenn/#_Matlab_Software, 2004. [Online; accessed 31-Aug. 2018].

[104] C. Uluisik, G. Cakir, M. Cakir, and L. Sevgi, "Radar cross section (RCS) modeling and simulation, part 1: a tutorial review of definitions, strategies, and canonical examples," *IEEE Antennas and Propagation Magazine*, vol. 50, no. 1, pp. 115–126, 2008.

[105] N. Goddemeier, K. Daniel, and C. Wietfeld, "Role-based connectivity management with realistic air-to-ground channels for cooperative UAVs," *IEEE Journal on Selected Areas in Communications*, vol. 30, no. 5, pp. 951–963, 2012.

[106] R. Amorim, H. Nguyen, P. Mogensen, I. Z. Kovcs, J. Wigard, and T. B. Srensen, "Radio channel modeling for UAV communication over cellular networks," *IEEE Wireless Communications Letters*, vol. 6, no. 4, pp. 514–517, 2017.

[107] C. Yan, L. Fu, J. Zhang, and J. Wang, "A comprehensive survey on UAV communication channel modeling," *IEEE Access*, vol. 7, pp. 107769–107792, 2019.

[108] M. Kim and J. Lee, "Impact of an interfering node on unmanned aerial vehicle communications." https://arxiv.org/abs/1903.08154. [Online; V2 accessed 27 Nov. 2019].

[109] W. Khawaja, I. Guvenc, and D. Matolak, "UWB channel sounding and modeling for UAV air-to-ground propagation channels," in *2016 IEEE Global Communications Conference (GLOBECOM)*, pp. 1–7, Dec 2016.

[110] D. W. Matolak and R. Sun, "Air-ground channels for UAS: Summary of measurements and models for L- and C-bands," in *Integrated Communications Navigation and Surveillance (ICNS)*, pp. 8B2–1–8B2–11, April 2016.

[111] J. Holis and P. Pechac, "Elevation dependent shadowing model for mobile communications via high altitude platforms in built-up areas," *IEEE Transactions on Antennas and Propagation*, vol. 56, no. 4, pp. 1078–1084, 2008.

[112] T. S. Rappaport, *Wireless Communications: Principles and Practice*. Prentice hall PTR New Jersey, 2 ed., Dec. 2001.

[113] R. Geise, A. Enders, H. Vahle, and H. Spieker, "Scaled measurements of instrument-landing-system disturbances due to large taxiing aircraft," *IEEE Transactions on Electromagnetic Compatibility*, vol. 50, no. 3, pp. 485–490, 2008.

[114] A. Wongkeeratikul, P. Supnithi, S. Noppanakeepong, N. Leelaruji, and N. Hemmakorn, "Modeling and measurement of airplane flutter phenomena on tv broadcasting signal," *IEEE Transactions on Broadcasting*, vol. 54, no. 2, pp. 173–181, 2008.

[115] D. Arnaud, C. Brousseau, and A. Bourdillon, "Study of flight route effects on aircraft RCS signature at VHF frequencies by means of wire grid models," in *IEEE 2000 International Radar Conference [Cat. No. 00CH37037]*, pp. 231–235, 2000.

[116] J. D. Wang, T. H. S. Chao, and B. R. Saltzberg, "Training signal and receiver design for multipath channel characterization for TV broadcasting," *IEEE Transactions on Consumer Electronics*, vol. 36, no. 4, pp. 794–806, 1990.

[117] A. Wonggeeratigun, P. Sangonchat, S. Noppanakeepong, N. Leelaruji, and Y. Moriya, "The observation and simulation of the airplane flutter on low

band television broadcasting signal," in *Student Conference on Research and Development, 2003.*, pp. 118–122, Aug 2003.

[118] M. L. Bucher, "Simulation of multipath fading/ghosting for analog and digital television transmission in broadcast channels," *IEEE Transactions on Broadcasting*, vol. 38, no. 4, pp. 256–262, 1992.

[119] H. Miyazawa, "Evaluation and measurement of airplane flutter interference," *IEEE Transactions on Broadcasting*, vol. 35, no. 4, pp. 362–367, 1989.

[120] Routehappy, "Routehappy 2018 Wi-Fi report evaluates global in-flight Wi-Fi [Accessed on: 5 Aug. 2018]," 2018.

[121] MarketsandMarkets, "In-flight Entertainment & Connectivity (IFEC) Market by End User (OEM, Aftermarket), Aircraft Type (NBA, WBA, VLA, Business Jets), Product (IFE Hardware, IFE Connectivity, IFE Content), and Region - Global Forecast to 2023 [Accessed on: 5 Aug. 2018]," 2018.

[122] Honeywell, "Honeywell 2014 in flight connectivity survey [Accessed on: 5 Aug. 2018]," 2014.

[123] Inmarsat, "Demand for inflight Wi-Fi is driving airline loyalty amongst passengers [Accessed on: 5 Aug. 2018]," 2018.

[124] Air Transport Action Group, "Aviation benefits beyond borders [Accessed on: 5 Aug. 2018]," July 2016.

[125] J. P. Rula, J. Newman, F. E. Bustamante, A. M. Kakhki, and D. Choffnes, "Mile high WiFi: A first look at in-flight internet connectivity," in *World Wide Web Conference*, pp. 1449–1458, 2018.

[126] GoGo, "Gogo ATG-4 what is it, and how does it work? [Accessed on: 5 Aug. 2018]," Nov. 2014.

[127] GoGo, "How Gogo is well prepared to improve 2Ku now and in the future [Accessed on: 5 Aug. 2018]," Feb. 2018.

[128] Inmarsat, "The european aviation network [Accessed on: 14 Aug. 2018]," April 2016.

[129] Inmarsat, "Network completed: Ean ready to take off! [Accessed on: 14 Aug. 2018]," Feb. 2018.

[130] A. Jahn, M. Holzbock, J. Muller, R. Kebel, M. D. Sanctis, A. Rogoyski, E. Trachtman, O. Franzrahe, M. Werner, and F. Hu, "Evolution of aeronautical communications for personal and multimedia services," *IEEE Commun. Magazine*, vol. 41, no. 7, pp. 36–43, 2003.

[131] E. Sakhaee and A. Jamalipour, "The global in-flight internet," *IEEE Journal on Selected Areas in Commun.*, vol. 24, pp. 1748–1757, Sep. 2006.

[132] H. D. Tu, P. Jingyu, S. Shimamoto, and J. Kitaori, "Oceanic air traffic control based on space-time division multiple access," in *IEEE Digital Avionics Systems Conference*, pp. 7.D.2–1–7.D.2–13, Oct. 2009.

[133] D. Medina and F. Hoffmann, *Future Aeronautical Communications*, ch. The Airborne Internet, pp. 349–374. Germany: InTech, Sep. 2011.

[134] D. Medina, F. Hoffmann, F. Rossetto, and C.-H. Rokitansky, "A crosslayer geographic routing algorithm for the airborne internet," in *IEEE International Conference on Communications*, pp. 1–6, May 2010.

[135] X. Fan, Y. Qin, S. Shang, D. Song, W. Sun, D. Li, and X. Luo, "Research on the bastatic rcs characteristics of stealth aircraft," in *Asia-Pacific Microwave Conference (APMC)*, vol. 3, pp. 1–3, Dec 2015.

[136] L. Zhu, X. Liang, J. Li, and R. Li, "Simulation analysis on static scattering characteristics of stealth aircraft," in *IEEE Advanced Information Management, Communicates, Electronic and Automation Control Conference (IM-CEC)*, pp. 1774–1778, Oct 2016.

[137] E. F. Knott, *Radar cross section measurements.* Springer Science & Business Media, 2012.

[138] M. Cherniakov, *Bistatic Radar: Principles and Practice.* John Wiley & Sons Ltd, 2007.

[139] S. R. Saunders and A. Aragï, *Antennas and propagation for wireless communication systems.* John Wiley & Sons, 2007.

[140] J. Liu, *Spacecraft TT&C and Information Transmission Theory and Technologies.* Springer-Verlag Berlin Heidelberg, 2015.

[141] S. J. Nawaz, N. M. Khan, M. I. Tiwana, N. Hassan, and S. I. Shah, "Airborne internet access through submarine optical fiber cables," *IEEE Transactions on Aerospace and Electronic Systems*, vol. 51, no. 1, pp. 167–177, 2015.

[142] Airbus S.A.S, "Aircraft characteristics airport and maintainence planning," 01 Dec 2016.

[143] Airbus S.A.S, "Autocad 3-view aircraft drawings," 10 May 2012.

[144] F. Chatzigeorgiadis and D. C. Jenn, "A matlab physical-optics rcs prediction code," *IEEE Antennas and Propagation Magazine*, vol. 46, no. 4, pp. 137–139, 2004.

[145] C. C. Ferguson, "Intersections of ellipsoids and planes of arbitrary orientation and position," *Journal of the International Association for Mathematical Geology*, vol. 11, no. 3, pp. 329–336, 1979.

[146] P. P. Klein, "On the ellipsoid and plane intersection equation," *Applied Mathematics*, vol. 3, no. 11, pp. 1634–1640, 2012.

[147] A. Paulraj, D. Gesbert, and C. Papadias, "Smart antennas for mobile communications," *Encyclopedia for Electrical Engineering*, pp. 1–15, 2000.

[148] P. P. Klein, "On the ellipsoid and plane intersection equation," *Applied Mathematics*, vol. 3, no. 11, p. 1634, 2012.

Appendix A

Proof of the Intersection Ellipse Formed as a Result of Plane Cross-Section of Prolate Spheroid at its Focal Point

A.1   Prolate Spheroid with Successive Elliptical Rings

Consider a prolate spheroid with dimensions c_p along z-axis, a_p along x-axis and b_p along y-axis. A prolate spheroid is a surface of revolution usually constructed by rotating an ellipse along its major axis. An illustration of prolate spheroid to describe its axes representation is shown in Fig. A1. In the figure, one elliptical ring of maximum dimension (covering outer boundary of prolate spheroid along major axis) can be envisioned with its semi-major and semi-minor axes equivalent to c_p and a_p respectively. Furthermore, the circular ring shown in the Fig(1) has radius a_p because according to the properties of prolate spheroid, the two minor axes of prolate spheroid are equal *i.e* $a_p = b_p$. Following the axes properties, the elliptical ring lies in xz-plane while the circular ring lies in xy-plane as perpendicular to the plane of elliptical ring. From now onwards, the elliptical and circular rings will be mentioned as E_r and C_r respectively. By visualizing the concept of elliptical rings, the three dimensional prolate spheroid can be represented with the help of successive elliptical rings located in yz-plane with specific lengths of semi-major
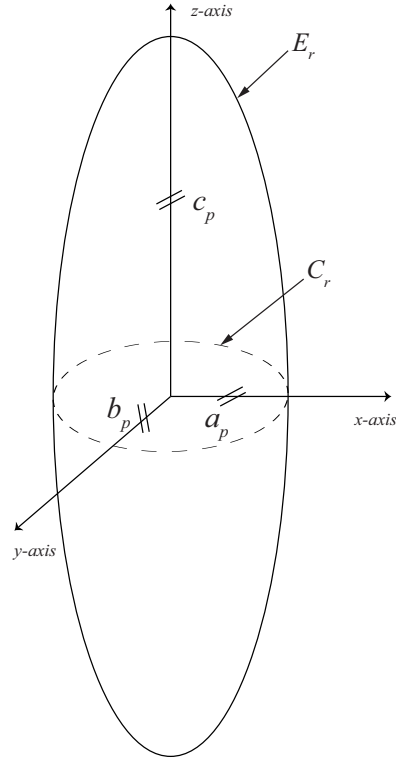
FIGURE A1: Axes representation of a triaxial prolate spheroid with a perspective of elliptical and circular rings .

and semi-minor axes according to E_r and C_r respectively. An illustration to express the methodology of successive elliptical rings is shown in the Fig. A2. Consider a total of N elliptical rings are possible to cover the whole surface of prolate spheroid. The elliptical ring located at the origin (Center) has lengths of semi major and minor axes equivalent to the lengths of semi major and semi minor axes of prolate spheroid, which are c_p and a_p. For simplicity, the successive elliptical rings located in yz-plane are termed as E_{sr}. The length of major and minor axes of E_{sr} decreases as when the E_{sr} moves away from the origin and becomes zero when it reaches at a distance equal to semi-minor axis a_p of prolate spheroid. Consequently, it can be concluded that the lengths of semi-major and semi-minor axes of E_{sr}'s would change according to the distances of E_{sr}'s from the origin, where they are located. From the observation of the lengths of major and minor axes of E_{sr}s, it is observed that the lengths of major axis of E_{sr} follows elliptical properties of E_r while minor axis adopts circular characteristics of C_r. Hence, in a precise manner, each E_{sr} can be characterized with the help of crossed elliptical ring E_r and circular ring
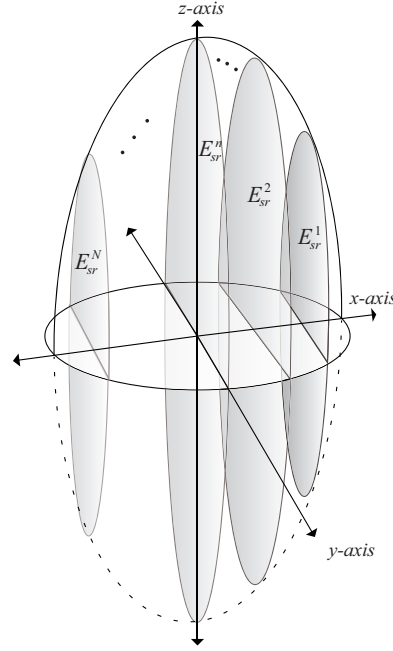
FIGURE A2: An illustration of successive ellipses of a prolate spheroid in yz-plane.

C_r. From the viewpoint of plane cross-section of prolate spheroid along its major axis, these elliptical rings give information of major and minor axes of intersection ellipse as a result of plane cross section of prolate spheroid.

With the help of polar radial length r_0 of elliptical ring E_r originated at origin, the semi-major and semi-minor lengths of E_{sr}^n (say nth successive elliptical ring) can be calculated by using the following expressions.

$$
\begin{aligned}
a_{nsr} &= r_0 \sin(\phi_n) && \text{(A.1)} \\
&= \frac{c_p a_p \sin(\phi_n)}{\sqrt{a_p^2 + (c_p^2 - a_p^2)\cos^2(\phi_n)}}
\end{aligned}
$$

and

$$
b_{nsr} = a_p \sin(\tilde{\phi}_n) \tag{A.2}
$$

where, ϕ_n is the angle between the x-axis and the line formed by joining the one end point of major axis of E_{sr}^n with the center. With the same manner, $\tilde{\phi}_n$ is the angle between the x-axis and the line formed by joining the one end point of minor axis of E_{sr}^n with the center. An illustrative view of both the angles is shown in

Fig. A3 along with the perspective of side and top view.
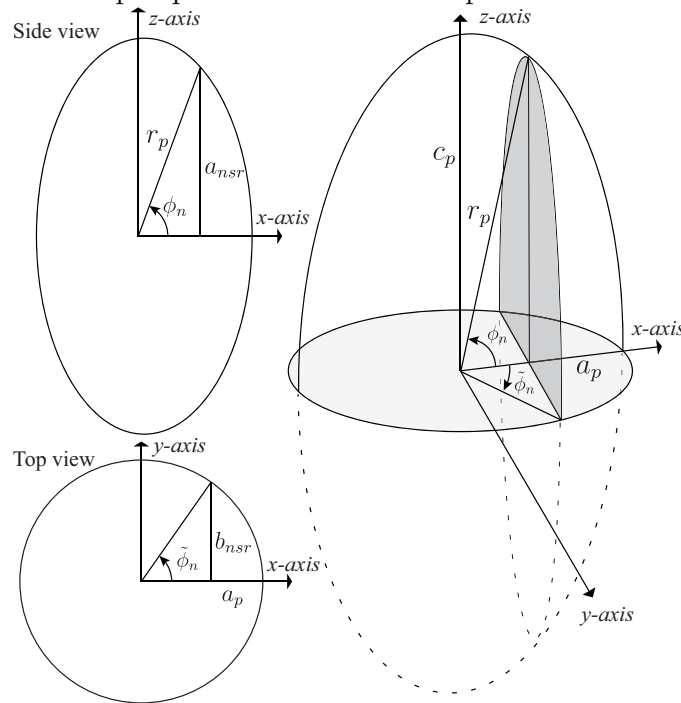
FIGURE A3: Top and side perspective view of elliptical and circular ring around prolate spheroid.

A.2 Major and Minor Axes of the Ellipse Resulted from the Prolate Intersectioned With Plane

In this section, the major and minor axes of plane cross-sectioned ellipse of prolate spheroid are formulated and expressed in detail. An illustration of intersection ellipse as a result of plane cross-section of a prolate spheroid is shown in Fig. 4(a). The major and minor axes of the intersection ellipse are termed as a_{cs} and b_{cs} respectively.
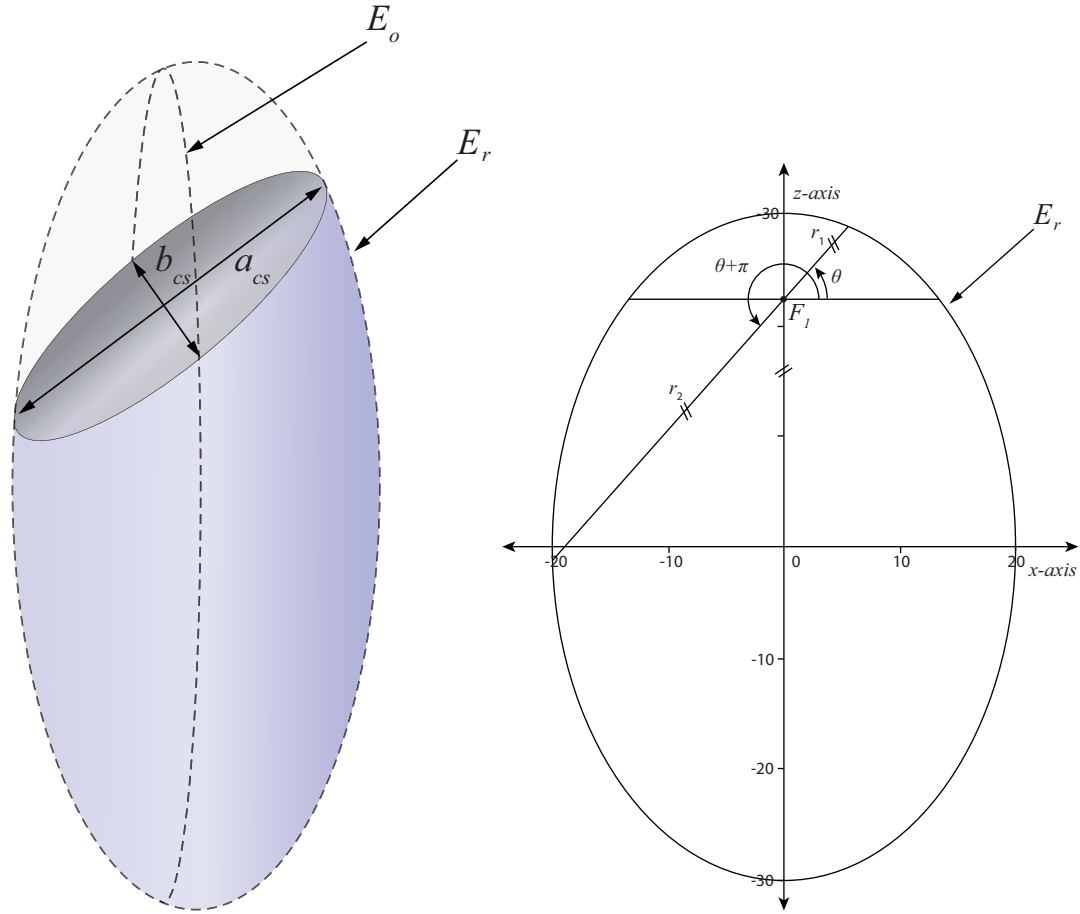
(a) Formation of intersection ellipse through a plane cut of prolate spheroid.

(b) Focal chord of the elliptical ring E_r with respective radial lengths r_1 and r_2.

FIGURE A4: A perspective diagram of the intersection ellipse and corresponding elliptical ring for the calculation of its major axis.

A.2.1 Major Axis of Intersection Ellipse

The major axis of ellipse formed through a plane cross-section of prolate spheroid at its focal point f is obtained by considering an elliptical ring E_r of maximum dimension. The elliptical ring E_r covers the outer boundary of prolate spheroid along xz-plane with its major axis along z-axis and minor axis along x-axis, as mentioned earlier in Fig. A1. Since, the length of semi-major axis c_p and semi-minor axis a_p of prolate spheroid is known, therefore, the elliptical ring E_r can be formed and characterized by labeling c_p and a_p as its semi-major and semi-minor axes i.e $a_m = c_p$ and $b_m = a_p$. The equation of the elliptical ring E_r can be written as follows.

$$\frac{z^2}{a_m^2} + \frac{x^2}{b_m^2} = 1 \quad ; \qquad a_m > b_m \tag{A.3}$$

By considering the parametric equations, $x = r\cos(\theta)$ and $z = f_m + r\sin(\theta)$ the polar form of Eq. (A.3) can be expressed as follows.

$$r = \frac{b_m^2}{a_m + \sqrt{a_m^2 - b_m^2}\sin(\theta)} \tag{A.4}$$

Where, $f_m = \sqrt{b_m^2 - a_m^2}$ is the focal point of elliptical ring and θ is the angle between r_1 and the line parallel to the x-axis as shown in the Fig. 4(b). In terms of eccentricity $e_m = \frac{f_m}{a_m}$ the Eq. (A.4) can be rewritten as

$$r = \frac{a_m(1 - e_m^2)}{1 + e_m\sin(\theta)} \tag{A.5}$$

Following the angular geometry, as shown in Fig. 4(b), the radial lengths r_1 and r_2 can be calculated by substituting angles θ and $\theta + \pi$. Hence, the length of the major axis of the intersection ellipse formed through plane cross section of prolate spheroid at its focal point can be obtained by summing both the radial lengths r_1 and r_2 respectively. By adjusting the equivalent major and minor axes lengths of prolate spheroid, the following expression yields length of semi-major axis of intersection ellipse.

$$\begin{aligned}
a_{cs} &= \frac{r_1 + r_2}{2} \tag{A.6}\\
&= \left[\frac{a_p^2}{c_p + \sin(\theta)\sqrt{c_p^2 - a_p^2}} + \frac{a_p^2}{c_p + \sin(\theta + \pi)\sqrt{c_p^2 - a_p^2}}\right] \times \frac{1}{2}\\
&= \frac{c_p a_p^2}{c_p^2\cos^2(\theta) + a_p^2\sin^2(\theta)}
\end{aligned}$$

Whereas, the center of the cross sectioned ellipse is the mid point of the focal chord PQ. With coordinates $P(r_1\cos(\theta), r_1\sin(\theta))$ and $Q((r_2\cos(\pi + \theta), r_2\sin(\pi + \theta)))$ the coordinates of the center of the cross-sectioned ellipse can be calculated as follows.

$$\begin{aligned}
C &= (\frac{r_1\cos(\theta) + r_2\cos(\pi + \theta)}{2}, f_m + \frac{r_1\sin(\theta) + r_2\sin(\pi + \theta)}{2})\\
&= (\frac{r_1\cos(\theta) - r_2\cos(\theta)}{2}, \frac{2\sqrt{c_m^2 - a_m^2} + r_1\sin(\theta) - r_2\sin(\theta)}{2}) \tag{A.7}
\end{aligned}$$

For a special case, when $\theta = 0$ the focal chord turns to become a latus rectum and the center point turns to focal point of prolate spheroid.

A.2.2 Minor Axis of Plane Cross-Sectioned Ellipse

The length of the minor axis of the plane cross-sectioned ellipse is calculated after correctly finding an accurate elliptical ring (E_0) among E_{sr}'s along yz-plane, which exactly lie at mid point of the focal chord of the elliptical ring E_r along xz-plane. After locating and characterizing the accurate E_0 elliptical ring, the length of the chord of E_0 passing through the mid point of the focal chord would define the length of minor axis of plane-cross sectioned ellipse.

The elliptical ring E_0 is characterized by using elliptical ring E_r, circular ring C_r and the line $x = x'$, where $x' = \frac{r_1 \cos(\theta) - r_2 \cos(\theta)}{2}$. The major axis of the E_0 is defined as the distance between the intersection points of E_r and the line $x = x'$, while, the minor axis is obtained by calculating the distance between the intersection points of C_r and the line $x = x'$. The length of semi-major and semi-minor axes of E_0 are thus defined as follows.

$$a_{E_0} = \frac{c_p}{2a_p}\sqrt{4a_p^2 - (r_1 - r_2)^2 \cos^2(\theta)} \tag{A.8}$$

$$b_{E_0} = \frac{\sqrt{4a_p^2 - (r_1 - r_2)^2 \cos^2(\theta)}}{2}$$

After perfect characterization of E_0, it will define the length of semi-minor axis of the cross-sectioned ellipse of prolate spheroid. The length of the minor axis of the cross sectioned ellipse is obtained by finding the distance between the intersection points of ellipse E_0 and the line $z = z'$, where $z' = \frac{2\sqrt{c_m^2 - a_m^2} + r_1 \sin(\theta) - r_2 \sin(\theta)}{2}$. Hence, the following expression is obtained to define the semi-minor axis of the plane cross-sectioned ellipse of prolate spheroid.

$$b_{cs} = \frac{b_{E_0}}{a_{E_0}}\sqrt{a_{E_0}^2 - z'^2} \tag{A.9}$$

A.3 Numerical Result Verification of the Proposed Closed-Form Expression

In order to verify the validity and the correctness of the proposed closed-form expressions, a commercial computer aided design software PTC Creo-Parametric$^{©}$ 4.0 is used to generate a prolate spheroid and a plane. A prolate spheroid with its semi-major axis of length 30 along z-axis and semi-minor axis of length 20 along x-axis is developed. In order to obtain plane cross-section region of the prolate spheroid, a plane making angle $\theta°$ with the line parallel to x-axis at focal point of the prolate spheroid is cross-sectioned with the prolate spheroid. During this verification, five different plane cross-section angles ($\theta = 0°, 30°, 45°, 60°, 75°$) are considered to construct the intersection ellipse specimens for the measurement of major and minor axis lengths as shown in Fig. A5. The Fig. A5 presents four different cases of intersection ellipse formation at cross-section angles $30°, 45°, 60°$ and $75°$ in Fig. 5(a), 5(b), 5(c) and 5(d) respectively. Moreover, the results are also compared with the closed-form expression derived in [148]. A comparison between the results of semi major and minor axes lengths obtained through the proposed closed-form expression, Creo-Parametric$^{©}$ and Klein [148] is tabulated in Table.A1. The lengths of semi-major and semi-minor axes of the intersection ellipse calculated through the proposed closed-form expression shows dissimilarity with the results of Creo-Parametric© and Klein [148]. By comparing the results, it can be concluded that the result of the proposed closed-form expressions would be more accurate and reliable than the calculations of CAD software and Klein [148]. This is due to the fact that in CAD softwares, some precision error may occur during the computation of the point to point distances which may degrade the accuracy at insignificant level. In contrast, Klein [148] method uses differential geometry to obtain the intersection ellipse between the plane and the spheroid which may also induce insignificant error. In comparison, the proposed closed-form expression uses simple direct formulation which do not involve any estimation procedure, therefore, the proposed expression will always provide the exact calculations with higher precision level of accuracy than Creo-Parametric©

(a) $\theta = 30°$

(b) $\theta = 45°$

(c) $\theta = 60°$

(d) $\theta = 75°$
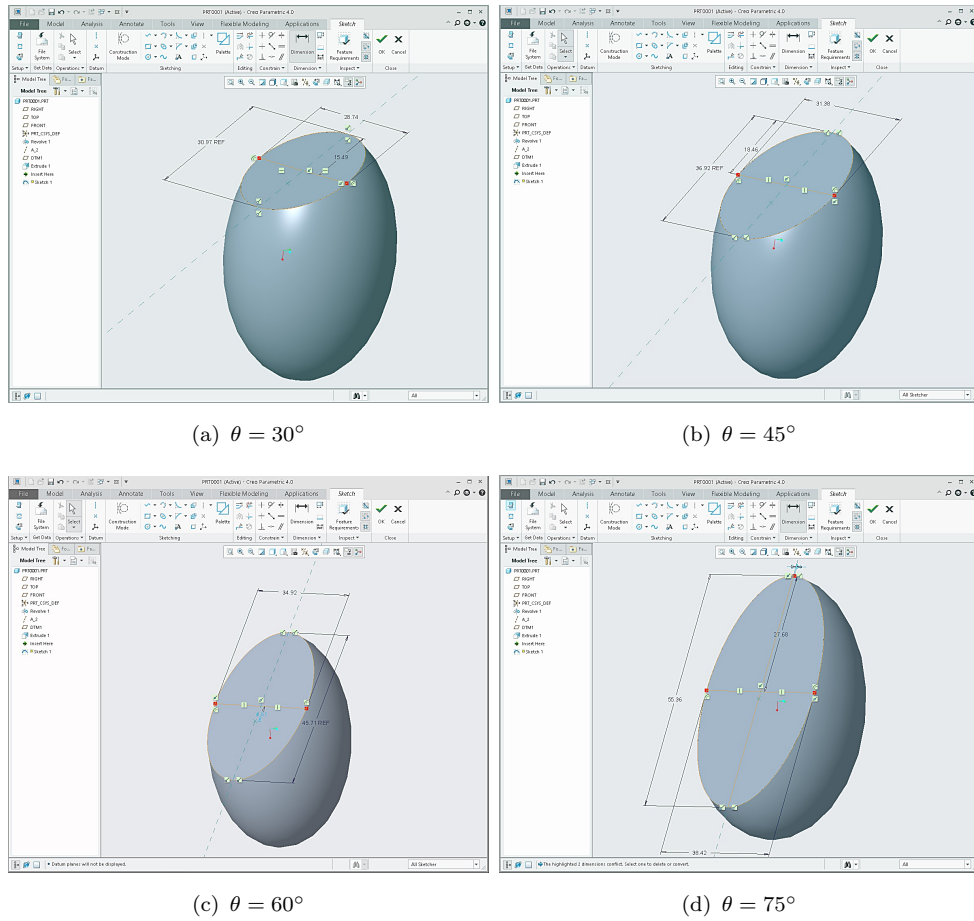
FIGURE A5: Formation of intersection ellipses with the help of CAD software Creo-Parametric$^©$ 4.0 at angles $\theta = 30°, 45°, 60°, 75°$.

and Klein [148].

TABLE A1: Accuracy comparison of the proposed closed-form expression.

Evaluation mechanism	Klein [148]		Creo-Parametric$^©$		Proposed	
$\boldsymbol{\theta°}$	a_{cs}	b_{cs}	a_{cs}	b_{cs}	a_{cs}	b_{cs}
0	13.3300	13.3300	13.3338	13.3338	13.3300	13.3300
30	15.4843	14.3680	15.4850	14.3700	15.4839	14.3684
45	18.4600	15.6900	18.4600	15.6900	18.4615	15.6893
60	22.8550	17.4600	22.8550	17.4600	22.8571	17.4574
75	27.5218	19.1006	27.6800	19.2100	27.6821	19.2118